

# **NMR, EM and functional studies on TBsmr, a small multidrug transporter from *M. tuberculosis***

Dissertation  
zur Erlangung des Doktorgrades  
der Naturwissenschaften

Vorgelegt beim Fachbereich 14  
der Johann Wolfgang Goethe-Universität  
in Frankfurt am Main

von  
**Daniel Basting**

aus Göttingen

Frankfurt am Main 2007

(D30)

Vom Fachbereich Chemische und Pharmazeutische Wissenschaften der Johann Wolfgang Goethe-Universität Frankfurt als Dissertation angenommen.

|            |                         |
|------------|-------------------------|
| Dekan:     | Prof. Harald Schwalbe   |
| Gutachter: | Prof. Clemens Glaubitz  |
|            | Prof. Joseph Wachtveitl |

Datum der Disputation:

# Contents

|          |  |           |
|----------|--|-----------|
| <b>1</b> | <b>Introduction</b>  | <b>4</b>  |
| 1.1      | Multidrug resistance . . . . .                               | 4         |
| 1.2      | Efflux pumps . . . . .                                       | 5         |
| 1.3      | Solid-state NMR for the study of membrane proteins . . . . . | 13        |
| 1.4      | Isotope labeling . . . . .                                   | 16        |
| 1.5      | TBsmr from <i>M. tuberculosis</i> . . . . .                  | 17        |
| 1.6      | Outline of this thesis . . . . .                             | 19        |
| <br>     |  |           |
| <b>2</b> | <b>Materials and Methods</b>                                 | <b>21</b> |
| 2.1      | Prediction methods . . . . .                                 | 21        |
| 2.2      | Cloning of TBsmr mutants . . . . .                           | 21        |
| 2.3      | Expression and Purification . . . . .                        | 22        |
| 2.4      | Chymotrypsin digestion . . . . .                             | 24        |
| 2.5      | SDS-PAGE . . . . .   | 24        |
| 2.6      | Dot blot . . . . .   | 25        |
| 2.7      | Western blot . . . . .                                       | 25        |
| 2.8      | Mass spectrometry . . . . .                                  | 26        |
| 2.9      | Gel filtration . . . . .                                     | 27        |
| 2.10     | Crystallization . . . . .                                    | 27        |
| 2.11     | Reconstitution . . . . .                                     | 28        |
| 2.12     | Density gradients . . . . .                                  | 29        |
| 2.13     | TPP <sup>+</sup> transport assay . . . . .                   | 30        |
| 2.14     | Freeze-fracture electron microscopy . . . . .                | 30        |
| 2.15     | Fluorescence assay . . . . .                                 | 31        |
| 2.16     | NMR spectroscopy . . . . .                                   | 33        |
| <br>     |  |           |
| <b>3</b> | <b>Reconstitution and 3D crystallization</b>                 | <b>38</b> |

---

|          |   |           |
|----------|---|-----------|
| 3.1      | Introduction . . . . .  | 38        |
| 3.2      | Results . . . . .   | 40        |
| 3.2.1    | Expression and Purification . . . . .   | 40        |
| 3.2.2    | Monodispersity and stability in different detergents . . . . .  | 43        |
| 3.2.3    | Crystallization . . . . .   | 44        |
| 3.2.4    | Reconstitution into lipid vesicles . . . . .  | 46        |
| 3.3      | Discussion . . . . .  | 49        |
| 3.4      | Conclusion . . . . .  | 53        |
| <b>4</b> | <b>Lipids influence the oligomerization and function of TBsmr: EM and TPP<sup>+</sup> transport study</b>       | <b>54</b> |
| 4.1      | Introduction . . . . .  | 54        |
| 4.2      | Results . . . . .   | 55        |
| 4.2.1    | Reconstitution into different lipids . . . . .  | 55        |
| 4.2.2    | Drug transport: TPP <sup>+</sup> assay . . . . .  | 56        |
| 4.2.3    | Lipids influence TPP <sup>+</sup> transport . . . . .   | 59        |
| 4.2.4    | Analysis of the freeze-fracture EM images . . . . .   | 61        |
| 4.3      | Discussion . . . . .  | 65        |
| 4.4      | Conclusion . . . . .  | 67        |
| <b>5</b> | <b>Transport cycle intermediate in small multidrug resistance protein is revealed by substrate fluorescence</b> | <b>68</b> |
| 5.1      | Introduction . . . . .  | 68        |
| 5.2      | Results . . . . .   | 70        |
| 5.3      | Discussion . . . . .  | 77        |
| 5.3.1    | Formation of an intermediate substrate-protein complex . . . . .  | 77        |
| 5.3.2    | Characterization of an intermediate substrate-protein complex . . . . .   | 81        |
| 5.3.3    | Relevance for transport models . . . . .  | 82        |
| 5.4      | Conclusion . . . . .  | 82        |
| <b>6</b> | <b>Liquid-state NMR study on detergent-solubilized TBsmr</b>  | <b>84</b> |
| 6.1      | Introduction . . . . .  | 84        |
| 6.2      | Results and discussion . . . . .  | 84        |
| 6.2.1    | NMR sample optimization . . . . .   | 84        |
| 6.2.2    | Backbone resonance assignment . . . . .   | 87        |

---

|          |   |            |
|----------|---|------------|
| 6.2.3    | EtBr interacts non-specifically with TBsmr in detergent . . . . .   | 89         |
| 6.2.4    | TBsmr is monomeric in LPPG . . . . .                                | 89         |
| 6.3      | Conclusion . . . . .  | 92         |
| <b>7</b> | <b>Solid-state NMR study on TBsmr proteoliposomes</b>               | <b>93</b>  |
| 7.1      | Introduction . . . . .  | 93         |
| 7.2      | Results . . . . .   | 93         |
| 7.2.1    | <sup>15</sup> N solid-state NMR experiments . . . . .               | 93         |
| 7.2.2    | Attempt to identify conserved Glu-13 . . . . .                      | 96         |
| 7.2.3    | <sup>19</sup> F solid-state NMR experiments . . . . .               | 97         |
| 7.2.4    | Trp 63 labeling (Involvement of W63 in substrate binding) . . . . . | 99         |
| 7.3      | Discussion . . . . .  | 102        |
| 7.4      | Conclusion and outlook . . . . .                                    | 105        |
| <b>8</b> | <b>Summary</b>  | <b>107</b> |
| <b>9</b> | <b>Zusammenfassung</b>  | <b>109</b> |
|          | <b>Appendix</b>   | <b>116</b> |
|          | <b>List of Tables</b>   | <b>120</b> |
|          | <b>List of Figures</b>  | <b>121</b> |
|          | <b>Abbreviations</b>  | <b>124</b> |
|          | <b>Acknowledgements</b>   | <b>128</b> |
|          | <b>References</b>   | <b>129</b> |

# 1 Introduction

## 1.1 Multidrug resistance

Antibiotic resistance of pathogenic bacteria is a major worldwide problem. For example, *Mycobacterium tuberculosis* is one of the leading causes for mortality and responsible for the deaths of 1.6 million people in 2005 (WHO Report 2007). The widespread use of antibiotics over a number of years means they no longer provide effective control against many infectious diseases (Fig. 1.1). Even more troublesome is the appearance of strains that are resistant to more than one antibiotic, which is called multidrug resistance (MDR). Bacteria can resist antibiotics through several mechanisms (Fig. 1.2) like drug inactivation by blocking the reaction of the pro-drug to the active compound (Raynaud et al., 1999) or mutation of the drug target (Takiff et al., 1994). Other mechanisms reduce the accumulation of toxic agents inside the organism by decreasing the cell wall permeability to prevent the drug from entering the cell or by active efflux due to multidrug transporters (Li et al., 2004).

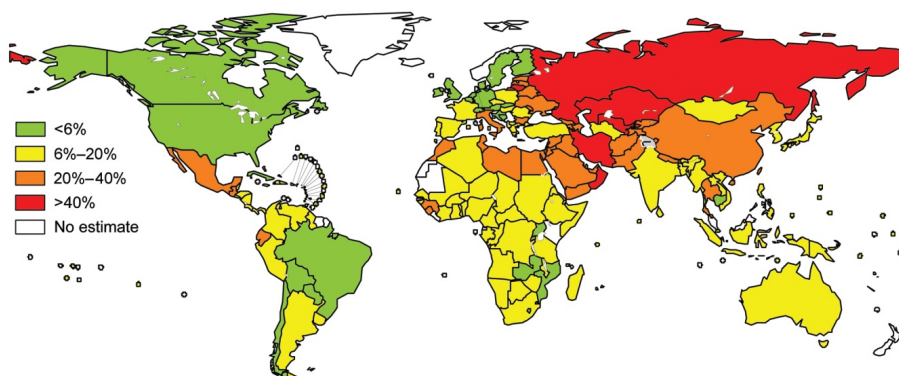


**Figure 1.1:** Distribution of multidrug-resistant tuberculosis rates among previously treated cases (Source: Zignol et al., 2006).

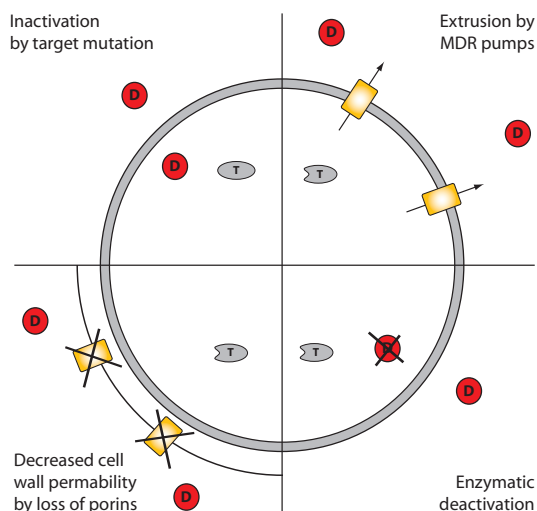


**Figure 1.2:** Multidrug resistance mechanisms (Target proteins, T; drugs, D).

## 1.2 Efflux pumps

Genes for efflux pumps are present in all organisms and are located on the chromosome or on transmissible plasmids (Gros et al., 1986; Tennent et al., 1985). When expressed, they can increase the tolerance of the organism to antibiotics. While some extrude specific targets, others transport a wide range of structurally dissimilar compounds. The widespread existence cannot be explained by their function in drug resistance alone. Instead it could be that the drug efflux is a by-product of a physiological role (Piddock, 2006). For example the MDR transporter, LmrA can act as a lipid flippase and as a multidrug transporter if this function is needed (Margolles et al., 1999).

Since the first evidence for multidrug efflux (Juliano and Ling, 1976), the important role of efflux pumps in multidrug resistance has been recognized. Multidrug resistance can be intrinsic or acquired. An intrinsic drug resistance is inherent to every member of the species. For example, bacteria lacking peptidoglycan are not affected by  $\beta$ -lactam antibiotics. However, intrinsic drug resistance is not restricted to passive mechanisms, a basal level of drug efflux can also contribute to intrinsic drug resistance (Ramon-Garcia et al., 2007).

An acquired drug resistance is the result of exposure to non-lethal drug concentrations. It is reflected in an increase of minimum inhibitory concentrations (MICs) of those drugs. The drugs themselves can stimulate the expression of multidrug transporters by binding to regulatory proteins (Hillen and Berens, 1994). A permanent upregulation can result

from mutations in the regulatory system (Srikumar et al., 2000). Alternatively, multidrug transporter genes located on transmissible plasmids can spread the acquired resistance (Welch et al., 2007).

In clinical strains, they mostly provide a low-level resistance phenotype. Combined with the fact that often mutations of the drug target are the cause for high-level resistance in pathogens (Takiff et al., 1994), the clinical relevance of efflux transporter is still unresolved. However, efflux mechanisms are found in most basal and high-level drug resistant isolates of pathogens (Peric et al., 2003), and a recent study reported a high-level resistance based entirely on multidrug efflux (Daporta et al., 2004).

## Classes of MDR efflux pumps

Bacterial efflux pumps are classified in five families (Saier and Paulsen, 2001), the major facilitator superfamily (MFS; TC# 2.A.1), the ATP-binding cassette superfamily (ABC; TC# 3.A.1), the multidrug and toxic compound extrusion family (MATE, TC# 2.A.66.1), the resistance nodulation division superfamily (RND; TC# 2.A.6) and the small multidrug resistance family (SMR, TC# 2.A.7.1) based on the number of transmembrane helices, type of substrate and energy source (transport classification database, [www.tcdb.org](http://www.tcdb.org)). Common examples of every family and typical substrates are shown in Fig. 1.3.

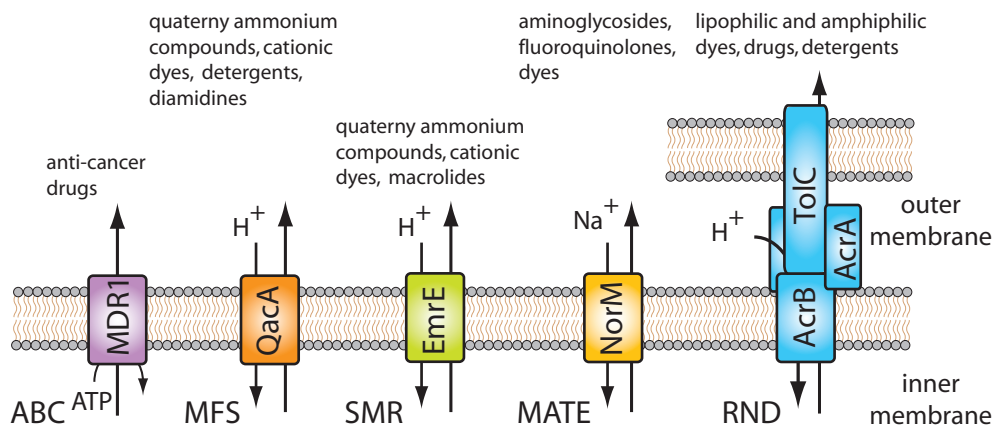


**Figure 1.3:** Schematic comparison of the five families of multidrug-resistant efflux pumps.

Most organisms have one or more genes from every family ([www.membranetransport.org](http://www.membranetransport.org)). The simultaneous overexpression of two RND efflux pumps was detected in clinical isolates of *Pseudomonas aeruginosa* (Llanes et al., 2004).

The ABC transporters, otherwise known as primary efflux pumps, utilize energy derived from ATP hydrolysis for active transport of substrates. The other families, MFS, MATE, RND and SMR, are termed secondary active transporters because the substrate efflux is coupled to an opposite electrochemical gradient of  $H^+$  or  $Na^+$  ions across the membrane.

At present, ABC transporter constitute the only multidrug efflux systems in eukaryotes. In human, the clinically relevant protein MDR1 (Roninson et al., 1986), also known as P-glycoprotein, is an attractive drug target because it can extrude nearly every known anti-cancer drug. However, few ABC transporters are involved in multidrug resistance in prokaryotes. Members of the RND superfamily are found ubiquitously in archaea, bacteria and eubacteria, but they contribute to multidrug resistance only in gram negative bacteria. There, they are associated with clinically relevant MDR (Piddock, 2006). RND proteins are organized in a tripartite system that bridges the inner and outer membrane. The best studied RND multidrug efflux protein is the AcrAB-TolC system which binds a broad range of substance from the cytoplasm and periplasm and transports them through a channel formed by TolC directly to the external medium (Seeger et al., 2006). In gram positive strains such as *Staphylococcus aureus*, clinical relevant multidrug resistance is associated with MFS exporters. QacA/B was found on transmissible plasmids in 41.6% (372/894) of the isolates of methicillin-resistant *S. aureus* (Noguchi et al., 2005). The major facilitator superfamily is the largest secondary transport family. Its members are uniporter, symporter and antiporter which transport a variety of substrates including sugars, ions, drugs (Pao et al., 1998). The recently discovered protein NorM from *Vibrio parahaemolyticus* showed no sequence identity to the other multidrug transporter families and was assigned to the new MATE family (Brown et al., 1999). Proteins of that family that have been found to export toxins with a preference for cationic compounds in exchange for  $H^+$  or  $Na^+$  ions (Omote et al., 2006).

### Small multidrug resistance

Due to their small size, the SMR proteins are a paradigm to study multidrug efflux and will be the focus of this study. Proteins of the SMR family are small integral membrane proteins of approximately 110 amino acids (aa) with a predicted four-helix transmembrane topology. They have been found in archaea and bacteria (Grinius et al., 1992; Ninio and Schuldiner, 2003). Generally, SMR proteins show a pmf-promoted efflux of a wide range of quaternary ammonium compounds (QACs) such as methyl viologen ( $MV^{2+}$ ) and



protein and the other an extended c-terminal tail (e.g. *Bacillus subtilis* EbrA has 105 aa and EbrB 117 aa). While some paired SMR proteins extrude multiple drugs similar to the SMPs (Masaoka et al., 2000), YvdR and YvdS did not confer a drug resistance phenotype when expressed either individually or alone, and have been suggested to serve a function not related to drug resistance (Chung and Saier, 2001). This observation is also reflected in a phylogenetic analysis where proteins of the PSMR subclass form small branches in the SUG and SMP clusters (Bay et al., 2007).

The distinct subclass of SUG proteins is based on the conferred phenotype of SugE to suppress mutations in the molecular chaperon gene *groEL* (Greener et al., 1993) and phylogenetic analysis (Paulsen et al., 1996). In contrast to proteins of the SMP subclass, SugE transports a narrow range of QACs (Chung and Saier, 2002).

The phenotype of multidrug resistance, associated with the SMR family, is primarily caused by proteins of the SMP subclass. The multidrug pumps are found on plasmids, e.g. QacC, and encoded on the chromosome as the *E. coli* EmrE (Littlejohn et al., 1991; Purewal, 1991).

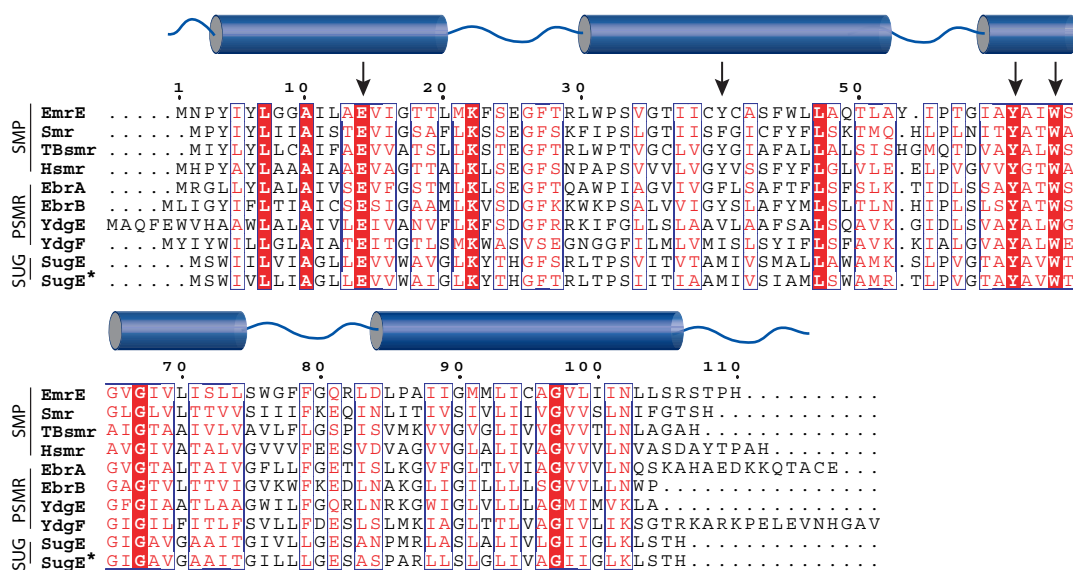


**Figure 1.5:** Sequence alignment of SMR proteins. Residues important for substrate binding are marked with an arrow. The secondary structure was predicted with TMHMM (Sonnhammer et al., 1998) for TBsmr. (*E. coli*: EmrE, YdgE, YdgF, SugE; *S. aureus*: Smr; *M. tuberculosis*: TBsmr; *Halobacterium salinarium*: Hsmr *B. subtilis*: EbrA, EbrB; *Citrobacter freundii*: SugE\*).

**Key residues** *E. coli* EmrE has been studied extensively and is a paradigm for the SMR family (Schuldiner et al., 2001). The conserved glutamate 14 is the primary active

site of EmrE shared mutually exclusive for substrate and proton binding (Yerushalmi and Schuldiner, 2000c). From all glutamates in the protein, E14 is the only carboxylate residue necessary for drug transport (Yerushalmi et al., 2001). Its high  $pK_a$  of  $\sim 7.5$  is essential for coupling the proton and substrate fluxes, and even a conservative mutation to aspartate leads to an impaired protein (Yerushalmi and Schuldiner, 2000b; Soskine et al., 2004). Mutagenesis studies on the PSMR protein EbrAB showed that only one glutamate in the dimer is essential for drug binding (Zhang et al., 2007). The asymmetry of the the two E14 residues has been shown in an electron paramagnetic resonance (EPR) and a solid-state NMR study for EmrE, too. (Koteiche et al., 2003; Lehner et al., 2007).

A number of conserved aromatic residues which are necessary for drug transport have been identified. The residues Y40, Y60 and W63 in transmembrane segment (TMS) 2 and 3 take part in substrate binding (Sharoni et al., 2005; Elbaz et al., 2005; Rotem et al., 2006), whereas Y4 is required for proper coupling between the substrate transport and the proton gradient (Rotem et al., 2006). In addition, important residues that are part of the binding cavity in the dimer have been identified in TMS1-3. Site-directed spin labeling experiments suggest that TMS1 from two different subunits are in close proximity and form a V-shaped chamber (Koteiche et al., 2003). Cross-linking studies and the accessibility to alkylation reagents have identified the conserved residues L7, A10, I11 and T18, which cluster on the same side of TMS1 as the conserved E14, to participate in the binding pocket (Mordoch et al., 1999; Gutman et al., 2003; Sharoni et al., 2005). A sequence alignment of SMR proteins of all three subgroups is shown in Fig. 1.5 in which conserved residues and residues important for substrate binding are highlighted. The data of residues affecting the substrate translocation has been used to validate a  $C^\alpha$  model of transmembrane region constructed from the cryo-EM data of EmrE (Fleishman et al., 2006).

***Oligomeric state, topology and structure*** All SMR proteins are approximately 11-12 kDa in size, and share a four-helix topology, which has been confirmed by Fourier transform infrared (FTIR) and liquid-state NMR spectroscopy for EmrE (Arkin et al., 1996; Schwaiger et al., 1998).

The oligomeric state of SMR proteins is still unresolved. Given that transporters of the other families typically contain 10-14 helices, it seems unlikely that the functional transporter is a monomer. There is evidence for EmrE monomers from a size exclusion chromatography (SEC) study (Winstone et al., 2005), but biophysical studies such

as electrospray ionization mass spectrometry (ESI-MS), analytical ultracentrifugation and electron paramagnetic resonance (EPR) spectroscopy (Ilag et al., 2004; Butler et al., 2004; Koteiche et al., 2003), and biochemical studies such as monomer swapping and cysteine cross-linking of solubilized EmrE (Rotem et al., 2001; Soskine et al., 2002) support a dimeric state. In addition, paired SMR proteins which require both proteins to be expressed simultaneously to confer a resistance phenotype also support a functional dimer (Jack et al., 2000). However there is also evidence for higher oligomers: a trimeric arrangement was found by negative dominance and radioactive ligand binding studies (Yerushalmi et al., 1996; Muth and Schuldiner, 2000). Even though two electron microscopy (EM) projection structures of EmrE and cross-linking experiments revealed a dimeric arrangement, the existence of tetramers/dimers of dimers could not be ruled out (Tate et al., 2001; Elbaz et al., 2004; Ubarretxena-Belandia et al., 2003). A second, low affinity oligomerization site is also supported by a fluorescence resonance transfer study with a peptide of TMS 4 of Hsmr (Rath et al., 2006). The conflicting results could be due to different preparation techniques, constructs, or experimental conditions. The dimer was most frequently determined and probably is the minimal functional unit capable of binding substrate. However, it is not certain if the dimer is also capable of transport because a protein may bind substrate without completing the transport cycle (Smirnova and Kaback, 2003). The full activity of SMR proteins can only be shown in transport assays with protein reconstituted in proteoliposomes (Yerushalmi et al., 1995).

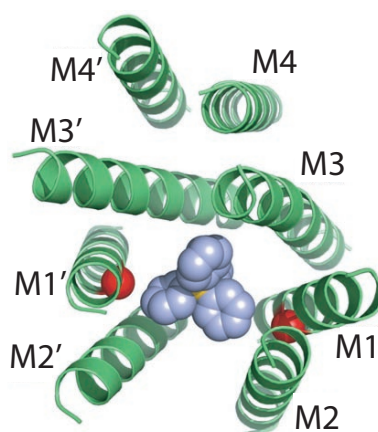


**Figure 1.6:** Backbone model of the transmembrane region of EmrE. TPP<sup>+</sup> was docked into the structure and the conserved E14 residues are highlighted in red (Source: Fleishman et al., 2006).

The discovery of dual topology proteins (anti-parallel) (Daley et al., 2005) sparked a controversy whether the two protomers in the functional EmrE dimer adopt a uni-

directional or bi-directional orientation (Schuldiner, 2007). Biochemical data, based on cross-linking studies (Soskine et al., 2006) support uni-directional arrangement, but a genetic study (Rapp et al., 2006, 2007) and an analysis of the cryo-EM structure of EmrE (Fig. 1.6) (Fleishman et al., 2006) agree with a bi-directional orientation, also known as dual topology. Recently, the retracted x-ray structures of EmrE (Ma and Chang, 2004; Pornillos et al., 2005; Chang et al., 2006) have been republished (Chen et al., 2007). Even though the resolution of 3.8 Å was too low to place the side chain atoms, an anti-parallel orientation of the dimer could clearly be identified in selenomethionine-labeled crystals, supporting the dual topology model.

***Drug-transport mechanism*** The uphill transport of substrate is solely driven by the proton motive force (pmf), which also determines the direction of transport (Littlejohn et al., 1992; Grinius and Goldberg, 1994; Yerushalmi et al., 1995). The proton motive force consists of two components, a pH gradient ( $\Delta\text{pH}$ ) and a charge difference (or membrane potential,  $\Delta\psi$ ) across the membrane. It is possible to study the two components separately and thus determine if a transport is electroneutral, or not. EmrE transports monovalent  $\text{TPP}^+$  and also divalent substrates. The electrogenic transport of  $\text{TPP}^+$  and electroneutral transport of divalent  $\text{MV}^{2+}$  support an exchange of two protons per substrate during each transport cycle (Rotem and Schuldiner, 2004). Besides proton-driven substrate transport, substrate/substrate exchange can also take place, albeit at a  $\sim 15$  times slower rate (Yerushalmi and Schuldiner, 2000b).

The transport of drugs across the membrane is thought to occur in two steps (Fleishman et al., 2006; Yerushalmi et al., 2001). Substrate binding induces a conformational change, so that the binding pocket faces the other side of the membrane. There, the lower pH causes a high concentration of protons which compete with the drug for binding to the two glutamates. The reprotonated dimer returns to its original conformation and the transport cycle is completed. It is unlikely that the transport cycle consists only of an inward and outward facing conformation but so far no further intermediate state has been detected.

The drug binding affinities of SMR proteins are in the nanomolar to micromolar range. Low binding affinities are expected for multidrug transporters because the substrate has to be released again during the transport cycle. For example, Smr has a low micromolar binding affinity for  $\text{TPP}^+$  (Poget et al., 2007) but transports it (Grinius and Goldberg, 1994), whereas EmrE has an unusually high affinity of 10 nM for  $\text{TPP}^+$  (Muth and

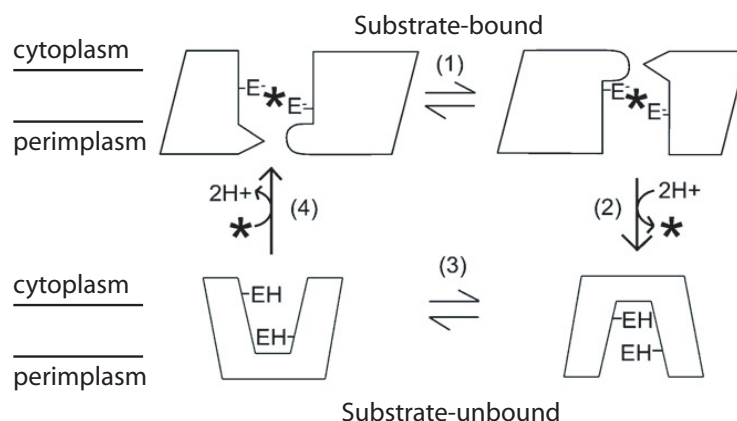


**Figure 1.7:** Alternate-access mechanism for proton-coupled translocation of substrates by the SMR family of proteins. (1) Two substrate-bound forms of the protein interconvert between conformations, in which the substrate, marked by an asterisk (\*) faces the cytoplasm or the periplasm due to conformational changes. (2) In the periplasmic-facing conformation, the substrate is supplanted by the binding of two protons to the Glu14 positions (marked by E-) on both monomers, thus driving the equilibrium towards substrate translocation. (3) A conformational change reorients the binding site towards the cytoplasm. (4) Substrate binding on the cytoplasmic side forces the protons out of the translocation chamber into the cytoplasm (Source: Fleishman et al., 2006).

Schuldiner, 2000) but the transport is slow (Rotem and Schuldiner, 2004). The binding affinity of EmrE for EtBr,  $MV^{2+}$  and  $TPP^+$  was also studied by isothermal titration calorimetry (ITC). Those measurements revealed binding affinities in the  $\mu M$  range in different membrane mimetics such as DDM, SDS and small uniform vesicles (Sikora and Turner, 2005a). The different results for  $TPP^+$  are probably related to the sample preparation. The unusual high affinity of EmrE for  $TPP^+$  seems to be the exception because only low or no  $TPP^+$  binding could be determined for the many other SMR proteins (BPsmr, TBsmr, PAsmr, SugE and Smr) (Ninio et al., 2001; Sikora and Turner, 2005b; Poget et al., 2007), and the affinity of EmrE is also in the micromolar range for other substrates such as EtBr and  $MV^{2+}$  (Sikora and Turner, 2005a; Chen et al., 2007).

### 1.3 Solid-state NMR for the study of membrane proteins

So far, 26 structures of the proteins AcrB, Sav1866, EmrE and EmrD from four multidrug transporter families have been determined (Seeger et al., 2006; Dawson and Locher, 2006; Chen et al., 2007; Yin et al., 2006a). Only AcrB and EmrE have been confirmed to be multidrug efflux transporter. Although the structures do not yet contain a representative from

all transporter families, this information is of great value for understanding the molecular mechanisms (Higgins, 2007). Furthermore, we must remember that each structure corresponds to a snapshot of the protein during its transport cycle. Therefore, additional approaches are needed to elucidate the transport kinetics, substrate-protein interactions or conformational changes during substrate translocation.

Solid-state nuclear magnetic resonance (ssNMR) spectroscopy has been widely used in membrane biophysics to study membrane bound peptides and increasingly for investigations of larger integral membrane proteins. Biological material contains protons, carbons and nitrogens which have at least one magnetic isotope ( $^1\text{H}$ ,  $^{13}\text{C}$ ,  $^{15}\text{N}$ ). When such a magnetic nucleus is placed in a magnetic field, it adopts two permitted states which are separated by an energy  $\Delta E$ . The energy difference depends not only on the magnetic field but is also sensitive to the environment. NMR spectroscopy can detect those interaction with the environment which are described by Hamiltonians:

$$\hat{H} = \hat{H}_{\text{CS}} + \hat{H}_{\text{CSA}} + \hat{H}_{\text{DC}} + \hat{H}_{\text{J}} \quad (1.1)$$

The chemical shift ( $\hat{H}_{\text{CS}}$ ) and the chemical shift anisotropy ( $\hat{H}_{\text{CSA}}$ ) contain information about the local chemical environment, whereas the dipolar coupling between nuclei ( $\hat{H}_{\text{DC}}$ ) can be used to determine the distance between them. The skalar coupling ( $\hat{H}_{\text{J}}$ ) is transmitted through bonds and contains information e.g. about dihedral angles.

Areas of application cover protein structure and dynamics, lipid-protein, substrate-protein, and substrate-membrane interactions. Static ssNMR applied to macroscopically ordered membrane samples has been used to elucidate secondary structure and topological organisation of membrane bound peptides (Ketchum et al. 1997). However, for larger membrane proteins, such as SMR proteins, static ssNMR techniques are of limited use. Instead, magic angle sample spinning (MAS) seems more promising as it imposes fewer restrictions with respect to sample preparations: The proteins can be studied in a number of states. But most importantly, anisotropic NMR interactions are averaged out by fast sample rotation (in practice 5-20 kHz) about the magic angle ( $54.7^\circ$  with respect to the magnetic field  $B_0$ ), leading to the type of well resolved spectra shown in Fig. 1.8.

The number of membrane proteins available for biophysical studies has been dramatically increased by the advent of microbial expression systems (e.g. *Escherichia coli*, yeast and baculovirus) and cell-free expression systems (Klammt et al., 2004) optimized for membrane proteins, the availability of detergent screens and advanced purification technologies, in addition to the sequencing of a number of prokaryotic and eukaryotic

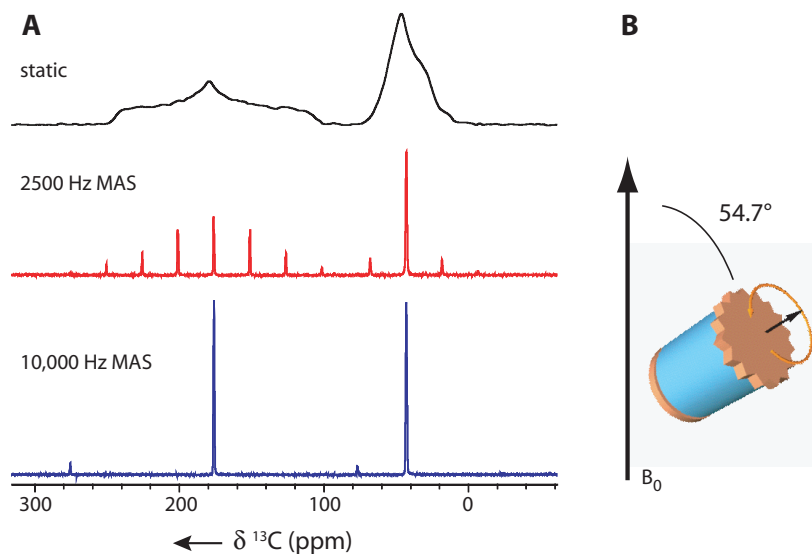


**Figure 1.8:** A)  $^{13}\text{C}$  solid-state NMR spectra of glycine at 100 MHz  $^{13}\text{C}$  lamor frequency. B) Schematic view of rotor with magic angle spinning.

genomes. Solid-state NMR is increasingly applied to isotope labeled membrane proteins in order to derive data about protein structure and dynamics. Details about the expression of isotope labeled protein in *E. coli* is given further down.

So far, only a limited number of solid-state NMR studies on transporters have been reported (for a review see Basting et al., 2006). Applications cover in principle three areas: interactions of substrates with the membrane, detection of substrates bound to transporters, and methodological studies describing how to prepare isotope labeled transporters. The first solid-state NMR applications to transporters were presented by the laboratories of Watts and Henderson who demonstrated the detection of substrate bound to the sugar transporter GalP (Spooner et al., 1994). This has triggered further studies aimed at obtaining structural information concerning the position of the binding site (Spooner et al., 1998), as well as the ligand/protein association constant (Patching et al., 2004). Recently, it has also been shown that isotope labelled transporters can be prepared at a quantity and purity suitable for ssNMR (Mason et al., 2004; Agarwal et al., 2007; Lehner et al., 2007).

The possibility of a complete de novo structure determination purely based on MAS NMR recoupling techniques was first demonstrated for small insoluble peptides (Jaroniec et al., 2004; Rienstra et al., 2002) and has been extended to soluble proteins studied in the solid state (Castellani et al., 2002; Seidel et al., 2005; Zech et al., 2004). However,

similar studies have not yet been successfully applied to membrane proteins largely due to limitations in spectral resolution. Nevertheless, a number of studies have reported promising MAS NMR spectra of membrane proteins prepared as 2D crystals (Hiller et al., 2005; Shastri et al., 2007), 3D crystals (Lorch et al., 2005a) and also in proteoliposomes (Andronesi et al., 2005). The latter is clearly the preparation of choice as it is closest to the protein's native environment. Lipid reconstituted samples also offer the option of investigating the dynamics of the protein as it binds ligands (Patching et al., 2004), goes through its reaction cycle (Mason et al., 2005) or responds to changes in the lipid environment (Yamaguchi et al., 2004). However, the currently very limited knowledge base does not yet allow to derive general rules about how to prepare membrane proteins for solid-state NMR and so screens have to be performed for each individual protein.

## 1.4 Isotope labeling

*E. coli* is also the most used expression system for preparing isotope labeled proteins for NMR spectroscopy. Overexpression of bacterial transporters has been repeatedly demonstrated in *E. coli* (Auer et al., 2001; Curnow et al., 2004; Masi et al., 2003; Xie et al., 2004; Yerushalmi et al., 1995). Complete labeling can be achieved by using minimal media, which contains all necessary nutrients and an isotope enriched carbon and/or nitrogen source. These well established standard procedures have been used, for example, to prepare the *E. coli* transporter EmrE for solution-state NMR (Schwaiger et al., 1998).

Unfortunately,  $\alpha$ -helical membrane proteins often have a low spectral dispersion, and therefore uniformly labeled proteins yield very crowded NMR spectra with many overlapping peaks (Krueger-Koplin et al., 2004). To circumvent this problem, selective labeling of single amino acid types can be achieved with a defined medium (synthetic rich) containing all amino acids (Muchmore et al., 1989). Selective labeling can be aided, and metabolic scrambling of NMR active nuclei avoided, with the use of auxotrophic *E. coli* strains. However, auxotrophs are not available for all amino acids and usually support only low levels of protein overexpression. An alternative to auxotrophs makes use of the T7 promoter and the action of the antibiotic rifampicin (Arkin et al., 1996; Lee et al., 1995) Rifampicin selectively binds to the *E. coli* RNA polymerase and blocks its transcription initiation, while the T7 RNA polymerase is not affected. This can be exploited by growing *E. coli* in unlabeled media to the desired cell density, pelleting the cells and inducing in fresh isotope labeled media (Almeida et al., 2001). Shortly after induction,

rifampicin is added and thus it is assured that protein contaminants are not isotope labeled and that the *E. coli* cell metabolism is reduced.

## 1.5 TBsmr from *M. tuberculosis*

TBsmr (gene accession number Rv3056, also known as mmr) was selected for this study because it is a small multidrug resistance protein from the clinically relevant *M. tuberculosis* and has 70% similarity and 43% identity to the well studied EmrE (Fig. 1.5) (De Rossi et al., 1998b). Both proteins impart resistance to TPP<sup>+</sup>, acriflavine, ethidium bromide (EtBr), benzalkonium, and methyl viologen (MV<sup>2+</sup>), whereas TBsmr also confers resistance to safranin O, pyronin Y, and erythromycin (Fig. 1.10). TBsmr can be expressed *in vivo* and *in vitro*, and has been shown to cause uptake of MV<sup>2+</sup> into proteoliposomes (Ninio et al., 2001; Elbaz et al., 2004). Attempts to increase the expression yield as a fusion protein with the maltose binding protein failed (Korepanova et al., 2007). A topology plot of the TBsmr construct is shown in Fig. 1.9.

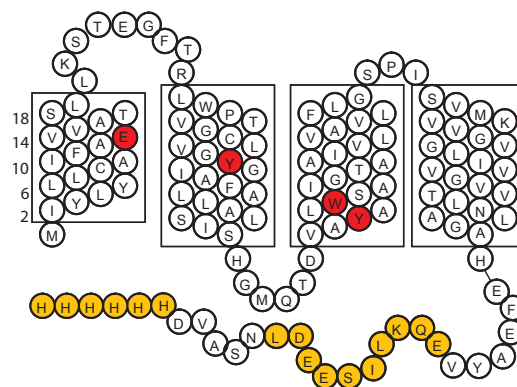


**Figure 1.9:** Topology model of the TBsmr construct. The position of the transmembrane helices were predicted with TMHMM. The myc/his-tag is shown in orange and important residues for substrate binding in red.

Tuberculosis (TB), caused by *Mycobacterium tuberculosis*, is a leading cause of mortality due to an infectious disease (Neralla and Glassroth, 2003). The bacillus has the ability to persist in a latent form for years before the active disease breaks out (Lillebaek et al., 2003). According to the World Health Organization, it has infected about 2 billion people, one third of the world's population, and killed 1.6 million people in 2005 (WHO/HTM/TB/2007.376).

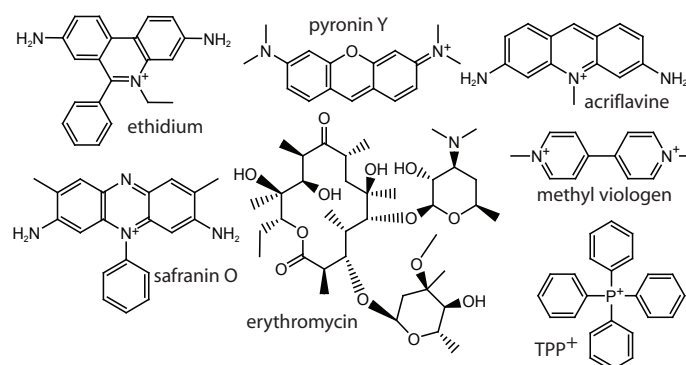


**Figure 1.10:** Substrates of TBsmr.

Even though the infection rates are going down world wide, control of the disease remains a challenge. Multidrug-resistant tuberculosis (MDR-TB), which does not respond to the first-line drugs isoniazid and rifampicin, poses a threat to public health because its treatment is difficult and costly (Prasad, 2007; Cox et al., 2006). An extensively drug-resistant tuberculosis (XDR-TB), resistant to first and second-line drugs, is particularly worrisome because treatment options are limited (Zignol et al., 2006).

Mutations in the genes encoding the drug target (Telenti et al., 1993) and the enzymes responsible for drug activation (Rouse et al., 1995) have been identified as the major mechanism of an acquired high-level resistance of *M. tuberculosis*. However, mutations cannot be the sole source for multidrug resistance. The development of multidrug resistance is attributed to two factors: A thick cell wall, with an extensive layer of peptidoglycan and an outer membrane made of mycolic acid in addition to the inner-membrane, limits the uptake of antibiotics (Brennan and Nikaido, 1995). The other mechanism, active drug extrusion, can be assigned to membrane-bound primary or secondary efflux pumps that extrude antibiotics that enter the cell (Colangeli et al., 2005). The genome of *M. tuberculosis* contains proteins from all of these families. Several mycobacterial drug efflux pumps have been identified (De Rossi et al., 2006) and are summarized in Tab. 1.1. Together these two mechanisms decrease the internal drug concentration and allow the infecting bacilli to survive long enough under fluctuating concentrations of antibiotics to develop additional mutations and convert from a drug tolerant to a fully resistant one.

## 1.6 Outline of this thesis

To understand the molecular mechanism of multidrug resistance, we have to gain information about the structure and function of these proteins. The research described in this thesis aimed to deduce details about the topology, transport cycle and key residues of TBsmr using biophysical techniques (Fig. 1.11). In Chapter 3, an enhanced protein prepara-

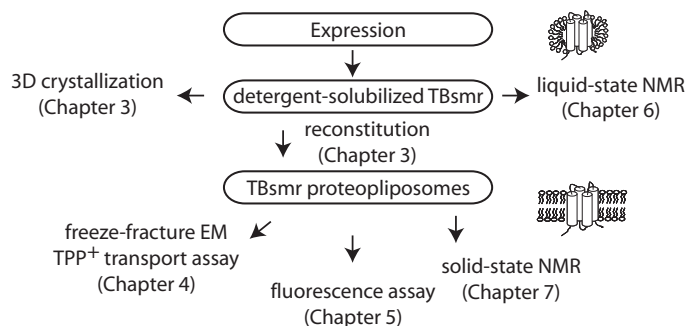


**Figure 1.11:** Biophysical techniques used to study TBsmr.

ration from *E. coli* which yields large amounts of protein usable for crystallization and reconstitution trials is described. TBsmr was reconstituted in a lipid bilayer suitable for further functional and structural studies. The influence of different lipids on the function and oligomerization of TBsmr was studied by freeze-fracture EM and a transport assay to determine the minimal functional unit capable of transport, which is shown in Chapter 4. A novel assay was established to study the transport cycle in more detail (Chapter 5). The functional assay revealed a transport cycle intermediate of the small multidrug resistance proteins by substrate fluorescence. The pH gradient needed for antiport was generated by co-reconstituting TBsmr with bacteriorhodopsin. The findings support a model with a single occluded intermediate state in which the substrate is highly immobile. To identify and characterize residues in the binding site, detergent-solubilized TBsmr was studied by liquid-state NMR but no specific interaction with the substrate EtBr has been found (Chapter 6). Functional protein could be prepared in liposomes. Membrane proteins in a lipid matrix can be investigated by solid-state NMR. In Chapter 7, it is shown how different isotope labeling approaches were applied to improve the spectra necessary for studying the protein by solid-state NMR. Two distinct sets of chemical shifts of the conserved key residue tryptophan-63 could be observed upon substrate binding which indicates a structural asymmetry in the binding pocket of TBsmr.

**Table 1.1:** Putative mycobacterial drug efflux pumps associated with reduced susceptibility to antibacterial agents (Source: De Rossi et al., 2006).

| Name                | Microorganism                                      | Resistance   | Cause of Resistance                                | References              |
|---------------------|--|--|--|-------------------------|
| iniA<br>(Rv0342)    | <i>M. tuberculosis</i>                             | Isoniazid  | Overexpression                                     | Colangeli et al. (2005) |
| <b>ABC</b>          |  |  |  |                         |
| PstB                | <i>M. smegmatis</i>                                | Fluoroquinolones   | Overexpression in a ciprofloxacin-resistant mutant | Bhatt et al. (2000)     |
| DrrAB               | <i>M. tuberculosis</i>                             | TET; ERY, ethambutol, norfloxacin, streptomycin, chloramphenicol, anthracyclines | Multicopy plasmid                                  | Chouhury et al. (2002)  |
| Rv2686c-2687c-2688c | <i>M. tuberculosis</i>                             | Fluoroquinolones   | Multicopy plasmid                                  | Pasca et al. (2004)     |
| <b>MFS</b>          |  |  |  |                         |
| LfrA                | <i>M. smegmatis</i>                                | Fluoroquinolones, EtBr, ACR, CET   | Gene amplification (multicopy plasmid)             | Takiff et al. (1996)    |
| Tet(V)              | <i>M. smegmatis</i>                                | TET  | Multicopy plasmid                                  | De Rossi et al. (1998a) |
| Tap                 | <i>M. tuberculosis</i> ; <i>M. fortuitum</i>       | Aminoglycosides, TET   | Multicopy plasmid                                  | Ainsa et al. (1998)     |
| P55                 | <i>M. bovis</i>                                    | Aminoglycosides, TET   | Multicopy plasmid                                  | Silva et al. (2001)     |
| Rv1634              | <i>M. tuberculosis</i>                             | Fluoroquinolones   | Multicopy plasmid                                  | De Rossi et al. (2002)  |
| Rv1258c             | <i>M. tuberculosis</i> , resistant clinical strain | Rifampicin, ofloxacin  | Overexpression after drug induction                | Siddiqi et al. (2004)   |
| <b>RND</b>          |  |  |  |                         |
| mmpL7               | <i>M. tuberculosis</i>                             | Isoniazid  | Multicopy plasmid                                  | Pasca et al. (2005)     |
| <b>SMR</b>          |  |  |  |                         |
| TBsmr<br>(Rv3065)   | <i>M. tuberculosis</i>                             | TPP <sup>+</sup> ; EtBr; ERY; ACR; safranin O; pyronin Y                         | Multicopy plasmid                                  | De Rossi et al. (1998b) |

ABC, ATP binding cassette; MFS, major facilitator superfamily; RND, resistance-nodulation-cell division; SMR, small multidrug resistance; ACR, acriflavine; CET, cetyltrimethylammonium bromide; ERY, erythromycin; FQs, fluoroquinolones; TET, tetracycline, TPP<sup>+</sup>, tetraphenyl phosphonium

## 2 Materials and Methods

All materials were purchased from Sigma-Aldrich Chemie GmbH (Munich, Germany) unless indicated otherwise.

### 2.1 Prediction methods

The GRAVY (grand average of hydropathicity; Kyte and Doolittle, 1982) score was calculated using the software program ProtParam (<http://www.expasy.org/>). The same software was used to calculate the molecular weight and the extinction coefficient. For a topology model, the transmembrane helices were predicted with TMHMM (Sonnhammer et al., 1998).

### 2.2 Cloning of TBsmr mutants

Mutants of TBsmr were cloned using the Quikchange<sup>®</sup> Site-Directed Mutagenesis Kit (Stratagene, Amsterdam, Netherlands). A forward primer and a reverse primer was used in a two-stage PCR reaction (Wang and Malcolm, 1999). For each primer, a PCR reaction mix (Tab. 2.1) was run for 3 cycles in a thermo cycler. The separate reaction mixtures were combined and run for another 16 cycles. The annealing temperature was kept at 55 °C for 1 min. The polymerase extension reaction was run at 68 °C for 8 min. Following the PCR reaction, the parental DNA template was digested with 1  $\mu$ L Dpn1 for 1 h at 37 °C. The mutated vector DNA was transformed into NEB turbo competent cells (New England Biolabs GmbH, Frankfurt). Positive clones were confirmed by sequencing.

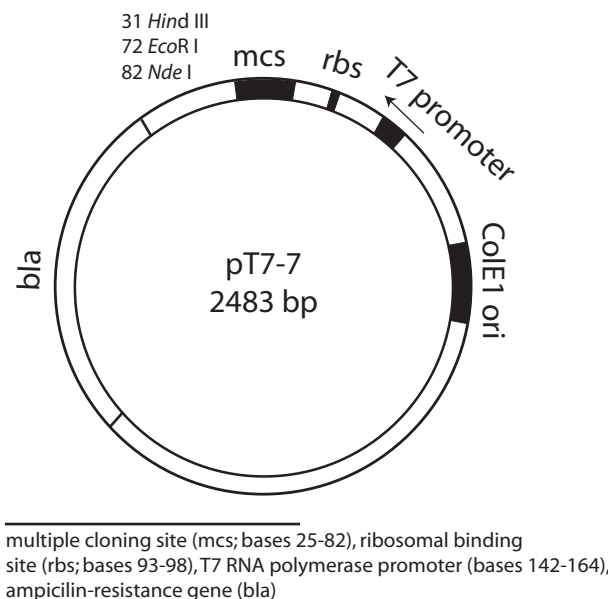
The mutant TBsmr E13A was cloned with the forward primer 5'-GCGATCTTCGCGG-CAGTGGTGGCAACC-3' and the reverse primer 5'-GGTTGCCACCACTGCCGCGA-AGATCGC-3'). The mutant TBsmr W30A was cloned using the the forward primer 5'-GGTTCACCTCGGTTGGCGCCCACGGTGG-3' and the reverse primer 5'-CCACCG-TGGGCGCCAACCGAGTGAACC-3'.

**Table 2.1:** PCR reaction mix

| Reagent                                      | Volume                   |
|--|--------------------------|
| 10x Pfu reaction buffer                      | 2.5 $\mu\text{L}$        |
| ds template DNA [68 ng/ $\mu\text{L}$ ]      | 0.37 $\mu\text{L}$       |
| primer [10 pmol/ $\mu\text{L}$ ]             | 0.5 $\mu\text{L}$        |
| NTP mix [10 mM]                              | 0.5 $\mu\text{L}$        |
| Pfu turbo polymerase [2,5 U/ $\mu\text{L}$ ] | 0.5 $\mu\text{L}$        |
| ddH <sub>2</sub> O                           | fill to 25 $\mu\text{L}$ |

## 2.3 Expression and Purification

The myc/his-tagged pT7-7 TBsmr-wt plasmid (Ninio et al., 2001) was kindly provided by Prof. Shimon Schuldiner (Hebrew University of Jerusalem). TBsmr was cloned into the pT7-7-His vector by removing the *emrE* gene from vector pT7-7-EmrE-His with restriction enzymes *NdeI* and *EcoRI* (Ninio et al., 2001). The plasmid map of the pT7-7 vector is shown in Fig. 2.1. The DNA sequence of the construct is shown in Fig. 2.2.

**Figure 2.1:** Plasmid map of pT7-7 vector

Overexpression and purification of TBsmr were adapted from protocols described by others (Yerushalmi et al., 1995; Ninio et al., 2001). *Escherichia coli* T7 Express (New England Biolabs GmbH, Frankfurt) were grown at 37 °C in the appropriate media, e.g.

Luria-Bertani (LB), defined or minimal media (Tab. A.1 and A.2). Four flasks of 750 mL media containing 100  $\mu\text{g/mL}$  ampicillin in a 2-L flask was inoculated with 15 mL of LB overnight culture. When necessary, the cells were pelleted at a cell density of  $A_{600}=1$  at 3080 g for 5 min and resuspended in a quarter of fresh isotope labeled media 10 min before induction. Expression of TBsmr was induced with 0.5 mM isopropyl  $\beta$ -D-thiogalactoside (IPTG) at a cell density of  $A_{600}=1$ . When applied, rifampicin was added 10 min after induction. Two hours later the cells were harvested by centrifugation (3080 g for 10 min at 4 °C). When heat shock induction was used, TBsmr was grown at 30 °C in *E. coli* TA15 that have previously been transformed with the pGP1-2 plasmid (Tabor and Richardson, 1985). pGP1-2 codes the T7 polymerase under the heat shock promoter  $\lambda P_L$ . For induction, the temperature was shifted rapidly in a water bath to 42 °C for 15 min and than back to 30 °C.

```

atgatctacctatacctcttgtgcgcgatcttcgcggaagtggaggcaaccagcctgctc
M I Y L Y L L C A I F A E V V A T S L L
aaaagcacggaaggggttcaactcgggttggggccacggggctgtctagtggttatggc
K S T E G F T R L W P T V G C L V G Y G
atcgctttcgcgctgctggccttgtcgatctcgcaaggcatgcagacggacgtcgctat
I A F A L L A L S I S H G M Q T D V A Y
gcgctgtggcggcaatcggtacggccgcatgtgctggcgcgactgtttctcggc
A L W S A I G T A A I V L V A V L F L G
tcgccgatatctgtgatgaaggtgggtggcgctggcctgattgtcgctggcgctggtcacg
S P I S V M K V V G V G L I V V G V V T
ttgaacctggcgggtgcccataatcgaaagcttacgtagaacaaaaactcatctcagaa
L N L A G A H E F E A Y V E Q K L I S E
gaggatctgaatagcggcgtcgaccatcatcatcatcatcattga
E D L N S A V D H H H H H H -

```

**Figure 2.2:** DNA and protein sequence of the TBsmr (Rv3065) construct with myc/his-tag.

Cells were resuspended in 5 mL lysis buffer/g wet cells (250 mM sucrose; 150 mM NaCl; 10 mM Tris-Cl pH 7.5; 2.5 mM  $\text{MgSO}_4$ ; and DNase I) and broken twice in a cell disrupter (Constant Systems Ltd., Daventry, England) at 1.5 kbar. The lysate was centrifuged at 4550 g for 10 min to remove cell debris. After centrifuging the supernatant at 223.000g for 30 min, the membrane fraction was resuspended in 15 mM Tris-Cl pH 7.5, 300 mM NaCl and centrifuged again. Then the membrane pellet was collected, frozen in liquid nitrogen and stored in fractions at -80 °C until usage. A fraction of the membrane pellet was solubilized for 40 min at 4 °C in solubilization buffer (15 mM Tris-Cl pH 7.5; 300 mM NaCl; 20 mM imidazole; 1% (w/v) n-dodecyl- $\beta$ -D-maltoside (DDM); and complete protease inhibitor (Roche Diagnostics GmbH, Mannheim, Germany). After centrifugation at 184.000 g for 50 min, the supernatant was mixed with nickel-nitrilotriacetic acid (Ni-NTA) resin (Qiagen, Hilden, Germany) for 80 min at 4 °C. The resin was washed

with buffer (15 mM Tris-Cl pH 7.5; 300 mM NaCl; 20 mM imidazole; and 0.08% DDM (w/v)) until the  $A_{280}$  was below 0.05. The protein was eluted with the same buffer containing 300 mM imidazole (elution buffer) and either reconstituted directly or stored at  $-80\text{ }^{\circ}\text{C}$  until usage. Protein concentration was determined at  $A_{280}$  using the elution buffer as a blank with an extinction coefficient of  $17780\text{ M}^{-1}\text{cm}^{-1}$  at 280 nm.

## Expression of amino acid selectively labeled TBsmr

Amino acid selectively labeled (Muchmore et al., 1989) TBsmr was expressed with the spin down technique (Almeida et al., 2001) and rifampicin (Lee et al., 1995) as described above. The cells were grown in unlabeled, defined media until they reached an optical density of  $A_{600}=1$ , when they were resuspended in  $1/4$  volume of defined media supplemented with 70 mg/L DL-5-fluoro-tryptophan (Fluorochem, Old Glossop, United Kingdom), 60 mg/L L- $^{15}\text{N}$ -leucine (Cambridge Isotope Laboratories (CIL), Andover, USA), 35 mg/L -L-tryptophan (U- $^{13}\text{C}11$ ,U- $^{15}\text{N}2$ , CIL) or 35 mg L-tyrosine ( $^{15}\text{N}$ , CIL) , and the protein expression was induced with IPTG.

## 2.4 Chymotrypsin digestion

Chymotrypsin was used to cleave off the C-terminal myc/his-tag at F109 or Y112. Detergent-solubilized TBsmr was digested with chymotrypsin at a 1:20 (w/w) ratio for 5 h at room temperature (15 mM Tris pH 7.5; 300 mM NaCl; 300 mM imidazole; 0.08% (w/v) DDM; 1 mM  $\text{CaCl}_2$ ). After stopping the reaction with Pefabloc<sup>®</sup> SC protease inhibitor (Roche, Mannheim, Germany), the tag was dialyzed out (Spectra/Por 4; molecular weight cut-off (MWCO): 12k Da; Spectrum Laboratories, Rancho Dominguez, USA) against a 1000x volume (target buffer: e.g. 15 mM Tris pH 7.5; 300 mM NaCl) overnight at  $4\text{ }^{\circ}\text{C}$ .

## 2.5 SDS-PAGE

Sodium dodecylsulfate polyacrylamide gel electrophoresis (SDS-PAGE) under denaturing conditions was carried out using 10% polyacrylamide separating gels according to the method of Schägger (Schägger and von Jagow, 1987). Before loading on a 10% polyacrylamide stacking gel, 10  $\mu\text{L}$  sample (0.1-5 mg/ml) was mixed with an equal volume of loading buffer (4% (w/v) SDS; 12% (w/v) glycerol; 50 mM Tris-Cl pH 6.8; 2% (v/v) mer-

captoethanol; 0.01% (w/v) Serva blue G) and heated for 30 min at 40 °C. The SDS-PAGE was run at constant voltage (150 V per gel ) for 60 min using 1x anode buffer (10x stock buffer: 2 M Tris-Cl pH 8.9) and 1x cathode buffer (5x stock buffer: 0.5 M Tris-Cl pH 6.8, 0.5 M Tricine, 0.5% (w/v) SDS), fixed in 50% (v/v) methanol and 10% (v/v) acetic acid for 30 min at RT and stained with 0.025% Serva blue G in 10% (v/v) acetic acid for 1-2 h. A complete background destaining of the gels was obtained by shaking the gels in 10% acetic acid over night.

**Table 2.2:** Schagger gel components (10%T, 2.7% C)

| Component                     | Stacking gel | Separation gel |
|-------------------------------|--------------|----------------|
| 40% acrylamide                | 0.625 ml     | 2.5 ml         |
| 3 M Tris pH 8.45, 0.3% SDS    | 1.55 ml      | 1.55 ml        |
| glycerol                      |              | 1.06 ml        |
| ddH <sub>2</sub> O            | 4.075        | 3.14 ml        |
| 10% (w/v) ammonium persulfate | 100 $\mu$ l  | 150 $\mu$ l    |
| TEMED                         | 10 $\mu$ l   | 15 $\mu$ l     |

## 2.6 Dot blot

For dot blot analysis, the cells (1 mL at  $A_{600}=1$ ) were solubilized in 20% SDS (w/v) and DNase I. The solution (100  $\mu$ L) was transferred on a nitrocellulose membrane using a Bio-Dot<sup>®</sup> dot blot apparatus from Bio-Rad (Munchen, Germany). The protein was detected with mouse c-myc antibodies (clone 9E10) from Acris (Hiddenhausen, Germany) as described in paragraph 2.7

## 2.7 Western blot

For western blot analysis, the proteins ( $\sim 0.1 \mu$ g) were separated on a 10% Schagger gel and transferred onto a nitrocellulose membrane (Schleicher & Schuell Bioscience, Dassel, Germany) with a Bio-Rad Trans-Blot<sup>®</sup> apparatus for 80 min at 360 mA. The membrane was then blocked for 30 min in blocking buffer: TBS-T (20 mM Tris-Cl; 150 mM NaCl; 0.1% t-octylphenoxypolyethoxyethanol (Triton X-100; w/v)) and 5% skim milk powder (w/v) (Carl Roth, Karlsruhe, Germany). The membrane was immunoblotted with mouse c-myc antibodies (dilution 1:10,000) and horseradish peroxidase-conjugated goat anti-mouse IgG (sc-2005) (diluted 1:5000) from Santa Cruz Biotechnology (Santa Cruz,

USA) as the primary and secondary antibodies, respectively. The membrane was washed three times with TBS-T after blocking and each antibody. The blots were analysed by chemiluminescence in a Lumi-imager F1<sup>TM</sup> (Roche Diagnostics, Mannheim, Germany) with 600  $\mu$ l ECL1 and ECL2 (1:1 ratio).

ECL1 solution was made of 5 mL Tris (1 M) pH 8.5, 0.5 mL luminol (250 mM), 220  $\mu$ l p-cumaric acid and filled to 50 ml with ddH<sub>2</sub>O. ECL2 was made of 5 ml Tris (1 M) pH 8.5, 32  $\mu$ l H<sub>2</sub>O<sub>2</sub> (30% (w/v)) and also filled to 50ml. Both solutions could be stored at 4 °C in the dark up to 7 days. Stock solutions of 250 mM luminol and 90 mM p-cumaric acid in DMSO were stored at -20 °C in the dark.

## 2.8 Mass spectrometry

### MALDI-TOF mass spectrometry

To determine the total mass of the protein, matrix assisted laser desorption/ionization-time of flight (MALDI-TOF) mass spectrometry (MS) spectra were measured by Björn Meyer (Prof. Karas, Institute of Pharmaceutical Chemistry, J. W. Goethe-University Frankfurt) on an Ultraflex TOF-TOF (Bruker Daltonics, Bremen) in linear mode. The protein sample (1:10 diluted) was added to an equal volume (1  $\mu$ L) of matrix buffer (40 mg/ml DHB (2,5-dihydroxy benzoic acid:2-hydroxy-5-methoxy benzoic acid; 10:1; (Tsarbopoulos et al., 1994) in 33% acetonitril, 0.1% trifluoric acid) directly on the MALDI plate and dried in the open air. The MS spectra were processed with the program Flex Analysis v2.2 (Bruker Daltonics, Bremen) and referenced to the internal standard cytochrome c (12361 Da).

### LILBID mass spectrometry

The laser induced liquid bead ion desorption (LILBID) MS spectra were measured by Nina Morgner (Prof. Brutschy, Institute of Physical and Theoretical Chemistry, J. W. Goethe-University Frankfurt) as described by Morgner et al. (2007). TBsmr was dialyzed in a Spectra/Por 4 dialyze bag (12-14 kDa MWCO) for 24 h with salt and detergent free buffer. Micro droplets of the sample with a diameter of 50  $\mu$ m were produced at 10 Hz by a piezo-driven droplet generator and transferred into vacuum by differential pumping stages. The droplets were irradiated by synchronized high-power mid-IR laser pulses of typically 5 ns pulse length. The wavelength was tuned to the absorption maximum of water at around 3  $\mu$ m to excite its stretching vibrations. Above threshold intensity the

radiation induced a rapid transition into the supercritical state followed by the explosion of the droplets. The pre-formed ions in the liquid escaped into the gas phase, where they were analyzed in a TOF reflectron mass spectrometer. For data acquisition and analysis user-written LabVIEW programs were used. The signal-to-noise ratio was improved by subtracting the unstructured background, caused by metastable loss of water and buffer molecules, from the original ion spectra. These difference spectra were smoothed by averaging the signal over multiple experiments, with the smoothing interval always lying within the time resolution of the TOF mass spectrometer.

At low laser intensity (ultra soft mode), LILBID gently desorbs ions out of the liquid enabling detection of the non-covalently assembled membrane protein complexes where the ions still carry an average of 10% of the detergent molecules from their micelle.

## 2.9 Gel filtration

Determination of monodispersity by size-exclusion HPLC was carried out on an ÄKTA purifier<sup>TM</sup> (GE Healthcare, München, Germany). Aggregates were removed by centrifugation (5 min at 16,380g) in a Beckman Allegra X22. Various detergents were added to aliquots of protein in 0.1% DDM, until a final concentration of 0.2% above the cmc was reached for the added detergent. The samples were incubated for 30 min at 25 °C. 50-250 µg of TBsmr (50 µl) sample was loaded on a Superose 12 PC 3.2/30 (GE Healthcare, München, Germany) analytical size exclusion column equilibrated with 15 mM Tris pH 7.5, 50 mM NaCl, 0.1% DDM (w/v) and run at 0.1 ml/min. The presence of protein in the eluent was measured at A<sub>280</sub> and integrated to determine the proportion of monodisperse and aggregated TBsmr. The void volume V<sub>0</sub> was obtained using dextran blue 2000 (2 MDa).

## 2.10 Crystallization

Protein samples were used directly after Ni-NTA purification and concentrated with Vivaspin 4 PES (100 kDa MWCO) concentrators from Satorius (Göttingen, Germany). Imidazole was removed with a HiTrap desalting column (GE Healthcare). Immediately before setting up the crystallization trials, aggregates were removed by ultracentrifugation at 175,000g for 30 min. Protein samples used for crystallization trials contained 5 mg/ml TBsmr in 0.04% DDM (w/v) or 0.1% Fos-12 (w/v) and 15 mM Tris pH 7.5, 150 mM

NaCl, 2.3 mM TPP<sup>+</sup>. Benzamidine was added at a final concentration of 2.4% in the drop to enhance crystallization.

Crystallization trials were performed in cooperation with Gregor Madej (Dr. Lancaster, Department of Molecular Membrane Biology, Max Planck Institute of Biophysics, Frankfurt). The trials were set up at 18 °C by combining protein and reservoir solution at 1:1 - 3:1 ratios with the sitting/hanging drop vapor diffusion technique and a spread matrix of different pH and precipitants (Madej and Lancaster, unpublished results). Drop sizes ranged from 600 nl to 6  $\mu$ l. Submicroliter screens were performed with a crystallization robot in Greiner sitting drop plates (CrystalQuick 96-well standard profile, round bottom). Screens with larger drops were carried out in 24-well plates equipped with micro-bridges (round bottom, 12  $\mu$ l capacity) or boxes with 50  $\mu$ l-capacity bridges. For hanging drops, the protein solution was placed on silanized glass cover slides.

For a detergent screen, TBsmr was purified in DDM and exchanged on the Ni-NTA column to 0.02% (w/v)  $\alpha$ -DDM, 0.09% n-decyl- $\beta$ -D-thiomaltoside (DTM; Anatrace, Maumee, USA), 0.2% (w/v) decyl- $\beta$ -D-maltoside (DM; Glycon), 0.06% (w/v) 6-cyclohexyl-1-hexyl-D-maltoside (cymal-6; Anatrace) or 0.1% (w/v) n-dodecylphosphocholine (Fos-12; Anatrace).

## 2.11 Reconstitution

All lipids were purchased from Avanti Polar Lipids Inc., Alabaster, USA.

### Reconstitution by dialysis

The dialysis reconstitution was performed based on a protocol by Sarika Shastri (Prof. Glaubitz, Institute of Biophysical Chemistry, J. W. Goethe-University Frankfurt). 4 mg of lipids were solubilized in 1 ml of 15 mM Tris-Cl pH 7.5, 50 mM NaCl and 3.75 mg Fos-12. TBsmr in Fos-12 was added to achieve a final mol ratio of 1:100:200 (protein:lipid:detergent). 400  $\mu$ l of Protein-lipid mixture were dialyzed at room temperature in a Spectra/Por 4 dialyze bag (12-14 kDa MWCO) against 1.5 l buffer (15 mM Tris-Cl pH 7.5; 50 mM NaCl; 0.02% (w/v) NaN<sub>3</sub>). The dialysis buffer was exchanged on the third and 6th day and the resulting proteoliposomes pelleted by centrifugation at 150.000g for 30 min on the 13th day. Two parameter were screened: the type of lipid (*E. coli* total lipids and DOPC) and  $\pm$ 20% (v/v) glycerol.

## Rapid dilution reconstitution

Detergent solubilized TBsmr (0.08% DDM (w/v)) was mixed with 3.3x (w/w) DOPC lipids and diluted 11.5 fold in detergent free buffer (15 mM Tris-Cl p 7.5, 150 mM NaCl).

## Reconstitution using biobeads

Reconstitution with polystyrene beads was carried out according to the procedure of Rigaud and Levy (2003). Liposomes of 10 mg of *E. coli* total lipids in 1 mL of 150 mM KCl , 5 mM K-EDTA pH 7.3 were formed by 10 passes through an extruder (Northern Lipids) with a 400 nm filter. The liposomes were destabilized with detergent. The detergents DDM, OG, Fos-12 and Triton X-100 were added at two different detergent-lipid ratios: detergent saturated liposomes on the onset of solubilization ( $R_{sat}$ ) and with total solubilization ( $R_{sol}$ ). The detergent concentration was calculated according to Eq. 2.1:

$$[det] = cmc + R_{sat/sol} \times [lipids] \quad (2.1)$$

R values were taken from the literature when available (Paternostre et al., 1988; Lambert et al., 1998). The appropriate amount of TBsmr in elution buffer was added to the resulting suspension to produce the desired protein-lipid ratio and incubated for 1 h, followed by a fast detergent removal through polystyrene beads. Excess detergent was removed with thirty times the amount of degassed SM-2 biobeads (Bio-Rad, Munich, Germany) in an overnight incubation of at room temperature. The biobeads were then removed.

## 2.12 Density gradients

For analysis, the proteoliposomes were pelleted by centrifugation and layered on a discontinuous 0-10-20-30-40% (w/v) sucrose density gradient and run overnight at 4 °C in a swing bucket rotor (SW28 at 83.000g or SW50.1 at 101.000g) from Beckmann Coulter (Krefeld, Germany). The proteoliposomes were collected for freeze fracture electron microscopy analysis.

## 2.13 TPP<sup>+</sup> transport assay

Proteoliposomes for the TPP<sup>+</sup> assay were prepared according to the Biobeads method at total solubilization. 1 mg of TBsmr was reconstituted in 4 mg/ml *E. coli* total lipids at a 1:25 protein-to-lipid w/w ratio (~1:500 protein-to-lipid molar ratio). After pelleting (180,000g for 30 min) and resuspending the resulting proteoliposomes in 1.5 mL “inside buffer” (15 mM Mops, pH 7; 150 mM NH<sub>4</sub>Cl; 1 mM DTT), they were aliquoted, frozen in liquid nitrogen and stored at -80 °C. Before assaying the activity, the samples were sonicated for 30 s in a Sonorex bath type sonicator (Bandelin, Berlin, Germany).

TPP<sup>+</sup> transport was measured as described previously (Grinius and Goldberg, 1994). The TPP<sup>+</sup> uptake into the proteoliposomes was measured with an ETH 1001 based calcium-selective electrode MI-600 and a Ag/AgCl reference electrode MI-402 from Microelectrodes (Bedford, USA) (Mootha et al., 1996). The TPP<sup>+</sup> transport was initiated by diluting the proteoliposomes (8 μL) in 1 mL “outside buffer” containing 2 μM TPP<sup>+</sup>. The solution in 2 mL Eppendorf cups as the reaction vessel was continuously mixed with a small stirring bar. For the experiments, all buffers were kept at room temperature.

For examining the effect of N,N'-dicyclohexylcarbodiimide (DCCD) on the TPP<sup>+</sup> transport, reconstituted TBsmr was incubated for 30 min at room temperature in a suspension of “inside” buffer containing 0.5 mM DCCD. The proteoliposomes were pelleted for 30 min at 180,000g and resuspended in fresh buffer before the measurement.

The TPP<sup>+</sup> transport rate was measured in a range of concentrations (0.5 - 30 μM TPP<sup>+</sup>).  $K_M$  and  $V_{max}$  values were determined by nonlinear least squares fitting to the following user-defined equation:  $Y = (V_{max} \times S) / (K_M + S)$  using the computer program ORIGIN 7.5 (OriginLab Corporation, Northampton, USA).

## 2.14 Freeze-fracture electron microscopy

The freeze-fracture electron microscopy (EM) micrographs were provided by Dr. W. Haase from the Department of Structural Biology at the MPI of Biophysics, Frankfurt. Proteoliposomes in sample holders were frozen in ethane cooled to -180 °C by liquid nitrogen. Fracturing at -120 °C and replication at a shadowing angle of 45° with platinum/carbon was performed with a BAF 060 freeze-fracturing unit from Bal-Tec Inc. (Principality of Lichtenstein). The fracture images were enlarged from a ×16k – ×25k primary magnification to a final magnification of ×116,800 – ×194,500 and digitized

(1024×1024 pixel). The diameter of the protein particles in the electronic images were measured with the software GIMP ([www.gimp.org](http://www.gimp.org)).

## 2.15 Fluorescence assay

### Bacteriorhodopsin

Bacteriorhodopsin in purple membrane patches was prepared from *Halobacterium salinarium* strain JW5, as described previously (Mason et al., 2005), and kindly provided by Ingrid Weber. Purple membrane was used directly after density gradient purification with three additional washing steps to remove the sucrose (Oesterhelt and Stoeckenius, 1974).

### Reconstitution of TBsmr for fluorescence assay

10 mg of *E. coli* total lipids (Avanti Polar Lipids Inc., Alabaster, USA) were solubilized in 1 mL of 150 mM KCl, 5 mM K-EDTA pH 7.3 and 20 mg/mL n-dodecyl- $\beta$ -D-maltoside (DDM; Glycon, Luckenwalde, Germany). To 0.752 mL of the resulting suspension 0.1 mg of TBsmr, in elution buffer, was added. Elution buffer was used to produce a final sample volume of 2.4 mL. Excess detergent was removed with 250 mg of degassed SM-2 biobeads (Bio-Rad, Munich, Germany) in an overnight incubation at room temperature.

### Fusion of bR with TBsmr-containing liposomes

Bacteriorhodopsin (0.41 mg) was added to 1 mL of the TBsmr-proteoliposomes. The mixture was freeze-thawed 3 times, which results in an ~90% inside-out orientation of bR in the vesicles (Perozo and Hubbell, 1993). If necessary, the sample was stored at -80 °C after the last freezing step. Proteoliposomes were centrifuged at 15000 g, 30 min, 15 °C, and the resulting pellet was resuspended in 1 mL of 150 mM KCl, 5 mM K-EDTA pH 7.3. The sample was sonicated in a water bath for 3 min to form unilamellar vesicles. The sample typically contained final concentrations of 11  $\mu$ M TBsmr, 15.4  $\mu$ M bR and 4.19 mM lipids.

## Fluorescence measurements

All fluorescence measurements were carried out with a Jasco FP 6500 fluorescence spectrometer (Jasco, Groß-Umstadt, Germany). A 1- x 1-cm cuvette was kept at 25 °C by a thermostatic circulating water bath. EtBr measurements were carried out with excitation and emission wavelengths of 545 and 610 nm, respectively. Emission slits were kept constant at 10 nm; excitation slits between 2.5 and 20 nm were used.

In the cuvette, 200  $\mu$ L of the bR/TBsmr proteoliposomes was diluted into 2 mL of 150 mM KCl, 5 mM K-EDTA pH 7.3 and EtBr. The sample was incubated in the dark for 5 min. Illumination at 545 nm excites EtBr and enables bacteriorhodopsin to pump protons. The change in EtBr fluorescence was measured over 200 s. Illumination was switched off and the system left to equilibrate for 5 min. EtBr control experiments without protein (Fig. 5.6) were measured in 150 mM KCl, 5 mM K-EDTA pH 7.3.

For inhibition with TPP<sup>+</sup>, the  $K_i$  was obtained from the IC<sub>50</sub> value using the Cheng-Prusoff equation (Cheng and Prusoff, 1973), where S is the concentration of EtBr and  $K_D$  the binding constant of EtBr to TBsmr:

$$K_i = \frac{IC_{50}}{1 + \frac{S}{K_D}} \quad (2.2)$$

Steady state anisotropy was measured using Melles Griot film polarizer (Bensheim, Germany) on the excitation and emission beam. Correct alignment of the polarizer was confirmed with dilute glycogen, which gave an anisotropy of  $r > 0.97$ . The fluorescence intensities were measured parallel ( $F_{\parallel}$ ) and perpendicular ( $F_{\perp}$ ) to the direction of the vertically polarized excitation light, where  $F_{\perp}$  was corrected for instrument bias by a G-factor of 2.89 at 610 nm. The component intensities of a dye-free blank were subtracted from the component sample intensities to give the net emission intensities. The total anisotropy  $r$  is defined by

$$r = \frac{F_{\parallel} - F_{\perp}}{F_{\parallel} + 2 \times F_{\perp}} \quad (2.3)$$

The anisotropy  $r$  is a superposition of anisotropies of all molecules in the sample. In our case, we have EtBr free in solution and bound to TBsmr. Both contribute differently according to  $r = \Delta f \times \Delta r + f_0 \times r_0$ , where  $f$  and  $\Delta f$  are the fractional fluorescence of EtBr before and during the generation of  $\Delta$ pH ( $\Delta f = \Delta F/F$ ,  $f_0 = F_0/F$ ) and  $r_0$  and  $\Delta r$  are the corresponding anisotropies. To determine the anisotropy of the intermediate  $\Delta r$ , the net emission intensities of the intermediate  $\Delta F$  were used (Eq. 3).  $\Delta F$  was obtained

by subtracting the parallel and perpendicular equilibrium fluorescence intensities ( $F_{\parallel}^0$  and  $F_{\perp}^0$ ) from the corresponding fluorescence  $F$  :

$$r_{\Delta} = (r - f_0 r_0) \times \left( \frac{1}{\Delta f} \right) = \frac{(F_{\parallel} - F_{\parallel}^0) - (F_{\perp} - F_{\perp}^0)}{(F_{\parallel} - F_{\parallel}^0) + 2 \times (F_{\perp} - F_{\perp}^0)} = \frac{\Delta F_{\parallel} - \Delta F_{\perp}}{\Delta F_{\parallel} - \Delta F_{\perp}} \quad (2.4)$$

For each quenching experiment, a fresh 5 M KI stock solution was made, and 0.1 mM  $\text{Na}_2\text{S}_2\text{O}_3$  was added to prevent  $\text{I}_3$  formation. Collision quenching of EtBr in assay buffer with  $\text{I}^-$  was determined as  $F_0/F = 1.2$  for 0.1 M KI using a Stern-Vollmer plot (Fig. 2.3). For the TBsmr/bR quenching experiments, 0.1 M KI was added to the cuvette before equilibrating the sample in the dark.

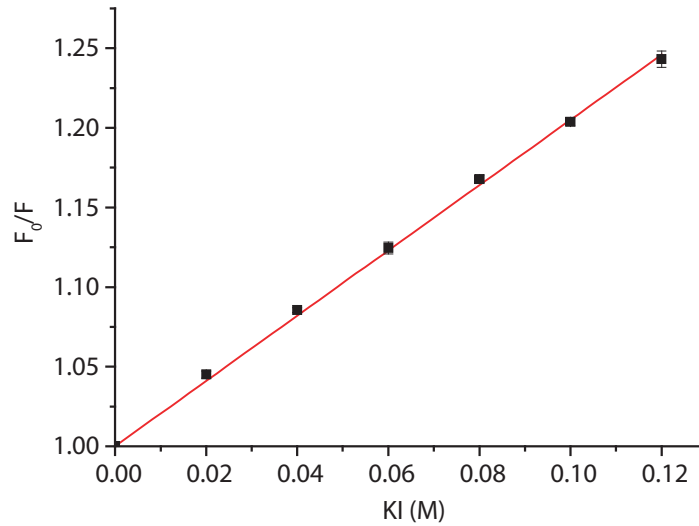


**Figure 2.3:** Stern-Vollmer plot of ethidium bromide. 15  $\mu\text{M}$  EtBr is quenched by increasing concentrations of KI

## 2.16 NMR spectroscopy

### Liquid-state NMR spectroscopy

#### Sample preparation

For liquid-state NMR experiments, uniformly  $^{13}\text{C}$ ,  $^{15}\text{N}$  labeled TBsmr was expressed and purified as described in chapter 2. The detergent was exchanged on the Ni column with 20 column volumes buffer containing 0.1% (w/v) 1-palmitoyl-2-hydroxy-sn-glycero-3-[phospho-RAC-(1-glycerol)] (LPPG). After elution, imidazole was removed by dialysis

(MWCO=12k Da, Spectra/Por 4) two times against buffer without imidazole and detergent overnight at 4 °C. The sample was concentrated at 1000 rcf (Vivaspin 4; MWCO=30k Da) to 0.7-1.2 mM TBsmr in 300  $\mu$ l and supplemented with LPPG in the Shigemi tube. The final sample buffer contained 20 mM Hepes pH 7.5, 100 mM NaCl, 2 mM TCEP (Pierce Biotechnology, Rockford, USA), 5% D<sub>2</sub>O, 10% (w/v) LPPG and 0.15 mM 2,2-dimethyl-2-silapentane-5-sulfonic acid (DSS).

### NMR measurements

Solution-state NMR measurements were carried out on Bruker 700, 800 and 900 MHz spectrometers equipped with cryoprobes. Proton chemical shifts were referenced internally with DSS. Nitrogen and carbon chemical shifts were referenced indirectly to the proton standard using a conversion factor derived from the ratio of the NMR frequencies (Markley et al., 1998).

The following triple resonance NMR experiments were recorded: TROSY-HNCA/TROSY-HN(CO)CA, TROSY-HNCO/TROSY-HN(CA)CO and TROSY-HNCACB (Salzmann et al., 1999). All experiments were run at 303 K. The HNCA spectrum was measured on a 900 MHz Avance spectrometer with 88 complex points in t1, 192 complex points in t2 and 16 scans per increment. The HN(CO)CA spectrum was obtained on an Avance 700 with 56 complex points in t1, 160 complex points in t2 and 32 scans per increment. The HNCO experiment was recorded on a 900 MHz Avance with 72 complex points in t1 (C'), 160 complex points in t2 (NH) and 16 scans per increment. The HN(CA)CO spectrum was acquired on a DRX 800 spectrometer with 64 complex points in t1, 192 complex points in t2 and 32 scans per increment. The HNCACB experiment was measured with 188 complex points in t1, 192 complex points in t2 and 16 scans per increment on a Avance 800. The measurements were set up by Dr. Frank Löhr (Prof. Dötsch, Institute for Biophysical Chemistry, J. W. Goethe-University Frankfurt).

All spectra we processed with Topspin 1.3 (Bruker) and analyzed using CARRA 1.8.5.

## Solid-state NMR spectroscopy

### Sample preparation

TBsmr was reconstituted into 1-palmitoyl-2-oleoyl-*sn*-glycero-3-phosphocholine (POPC; 760.1 g/mol), 1,2-dioleoyl-*sn*-glycero-3-phosphocholine (DOPC; 786.2 g/mol) or *E. coli* total lipids ( $\sim$  770 g/mol) at a protein to lipid mol ratio ranging from 1:33 to 1:100 using

the biobeads reconstitution technique. For substrate binding, the proteoliposomes were incubated with 15 mM EtBr ( $1000 \times K_d$ ; 300  $\mu\text{g}$  in 50  $\mu\text{l}$  volume) for 30 min at RT.

TBsmr proteoliposomes were sedimented in an ultracentrifuge for 30 min at 100.000g. The pellet was transferred into a 4 mm zirconium rotor by centrifugation at 14.000 rpm in a BioFuge pico (Heraeus) for 5 min and sealed with a top insert. For each experiment, the temperature was maintained at a fixed value  $\pm 1$  K between 190 – 280 K using air which was cooled with liquid nitrogen. For experiments carried out below the freezing point, balanced rotors were shock frozen in liquid nitrogen and inserted in a pre-cooled magnet.

### NMR measurements

Well resolved  $^1\text{H}$  solid-state NMR spectra are difficult to obtain because the strong dipolar couplings between protons can approach 100 kHz and are difficult to remove by MAS. As a result of these difficulties, often low- $\gamma$  (gyromagnetic ratio) nuclei (S) such as  $^{13}\text{C}$  or  $^{15}\text{N}$  with weaker dipolar couplings are used. To enhance the signal of these nuclei in a direct polarization experiment (DP), polarization can be transferred from abundant, high- $\gamma$  nuclei such as  $^1\text{H}$  by using a technique called cross polarization (CP) (Pines et al., 1973). The pulse sequences of these two solid-state NMR experiments are shown in Fig. 2.4.

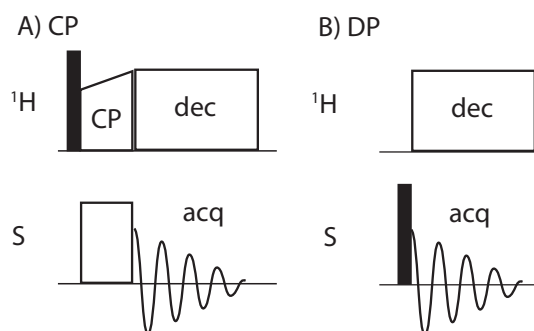


**Figure 2.4:** Pulse sequences of the cross polarization (A) and direct polarization (B) solid-state NMR experiments.

An effective approach to establish a dipolar contact between the different nuclei for CP is the simultaneous irradiation of both nuclei according to Hartmann and Hahn (Hartmann and Hahn, 1962). The maximum signal enhancement for a CP contact period under the Hartmann-Hahn condition is  $\gamma_I/\gamma_S$ . Heteronuclear coupling between the low- $\gamma$  nuclei and protons during the acquisition (acq) can cause a significant broadening of the spectrum. Therefore, an additional  $^1\text{H}$  radio-frequency (rf) pulse is applied to decouple the

protons from the detected spins. The simplest method is a continuous wave (cw) decoupling which rotates the proton nuclear spins and thus averages their magnetic moment and consequently the heteronuclear dipolar coupling to zero (Bloch, 1956).

One-dimensional  $^{15}\text{N}$  CP- and DP-MAS experiments were carried out on a Bruker Avance 400 MHz wide bore spectrometer (Karlsruhe, Germany) with a 4 mm triple resonance probe head. (Bruker). The contact time for ramped cross polarization was set to 1 ms. During acquisition, the protons were decoupled with power levels of 40-75 kHz (TPPM-15, Bennett et al., 1995). The spinning speed  $\nu_R$  was regulated to  $8.000 \pm 3$  Hz. All spectra were referenced externally to ammonium chloride (0 ppm).

$^{19}\text{F}$  solid-state DP NMR experiments were measured on an Avance 600 MHz wide bore spectrometer operating at a  $^{19}\text{F}$  resonance frequency of 564.68 MHz. The rotor was spun at 10-12 kHz in a 4 mm double resonance fluorine MAS probe (Bruker). Trifluoroacetic acid (0 ppm) was used for external referencing.

Solid-state  $^{13}\text{C}$  NMR experiments were recorded on the Avance 400 with a 4 mm triple resonance probe, or on the Avance 600 with a 4 mm triple resonance probe (Bruker). The sample was spun at 10 kHz and SPINAL-64 (Fung et al., 2000) used for proton decoupling. A contact time of 1.1 ms was used for cross polarization. All  $^{13}\text{C}$  NMR spectra were referenced against tetramethyl silane at 0 ppm.

The pulse sequence for a 2D  $^{13}\text{C}$ - $^{13}\text{C}$  Proton Driven Spin Diffusion (PDS) is shown in Fig. 2.5 A (Szeverenyi et al., 1982). After a CP from  $^1\text{H}$  and chemical shift evolution in the indirect dimension, the  $^{13}\text{C}$  magnetization is converted to z-magnetization with a  $90^\circ$  X-pulse. During a delay, the  $^{13}\text{C}$  spins recouple, and the magnetization can diffuse across the carbons. After reconversion to  $^{13}\text{C}$  x/y-magnetization with another  $90^\circ$  X-pulse, the FID is acquired.

The pulse sequence for a 2D  $^{13}\text{C}$ - $^{13}\text{C}$  Dipolar Assisted Rotational Resonance (DARR) is shown in Fig. 2.5 B (Takegoshi et al., 2001). After a CP from  $^1\text{H}$  and chemical shift evolution in the indirect dimension, the  $^{13}\text{C}$  magnetization is converted to z-magnetization with a  $90^\circ$  X-pulse. The polarization transfer between  $^{13}\text{C}$  spins is enhanced by recoupling the  $^{13}\text{C}$ - $^1\text{H}$  dipolar interaction through a weak  $^1\text{H}$  rf irradiation  $\nu_1$  which fulfills the rotary resonance condition  $\nu_1 = n\nu_R$  ( $n = 1$  or  $2$ ). During a delay, the  $^{13}\text{C}$  magnetization can recouple and diffuse across the carbons. After reconversion to  $^{13}\text{C}$  x/y-magnetization with another  $90^\circ$  X-pulse, the FID is acquired.

All spectra we processed and analyzed with Topspin 2.0 (Bruker). The spectra were plotted with CARRA 1.8.3 ([www.nmr.ch](http://www.nmr.ch)).

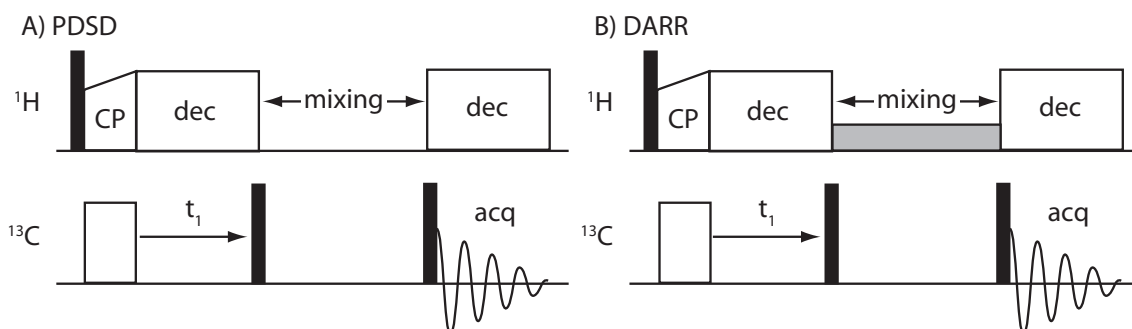


**Figure 2.5:** Pulse sequence for the PDSD (A) and DARR (B) experiments. All sequences begin with CP using a ramped pulse on the  $^1\text{H}$  channel. After the evolution period ( $t_1$ ), the magnetization is oriented along the z-axis with a  $90^\circ$  pulse and mixing occurs longitudinally with either a low power  $^1\text{H}$  recoupling pulse in the DARR experiment, or via  $^1\text{H}$  spin diffusion in the PDSD experiment. During the DARR mixing period, the  $^1\text{H}$  RF field strength is set to the  $n = 1$  rotational resonance condition. For spin diffusion in PDSD experiment, decoupling is turned off to reintroduce heteronuclear coupling. SPINAL-64 decoupling is used during acquisition and evolution.

For chemical shift anisotropy line shape fitting in Topspin 2.0 the Solids Lineshape Analysis tool was used with mixed Gaussian/Lorentzian line shapes.

# 3 Reconstitution and 3D crystallization

## 3.1 Introduction

At the beginning of these studies, an optimized procedure for the preparation of the small multidrug transporter TBsmr for solid-state NMR had to be established. Difficulties lie in the preparation of mg amounts of isotope labeled transporter (Wang et al., 2003) and preparation as microcrystals (Lorch et al., 2005a) or the functional reconstitution into liposomes (Mason et al., 2004).

It has been shown for the  $\alpha$ -helical diacylglycerol kinase (DGK), that 3D crystals of membrane proteins can be used for solid-state NMR (Lorch et al., 2005a). Even if the crystals do not diffract x-rays, they are promising for ssNMR. The advantage of crystals stems mainly from the higher protein concentration that can be achieved and from very well resolved ssNMR spectra which can be obtained under favorable circumstances (Martin and Zilm, 2003). The improvement of the NMR spectra is believed to be caused by a short-range order of the molecules in the crystals, leading to more homogeneous sample.

From the biochemical point of view, solid-state NMR studies on proteoliposomes are the approach of choice as this allows the preparation of functional membrane proteins. Promising NMR spectra were reported of proteoliposomes (Andronesi et al., 2005) and the  $\beta$ -barrel OmpG and the  $\alpha$ -helical proteorhodopsin in 2D crystals (Hiller et al., 2005; Shastri et al., 2007). For proteoliposomes, the difficulty of getting a large quantity of protein into the rotor is compounded by the presence of lipids. However the protein-to-lipid ratio can easily be controlled in detergent mediated reconstitution.

Even though the homologue EmrE, from *E. coli* has been studied for a long time, EmrE and TBsmr may behave differently. Therefore, the existing protocols for SMR proteins (Yerushalmi et al., 1995; Ninio et al., 2001; Curnow et al., 2004; Butler et al., 2004; Winstone et al., 2002) were evaluated with respect to the yield of protein and a high reconsti-

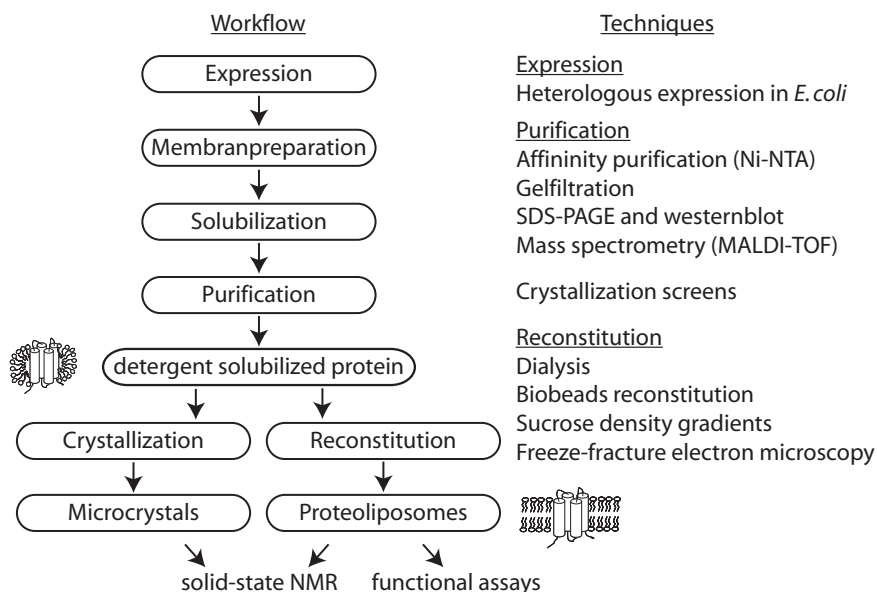


**Figure 3.1:** Schematic flowchart of the TBsmr sample preparation and the techniques used.

tution efficiency at a low protein-to-lipid ratio, while maintaining an active protein. For example, the protocol that worked well for the reconstitution of small quantities of TBsmr into liposomes for radioactive transport assays (Ninio et al., 2001) could not be used, as the requirements for ssNMR with respect to the amount of protein and the protein-to-lipid ratio are much higher.

The aim of the work described in this chapter was to prepare sufficient amounts of TBsmr in the mg range in a state suitable for a further biophysical characterization by solid-state NMR spectroscopy and functional studies. The workflow is shown in Fig. 3.1. For that, every step of the sample preparation as the expression, purification, crystallization and reconstitution was evaluated. It will be shown that high amounts of isotope labeled protein can be obtained and that in case of TBsmr, proteoliposomes are the best sample for solid-state NMR.

## 3.2 Results

### 3.2.1 Expression and Purification

#### Overexpression and labeling in *E. coli*

Even though an expression and purification scheme for TBsmr has been described (Ninio et al., 2001), an improved procedure was sought to obtain mg amount of isotope labeled protein suitable for ssNMR.

Different *E. coli* strains, in which the target gene is transcribed from the vector by the bacteriophage T7 RNA polymerase (Studier and Moffatt, 1986), were evaluated for expression because the bacteria stopped growing upon induction which indicated that TBsmr could be toxic to the host. The expression yields by IPTG induction were compared by dot blot analysis. BI21(DE3)plysS (Moffatt and Studier, 1987) provides a tighter control of the promoter and is used for expression of toxic proteins which inhibit cell growth. The strain C43(DE3) (Miroux and Walker, 1996), which is a double mutant of BL21(DE3), has been tailored to overcome toxic effects of membrane protein associated with overexpression. However, a comparison between BL21(DE3), BL21(DE3)plysS and C43(DE3) showed that TBsmr is expressed best in regular BL21(DE3) (see Fig 3.2). For the expression of isotope labeled protein, T7 Express (New England Biolabs, Frankfurt, Germany), which is a BL21(DE3) strain resistant to T1-phages, was used instead and gave the same yields.



**Figure 3.2:** Dot blot analysis of TBsmr expression yields in different *E. coli* strains. The bacteria were grown at 37 °C and induced with 0.5 mM IPTG. The cells were solubilized in 20% SDS (w/v) and the protein detected with anti-myc antibodies.

Other parameters tested, were the type of induction (heat shock and IPTG), expression media (LB, defined and minimal media), the antibiotic rifampicin and the “spin-down” procedure (Almeida et al., 2001).

Rifampicin is used to reduce the endogenous *E. coli* proteins expression by blocking the bacterial RNA polymerase, but does not affect proteins which are expressed under the T7 promoter. The “spin-down” exploits the fact that *E. coli* can be grown in unlabeled

media to the target cell density and are induced in a reduced volume of fresh isotope labeled media (Almeida et al., 2001). In Luria-Bertani (LB) broth and in defined media, where all amino acids were added individually, yields close to 1 mg per liter were obtained, comparable to published values (Winstone et al., 2002). There was no difference in expression between IPTG and heat shock induction. Therefore, the heat shock induction (TA15) was used for the production of large quantities of unlabeled protein in a fermentor, while T7 Express cells in flasks with an IPTG induction were used for the expression of labeled protein. When 100  $\mu\text{g/ml}$  rifampicin was added after induction, a seven fold increase in protein expression was observed. An additional “spin-down” step was added to the expression protocol to optimize the yield of protein per liter of isotope labeled medium further. Resuspending the bacteria in a four fold smaller medium did not affect the protein yield and thus quadrupled the yield per liter of labeled medium. Similar yields of ca. 23 mg per liter were also obtained in minimal media necessary for uniform  $^{15}\text{N}/^{13}\text{C}$  labeling. The data is summarized in table 3.1.

**Table 3.1:** Expression screen of TBsmr for optimum expression conditions: e.g. different media and induction techniques were tested. The best yield per labeled medium was obtained when the "spin down" was combined with the addition of rifampicin.

| Medium  | Conditions                     | Yield [mg/L] | Stdv |
|---------|--------------------------------|--------------|------|
| LB      | heat shock induction (HS)      | 0.67         | 0.06 |
| defined | HS                             | 0.63         | 0.04 |
| defined | rifampicin, HS                 | 5            | 0.7  |
| defined | rifampicin, 4x spin down, HS   | 24           | 4    |
| defined | rifampicin, 4x spin down, IPTG | 23           | 6    |
| minimal | rifampicin, 4x spin down, IPTG | 23           |      |

## Purification

TBsmr was purified essentially as described by others (Ninio et al., 2001). However, modifications to the protocol were made to improve the purity while maintaining a high yield. As demonstrated by SDS-PAGE and western blot analysis, TBsmr was obtained at a high purity after a single affinity column. Typical SDS-PAGE and western blots of TBsmr are shown in Fig. 3.3. After Ni-NTA metal affinity purification, TBsmr (14.3 kDa) can be seen as a major band of the monomer around 15 kDa with additional distinct and smeared bands at higher molecular weights (Fig. 3.3 lane a). The additional bands could be identified as higher oligomers of TBsmr because they were also detected by western

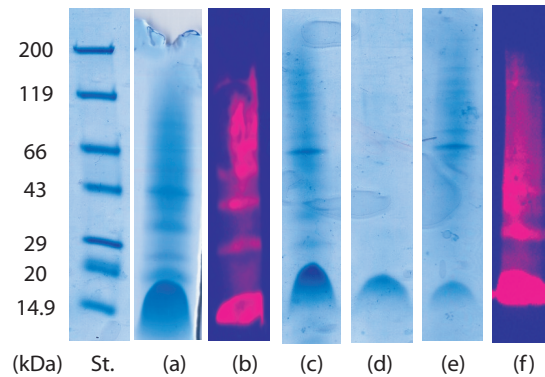


**Figure 3.3:** SDS-PAGE and western blot of TBsmr. The purity of TBsmr after different purification steps was evaluated by SDS-PAGE and western blot analysis. After Ni-NTA purification, a number of impurities could be seen on SDS-PAGE (lane a) besides monomeric TBsmr at 15kDa. Protein impurities were difficult to identify because TBsmr also showed additional bands on a western blot (lane b). Compared to the Ni-NTA purification (lane c), an additional size exclusion column (lane d) did not change the purity because the separated fraction in the void volume was also TBsmr (lane e, f).

blot with the specific anti-myc antibody (Fig. 3.3 lane b). Small changes in the apparent molecular weight were caused by different amounts of loaded protein.

Polypropylene columns (Qiagen, Germany) were used for the Ni affinity purification because higher protein yields were obtained and less buffer with detergents needed compared to an Äkta chromatography system. The salt concentration of the buffer for the Ni column was increased to 300 mM NaCl to suppress non-specific ionic interactions. Also, an additional mild wash step of the membrane fraction with Tris buffer was introduced to remove soluble and membrane anchored proteins (Schluesener et al., 2005).

An additional purification step by size exclusion chromatography gave a single, monodisperse peak in the detergent Fos-12 (Fig. 3.5). In the detergent DDM, an additional small peak in the void volume could be identified as aggregated TBsmr by SDS-PAGE and a western blot (Fig. 3.3 lane e, f). As expected for a single elution peak, no changes could be observed by SDS-PAGE (Fig. 3.3 lane d) besides a more dilute sample. Taken together, the gel filtration data agree with a pure protein preparation.

Because of the odd running behavior of TBsmr on gels, mass spectrometry, as an independent method, was carried out to verify the purity (Fig. 3.4). Singly (7174.4 Da) and doubly protonated (14,345.7 Da) ions of TBsmr can be seen in the resulting MALDI-TOF spectra (Karas and Hillenkamp, 1988) with a mass accuracy of 1-5 Da relative to the calculated mass of 14,344.9 Da. TBsmr (14317.67 Da) is shifted by a bound sodium (22.9 Da) and five  $^{15}\text{N}$  labeled tyrosines (5 Da). The spectra was referenced internally to cytochrome c (12361 Da). The correct molecular weight confirmed that TBsmr was

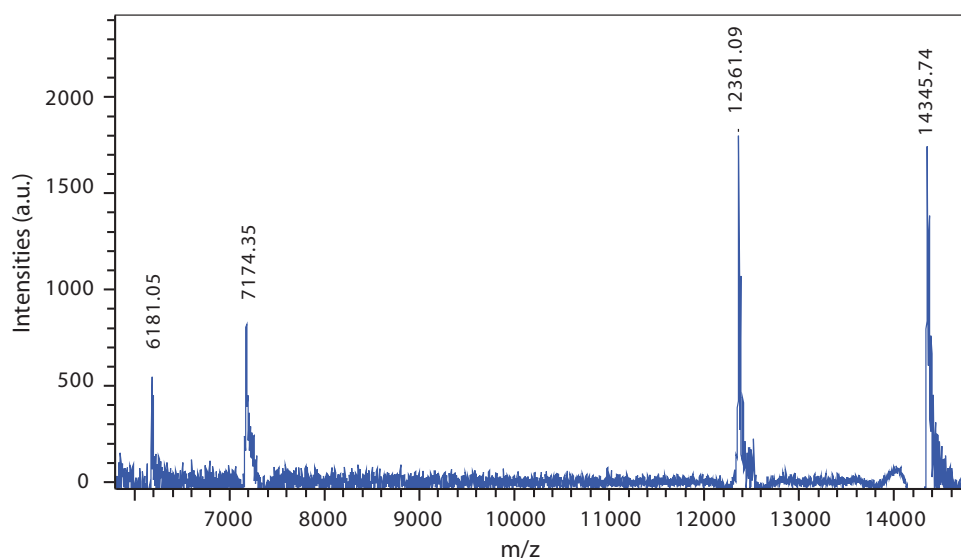


**Figure 3.4:** Mass spectrometry MALDI-TOF spectrum of purified TBsmr. Spectra obtained are consistent with doubly (7174.4 Da) and singly protonated (14,345.7 Da) ions of TBsmr and demonstrate a mass accuracy of 1-5 Da relative to the calculated mass of 14,344.9 Da. The spectrum was measured by Björn Meyer (Prof. Karas, Institute of Pharmaceutical Chemistry, J. W. Goethe-University).

expressed correctly and was not degraded by proteolytic activity.

In addition to SDS PAGE, mass spectrometry is a very sensitive tool to assess contamination with soluble proteins. However, membrane proteins are more difficult to detect by MS for two reasons: Firstly, hydrophobic membrane proteins are often underrepresented in MS proteomics approaches simply because they were not extracted from the membrane (Molloy et al., 1999) or were lost during an isoelectric focusing step (Klein et al., 2005). This is not a problem for a purified protein because it is present after all purification steps. Secondly, the high amount of detergents interfere with the measurements. This problem could be circumvented by a ten-fold dilution of the sample (0.08% DDM) in water before the measurements. The absence of other peaks in the spectrum supports a pure protein preparation.

### 3.2.2 Monodispersity and stability in different detergents

Monodispersity and stability of TBsmr protein in various detergent solutions were characterized according to a protocol from the literature (Boulter and Wang, 2001) by analytical gel filtration. The purpose of this study was identify detergents suitable for maintaining the protein in a monodisperse state for crystallization and reconstitution. Detergent puri-

fied TBsmr in 0.1% DDM was incubated for 2 h at 25 °C in the presence of the different detergents (0.7% octyl glucoside (OG) (w/v), 0.35% Triton X-100 (v/v), 0.25% (Fos-12 (w/v)) and analyzed by gel filtration. The detergent concentrations were chosen to be  $\sim 0.2\%$  higher than the cmc. (Fig. 3.5). The detergent Fos-12 was able to keep the protein monodisperse, whereas TBsmr was denatured by OG and aggregated rapidly. The monodispersity in different detergents was in the order: Fos-12 > DDM > Triton X-100 > OG. In addition, TBsmr in 0.1 % Fos-12 was stable over a period of two weeks at 4 °C (Fig. 3.6). The protein was also able to tolerate cycles of freezing and thawing in DDM and Fos-12.

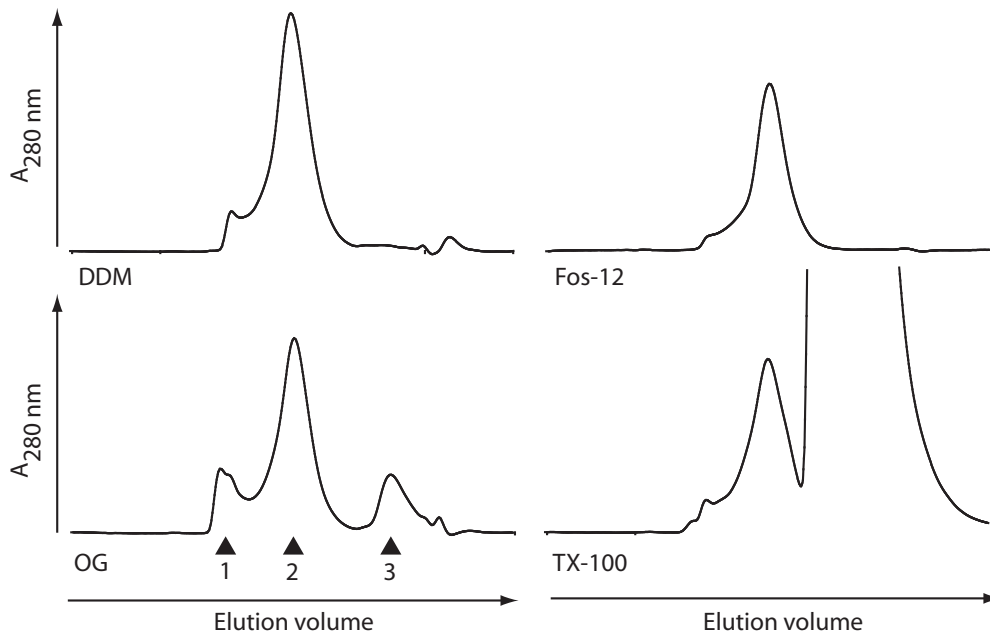


**Figure 3.5:** Monodispersity of TBsmr in different detergents assessed by gel filtration. The void volume of the column (1), the stable protein peak at 1.2 ml (2) and empty detergent micelles (3) are labeled. All samples were incubated with detergent for 2 h at 25 °C before the HPLC analysis.

### 3.2.3 Crystallization

The crystallization screens were performed in co-operation with G. Madej (Dr. Lancaster, Department of Molecular Membrane Biology, Max Planck Institute of Biophysics, Frankfurt). In an initial crystallization attempt, conditions for crystal growth were screened with the sitting drop vapor diffusion technique and a spread matrix of different pH and precipitants (Madej and Lancaster, unpublished results). However, acidic conditions were not

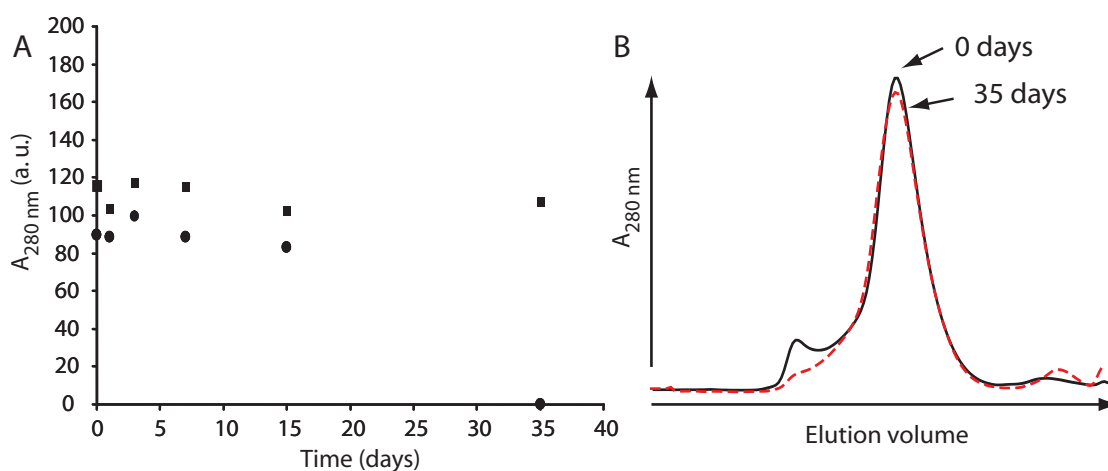


**Figure 3.6:** Long term stability of TBsmr in Fos-12 determined by gelfiltration. A) The protein samples were incubated in 15mM Tris, pH 7.5, 0.1% Fos-12, 50 mM NaCl (squares) and 500 mM NaCl (circles) at 4°C and analyzed by HPLC. B) Elution profiles of TBsmr in low salt buffer after 0 (filled black line) and 35 days (dashed red line).

optimal and further crystallization screening were limited to a basic pH (7 - 10) which also avoids proton mediated TBsmr-substrate dissociation when a substrate is added.

In further screens with the sitting/hanging drop vapor diffusion technique, the additive glycerol (10-25%) was included because it has been shown to enhance membrane protein solubility in numerous cases (Wang et al., 2003). In addition, an ultracentrifugation cycle was performed on the protein sample directly before setting up the crystallisation trials to make the sample more homogeneous and remove undesired protein aggregates (Horsefield et al., 2003) but did not lead to a particular improvement. From the substances tested (EtBr, TPP<sup>+</sup> and ciprofloxacin), co-crystallization in the presence of the substrate TPP<sup>+</sup> was found to be beneficial (Fig. 3.7 C). However, the crystallization trials in DDM yielded mainly detergent crystals (Fig. 3.7 A) and no x-ray diffraction could not be obtained from a promising crystal (Fig. 3.7 B) because it was destroyed in the measurement process. Improvements were found when the detergent DDM was exchanged to other detergents ( $\alpha$ -DDM, DDM, DM, cymal-6 and Fos-12). In the detergent screens, a large number of small, homogeneous crystals without aggregates were obtained with the detergent Fos-12 (Fig. 3.7 D). These microcrystals were identified as protein by SDS-PAGE and western blot (Fig. 3.7 E).

A solid-state NMR spectrum of <sup>15</sup>N isotope labeled microcrystals of TBsmr prepared under those conditions was recorded to compare the resolution of the NMR spectrum of the microcrystals to reconstituted TBsmr in proteoliposomes (Fig. 3.8). However,

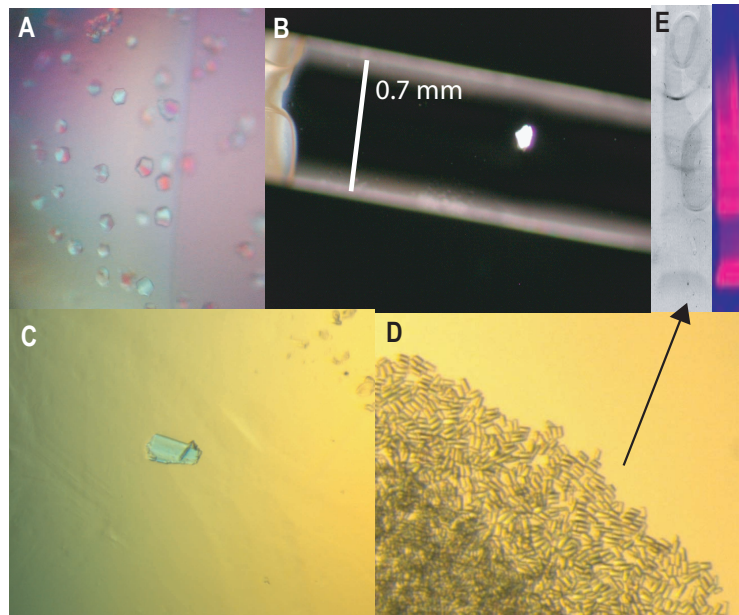


**Figure 3.7:** Crystals of TBsmr. A) DDM detergent crystals. B) crystal mounted in a capillary; 0.02% DDM; 2.1M  $(\text{NH}_4)_2\text{SO}_4$ ; 100 mM Tris pH 9; 25% glycerol; 2.4% benzamidine; 1.5% DMF. C) 0.02% DDM; 2.1 M  $(\text{NH}_4)_2\text{SO}_4$ ; 100 mM Tris pH 9; 25% (v/v) glycerol; 2.4% (w/v) benzamidine; 0.2 mM TPP<sup>+</sup>. D) 0.1% Fos-12; 20% (v/v) PEE 797; 1 M  $(\text{NH}_4)_2\text{SO}_4$ ; 100 mM Tris pH 9; 2.4% (w/v) benzamidine; 1% (v/v) DMF. E) SDS-PAGE and western blot of washed protein crystals.

since the crystallization was not quantitative and most of the protein remained in the supernatant, the signal-to-noise of the spectrum was very low and the spectrum had to be recorded at a very low temperature of 203 K to obtain a signal at all. Compared to a spectrum of proteoliposomes at 263 K, the microcrystals did not show to an improved resolution.

### 3.2.4 Reconstitution into lipid vesicles

#### Dialysis

Reconstitution can be achieved by removing the detergent through dialysis. However, it has been shown that the rate of detergent removal by dialysis relies on the relative cmc of the detergent, with a more rapid removal for a higher cmc (Allen et al., 1980). Depending on the cmc, dialysis expose the protein to the detergent for long time periods, which can be deleterious. Even though OG has a cmc of 0.5% (w/v), it was not tested because it denatured TBsmr (Fig. 3.5). Therefore dialysis reconstitution was attempted with Fos-12 in which TBsmr is extremely stable and homogeneous.

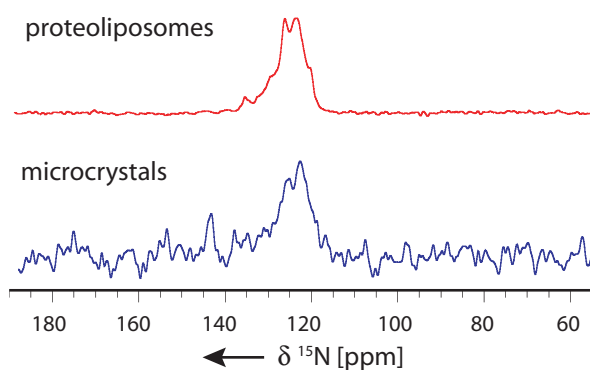


**Figure 3.8:**  $^{15}\text{N}$  CPMAS NMR spectrum of leucine labeled TBsmr (19 residues) microcrystals and proteoliposomes (Proteoliposomes: 263 K, 30k scans; Microcrystals: 203 K, 66k scans).

Successful reconstitution was monitored using discontinuous density gradient centrifugation to separate empty liposomes and proteoliposomes with different protein-to-lipid ratios as shown in Fig. 3.9 C (Chi-Rosso and Toole, 1987). Further characterization of proteoliposomes was achieved by freeze-fracture electron microscopy to assess sample homogeneity and protein aggregation (Viitanen et al., 1986). However, freeze fracture electron microscopy revealed little to no incorporation of protein (similar to Fig. 3.9 B). The failure seems to be caused by the detergent and not the technique, as the reconstitution with Fos-12 also failed when polystyrene beads were used.

### Dilution

Another procedure for obtaining proteoliposomes from micellar solutions consists of diluting the reconstitution mixture. Dilution lowers the detergent below its cmc and the protein proteoliposomes form spontaneously. While this method has been successfully employed for EmrE in OG (Yerushalmi et al., 2001) and DDM (Curnow et al., 2004), OG cannot be used for TBsmr as it denatures the protein. When TBsmr was reconstituted from DDM by dilution, little or no incorporation of TBsmr was found by freeze-fracture electron microscopy and sucrose density gradient centrifugation.

### Adsorption on polystyrene beads

Successful reconstitution of TBsmr was achieved by adsorption of detergent on polystyrene beads (biobeads) following the procedure developed by Rigaud et al. for membrane protein reconstitution (Levy et al., 1990). This method works also for detergents with low

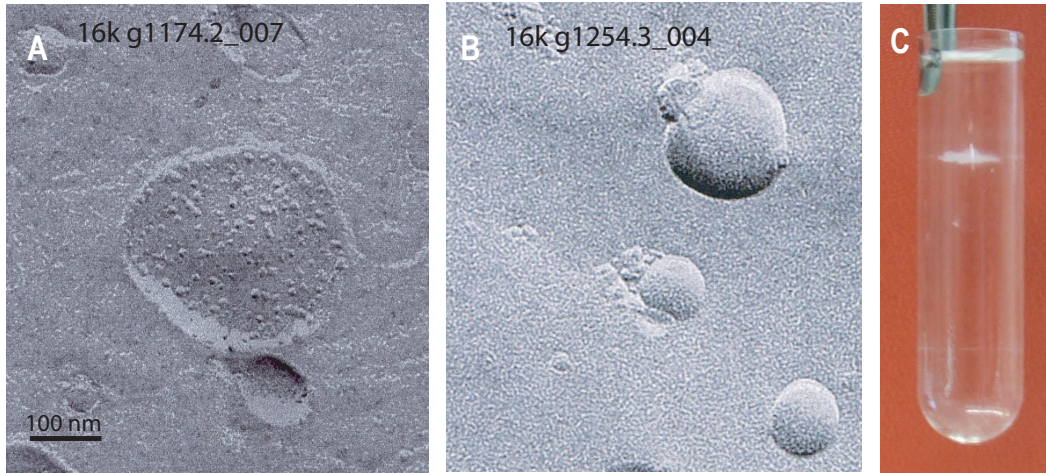


**Figure 3.9:** Freeze fracture electron micrographs of reconstituted TBsmr. TBsmr was reconstituted in *E. coli* total lipids (1:50 mol ratio) from total solubilization in DDM (2:1 detergent-lipid weight ratio) (A) and into *E. coli* total lipids (1:100 mol ratio) from total solubilization in Fos-12 (2:1 detergent-lipid weight ratio) (B). Sucrose density gradient of a successful reconstitution of TBsmr yields a single band (C). Freeze fracture electron microscopy was done by Dr. W. Haase (MPI of Biophysics, Frankfurt).

cmcs which are not readily removed by dialysis or rapid dilution. TBsmr was reconstituted with the batch procedure where the amount of added polystyrene beads can be controlled easily. The detergents DDM, OG, Fos-12 and Triton X-100 were tested at two different detergent-lipid ratios: detergent saturated liposomes on the onset of solubilization ( $R_{sat}$ ) and with total solubilization ( $R_{sol}$ ) followed by a fast detergent removal through the addition of polystyrene beads. The liposomes were saturated at weight ratios of 0.69, 0.3 and 0.5, whereas solubilization occurred at 1.2, 1, 1 with DDM, Triton X-100 and OG, respectively (Lambert et al., 1998; Paternostre et al., 1988). Turbidity measurement at  $A_{400}$  allowed the determination of  $R_{sol}=1$  (w/w) for Fos-12. Since the onset of solubilization could not be determined, it was estimated to be approximately half of  $R_{sol}$ .

The reconstitution efficiencies judged by sucrose density gradients are summarized in table 3.2. Homogeneity and quantity define the quality of a reconstitution. (i) Proteoliposomes of a homogeneous reconstitution will run at the same depth on the gradient and appear as one population. The more bands with proteoliposomes appear on the gradient, the more inhomogeneous the reconstitution. (ii) The sucrose percentage where the band appears is correlated to the reconstitution efficiency. The more protein is reconstituted successfully, the higher the sucrose percentage.

The results of the density gradients had to be validated by freeze-fracture electron microscopy because reconstituted protein and protein aggregated on the surface of the lipo-

**Table 3.2:** Detergent reconstitution screen: The effect of different detergents on reconstitution efficiencies were evaluated by sucrose density gradients and freeze fracture electron microscopy. Conditions that appear only as a single band on a gradient are marked (+), multiple bands (-). Protein insertion was analyzed by EM: good incorporation (+); inhomogeneous, sparse incorporation (0); or no incorporation (-). *E. coli* total lipids were used at a lipid-to-protein molar ratio of 100/1.  $R_{sat}$  and  $R_{sol}$  correspond the the onset of solubilization and total solubilization, respectively

| Detergent    | Detergent/lipid ratio (w/w) | Homogeneity | Incorporation |
|--------------|-----------------------------|-------------|---------------|
| DDM          | 0.69/1 ( $R_{sat}$ )        | -           | +             |
| DDM          | 1.1/1 ( $R_{sol}$ )         | +           | +             |
| Triton X-100 | 0.3/1 ( $R_{sat}$ )         | -           | 0             |
| Triton X-100 | 1/1 ( $R_{sol}$ )           | +           | 0             |
| OG           | 0.5/1 ( $R_{sat}$ )         | +           | 0             |
| OG           | 1/1 ( $R_{sol}$ )           | +           | 0             |
| Fos-12       | 0.5/1                       | -           | -             |
| Fos-12       | 2/1 ( $R_{sol}$ )           | +           | -             |

somes cannot be discriminated on a density gradient and can lead to false positives. While the reconstitution with Fos-12 looked very promising on density gradients, no incorporation was found in freeze-fracture micrographs (Fig 3.9 B). The best reconstitution result was obtained with *E. coli* total lipids solubilized totally in DDM (Fig 3.9 A).

### 3.3 Discussion

#### Expression and purification

The small multidrug resistance protein TBsmr from *M. tuberculosis* was successfully overexpressed in *E. coli* in high yields necessary for ssNMR. Overexpression and purification of TBsmr were adapted from protocols described by others (Ninio et al., 2001; Yerushalmi et al., 1995; Curnow et al., 2004) and improved to yield ~20 mg isotope labeled protein per liter of labeled medium.

While most parameter like the strain, the type of media, the type of induction and the expression time had little influence on the obtained yield (Fig. 3.2 and Tab. 3.1 ), two methods proved to be critical: the action of the antibiotic rifampicin (Lee et al., 1995; Arkin et al., 1996) and the spin down technique (Almeida et al., 2001). By combining the two methods, the yields were increased roughly twenty fold (see Tab. 3.1 ) compared to the normal expression of 1 mg/L for SMR proteins (Winstone et al., 2002). The optimized expression allows e.g. cost efficient uniform  $^{13}\text{C}$  labeling. The strong increase in

expression when rifampicin was used can be explained by the suppression of native protein expression and a decreased TBsmr degradation during the short induction time of two hours. On the other hand, the same explanation would be true for other SMR proteins like EmrE and Hsmr, where this dramatic increase was not observed. An alternative explanation would be that rifampicin is a substrate for TBsmr and thus a strong overexpression is favorable when the bacteria are grown in the presence of the antibiotic. However, it was found the TBsmr does not confer resistance to it when it is overexpressed in *M. smegmatis* (De Rossi et al., 1998b), nor is rifampicin a substrate for other SMR proteins like *M. smegmatis* SMR (Li et al., 2004). While the cause for the high overexpression with rifampicin remains elusive, the yields were highly reproducible.

The aim for the TBsmr purification was to achieve a high purity without losing too much of the isotope labeled sample. TBsmr preparations with a single Ni-NTA column contained no protein contamination as judged by SDS-PAGE, MALDI-TOF mass spectrometry and gel filtration (Fig. 3.3, 3.4 and 3.5). The established expression and purification protocol provides an ideal situation for biochemical and biophysical characterization of TBsmr.

The smeared bands on the SDS-PAGE and western blot gels could be due to aggregates, an oligomeric equilibrium or a lipid halo around the protein. Aggregates can be excluded because they do not enter polyacrylamide gels. While lipids could be co-purified, they cannot explain an almost ten-fold increase in molecular weight observed on the gels. The multiple distinct bands are due to dimers, trimers, tetramers and higher oligomers. Therefore, the smear between those bands suggests that there is dynamic exchange between the TBsmr oligomers during the SDS-PAGE run. These exchanging oligomers have also been observed by other groups (Ninio et al., 2001) and seem to be an intrinsic property of TBsmr.

While Hsmr shows a similar oligomeric pattern on a SDS-PAGE gel, EmrE often runs as a single band. The GRAVY score predicted for the whole *E. coli* proteome ranges from -2 to +2 (Wilkins et al., 1998), where a positive value corresponds to a more hydrophobic protein. The resistance of the TBsmr oligomers to SDS denaturing correlates with a higher hydrophobicity of TBsmr with a GRAVY score of 0.885 / 1.436 with and without tag compared to EmrE (0.617 / 1.048), and must be due to a stronger interaction between the monomers.

## Sample preparation for ssNMR

To prepare a sample for solid-state NMR some considerations with respect to the advantages and limitations of the method have to be taken into account. A great advantage that ssNMR has over other means of studying membrane proteins is, that it is compatible with a number of “solid” states such as protein frozen in detergent, proteoliposomes or protein crystals. However, observing the protein itself requires a sufficient amount of isotope-labeled ( $^{15}\text{N}$ ,  $^2\text{H}$ ,  $^{13}\text{C}$ ,  $^{19}\text{F}$ ) membrane protein. For example, to acquire a good quality 1D  $^{15}\text{N}$  spectrum during an overnight measurement requires more than  $0.2\ \mu\text{mol}$  of protein. 2D experiments demand even greater quantities in excess of  $1\ \mu\text{mol}$ . Given that the active volume of a standard ssNMR MAS (magic angle sample spinning) rotor with a 4 mm diameter is in the order of  $50\text{--}70\ \mu\text{l}$ , the protein concentration must be in the order of  $3\text{--}20\ \text{mM}$ , which means that  $2\text{--}10\ \text{mg}$  of a small  $12\ \text{kDa}$  membrane protein such as TBsmr has to fit into a MAS rotor. To overcome this concentration problem, the protein could be prepared more efficiently in the form of 3D crystals or reconstituted as proteoliposomes. Both approaches were evaluated for reliability and efficiency.

### Crystallization

It has been shown for  $\alpha$ -helical DGK that three-dimensional crystals (Lorch et al., 2005a) of membrane proteins can be used for ssNMR. Since large amounts of protein could be made, crystallization screens were initiated. Initial screens were hampered by the use of DDM where detergent crystals formed and protein was lost due to aggregation. The conditions and detergent N-nonyl- $\beta$ -D-glucoside used to crystallize EmrE (Ma and Chang, 2004; Pornillos et al., 2005) were not considered because the structures were at odds with biochemical data and later were retracted due to a software fault (Chang et al., 2006). Therefore the protein stability was screened in different detergents via gel filtration (Fig. 3.5) following the procedure of Auer et al. (2001). TBsmr was found to be monodisperse and highly stable in the detergent Fos-12. This improvement yielded small, homogeneous protein crystals (Fig. 3.7) without aggregates. The fact that protein crystals were obtained is a further indication of the homogeneity and purity of the sample preparation. However, since the crystallization conditions were difficult to reproduce and not quantitative, the reconstitution proved to be the more promising method to prepare a sample of TBsmr for ssNMR. In addition, no improved resolution of the NMR spectra could be obtained with TBsmr microcrystals compared to proteoliposomes (Fig. 3.8).

## Reconstitution

TBsmr was reconstituted using detergent based methods since it was extracted and purified through the use of detergents. Two important parameters were found for the reconstitution efficiency: the choice of the technique and detergent. A high protein stability in detergent solution is necessary for many applications such as crystallography and liquid-state NMR but also for the dialysis reconstitution. TBsmr was very stable in Fos-12 over 4 weeks (Fig. 3.6) but unfortunately the best detergent for long term stability did not lead to a successful reconstitution neither by dialysis nor with polystyrene beads. The detergent-protein interaction seems to be much stronger than the lipid-protein interaction, which leads to two independent mechanisms, one for the vesicle formation and one for the protein incorporation (Levy et al., 1992). When the liposomes have formed, the detergent Fos-12 is unable to incorporate the protein, leading to empty vesicles and aggregated protein on the surface of the liposomes. The results of the density gradient indicated a successful reconstitution while only the freeze fracture electron microscopy revealed the failure of incorporation (Fig. 3.9).

Since the type of detergent is critical for the reconstitution of membrane proteins, different detergents were tested. DDM was chosen as it is a mild detergent used to purify TBsmr and because it has been shown to be compatible with the biobeads method (Lambert et al., 1998). Its disadvantages are that it is difficult to remove completely, causing leaky liposomes (Fang et al., 1999), and forms large multi-lamellar vesicles upon slow removal (Lambert et al., 1998). OG has been used to reconstitute EmrE (Yerushalmi et al., 2001) and was also employed for TBsmr (Ninio et al., 2001). Even though OG seems to denature TBsmr (Fig. 3.5), OG has a high cmc and can be removed quickly by biobeads (Knol et al., 1996) and therefore could work for reconstitution. While Triton X-100 is not optimal for reconstitution by dialysis because of its low cmc, it has been employed successfully for a number of proteins like LacS (Knol et al., 1996) and bacteriorhodopsin (bR; Levy et al., 1990).

From the three techniques tested, dialysis, rapid dilution and detergent adsorption on polystyrene beads, only the biobeads method was successful. Some incorporation was obtained with all three detergents at  $R_{sat}$  and  $R_{sol}$  but total solubilization of the lipids consistently gave better results (Fig. 3.2). This indicates that the mechanism of reconstitution follows a micellar - lamellar phase transition where lipid and protein micelles are depleted simultaneously and the protein participates in the vesicle formation process (Lambert et al., 1998). Therefore a reconstitution by rapid dilution of TBsmr into a so-

lution containing preformed liposomes should not work and did not as predicted. The best results were obtained by a DDM mediated reconstitution at  $R_{sol}$ , which consistently gave the most homogeneous incorporation as judged by density gradients centrifugation and freeze-fracture EM. The reconstitution of TBsmr using polystyrene beads proved to be a robust technique which worked successfully, independently of the protein - lipid mol ratios up to of 1:50 (Tab. 4.2).

A comparison of crystallization and reconstitution of TBsmr clearly showed the latter technique to be superior when no specific conditions for either approach exists. The reconstitution trials were faster, needed less protein and were easier to set up. The key advantage was that the protein does not have to be stable in a specific detergent to be reconstituted. Therefore, even though stability problems and the tendency of TBsmr to aggregate in DDM when concentrated prevented crystallization, TBsmr could be reconstituted successfully from that detergent.

### 3.4 Conclusion

It was shown that TBsmr can be purified in high amounts, providing an optimal situation for further biochemical and biophysical experiments. The expression yields of TBsmr could be improved twenty fold with respect to the amount of isotope labeled media which allowed multi-dimensional solid-state NMR experiments. Even though the 3D crystallization was not successful, it was found that TBsmr can be reconstituted in proteoliposomes independently of protein-lipid ratio which enabled further structural and functional studies of TBsmr in a native-like membrane environment.

# 4 Lipids influence the oligomerization and function of TBsmr: EM and TPP<sup>+</sup> transport study

## 4.1 Introduction

Based on the successful reconstitution of the mycobacterial membrane protein TBsmr into *E. coli* lipid vesicles, two important questions had to be asked: Is the protein functional, and does the choice of lipids influence the function of TBsmr? Initial freeze-fracture EM data showed that the type of lipid influences the particle size of reconstituted TBsmr, which raised the question if the function of TBsmr is linked to its oligomeric state.

Biochemical and structural data supporting monomers, dimers, trimers or tetramers of EmrE have been reported and are summarized in Table 4.1. The conflicting results could be due to different preparation techniques, constructs, or experimental conditions. The dimer was most frequently determined and probably is the minimal functional unit capable of binding substrate. However, it is not certain if the dimer is also capable of transport.

Freeze-fracture EM (Eskandari et al., 1998) and a TPP<sup>+</sup> transport assay (Grinius and Goldberg, 1994) were used to correlate the oligomeric state of TBsmr in a lipid environment to its function. The experiments demonstrate that phospholipids influence the transport activity and oligomeric state of TBsmr. Furthermore the data suggests that the dimer is the minimal unit capable of transport but that structural tetramers also exist.

**Table 4.1:** Summary of experimental evidence for the oligomeric states of EmrE.

| Oligomeric state | Experimental methodology   | Reference                            |
|------------------|--|--------------------------------------|
| Monomer          | Analytical ultracentrifugation and size exclusion chromatography (SEC) | Winstone et al., 2005                |
| Dimer            | EPR spectroscopy   | Koteiche et al., 2003                |
|                  | EM structure   | Tate et al., 2001; Tate et al., 2003 |
|                  | Cysteine crosslinking  | Soskine et al., 2002                 |
|                  | Whole cell growth assay  | Jack et al., 2000                    |
|                  | Analytical ultracentrifugation and SEC                                 | Butler et al., 2004                  |
|                  | ESI-MS   | llag et al., 2004                    |
|                  | Monomer swapping   | Rotem et al., 2001                   |
|                  | Functional complementation of in vitro produced protein                | Elbaz et al., 2004                   |
| Trimer           | Helix-helix interactions   | Rath et al., 2006                    |
|                  | X-ray crystal structure  | Chen et al., 2007                    |
|                  | In vivo and in vitro negative dominance                                | Yerushalmi et al., 1996              |
| Dimer of dimers  | Radioactive ligand binding   | Muth and Schuldiner, 2000            |
|                  | Functional complementation of in vitro produced protein                | Elbaz et al., 2004                   |
|                  | EM structure   | Tate et al., 2001; Tate et al., 2003 |

## 4.2 Results

### 4.2.1 Reconstitution into different lipids

To determine the influence of the type of lipid on the reconstitution, pure synthetic lipids and different lipid compositions mimicing the *E. coli* membrane were tested.

TBsmr was reconstituted by detergent removal through adsorption on polystyrene beads. The lipids were dissolved completely with 1-5x (w/w) DDM in “inside buffer” (150 mM NH<sub>4</sub>Cl; 1 mM DTT; 15 mM MOPS, pH 7). The reconstitution efficiencies were analyzed by sucrose density gradients and are summarized in Table 4.2. The results were judged by two parameters: The number of bands on the gradient and the sucrose density where the proteoliposomes appeared. A single band corresponds to a homogeneous incorporation, while a high sucrose percentage corresponds to a more quantitative incorporation. The protein-to-lipid ratios were 1:450 or less to increase the protein content of the sample for future ssNMR measurements. The lipid mixture 1-palmitoyl-2-oleoyl-*sn*-glycero-3-phosphoethanolamine/ 1,1',2,2'-tetraoleoyl-cardiolipin (POPE/TOCL) could not be solubilized properly which might explain the inhomogeneous incorporation observed. Besides POPE/TOCL, all reconstitutions gave good results independent of the lipid type and

protein-to-lipid ratio indicating that the reconstitution of TBsmr is not affected by the type of lipid.

**Table 4.2:** Lipid reconstitution screen. The influence of lipids on the reconstitution with DDM was evaluated by sucrose density gradients. The number of bands on the gradient and their sucrose percentage were determined. An example of a sucrose density gradient is shown in Fig. 3.9. Conditions that appear only as a single band on a gradient represent a homogeneous reconstitution and are marked (+), whereas multiple bands corresponding to a inhomogeneous reconstitution are marked (-).

| Lipid (w/w)                 | Detergent-lipid ratio (w/w) | Lipid-protein ratio (mol/mol) | Bands | Sucrose percentage | Results |
|-----------------------------|-----------------------------|-------------------------------|-------|--------------------|---------|
| <i>E. coli</i> total lipids | 1/1                         | 100/1                         | 1     | 21%                | +       |
| DPOPE/ TOCL 7/3             | 1/1                         | 100/1                         | 1     | 22%                | +       |
| POPC/ POPG 5/1              | 2/1                         | 100/1                         | 1     | 22%                | +       |
| POPC/ POPG 5/1              | 2/1                         | 50/1                          | 1     | 23%                | +       |
| POPC                        | 2/1                         | 450/1                         | 1     |                    | +       |
| DMPC                        | 2/1                         | 450/1                         | 1     |                    | +       |
| POPE/ TOCL 7/3              | 5/1                         | 100/1                         | 2     | 15%, 22%           | -       |

1,2-dipalmitoleoyl-sn-glycero-3-phosphoethanolamine (DPOPE); 1,1',2,2'-tetraoleoyl-cardiolipin (TOCL); 1-palmitoyl-2-oleoyl-sn-glycero-3-phosphocholine (POPC); 1-palmitoyl-2-oleoyl-sn-glycero-3-phosphoglycerol (POPG); 1,2-dimyristoyl-sn-glycero-3-phosphocholine (DMPC)

#### 4.2.2 Drug transport: TPP<sup>+</sup> assay

TPP<sup>+</sup> transport was measured as described previously (Grinius and Goldberg, 1994). The basic layout of this assay is depicted in Fig. 4.1. The TPP<sup>+</sup> uptake into the proteoliposomes was measured with an TPP<sup>+</sup> selective electrode and a Ag/AgCl reference electrode MI-402 from Microelectrodes (Bedford, USA) (Mootha et al., 1996). The electrodes were connected to a high impedance pH meter CG825 from Schott (Mainz, Germany) and recorded with a Metrahit 22S A/D converter (GMC-I Gossen-Metrawatt, Nürnberg, Germany) and the software Metrawin 10 (V5.22).

Instead of constructing a TPP<sup>+</sup> electrode manually (Ohmizo et al., 2004), the TPP<sup>+</sup> uptake into the proteoliposomes was measured with an ETH 1001 based calcium-selective electrode MI-600 from Microelectrodes (Bedford, USA) (Mootha et al., 1996). The TPP<sup>+</sup> ions develop an electric potential (E) between the sensing ion selective electrode and the reference electrode which is measured in mV. The response of the electrodes was tested with varying concentrations of TPP<sup>+</sup> in “outside buffer” (15 mM Tris-Cl, pH 9.5; 150 mM KCl; 0.5 μg/mL valinomycin) (Fig. 4.2) and used to calibrate the electrode. Plotted on a logarithmic scale, the MI-600 calcium-selective electrode showed lineare response to

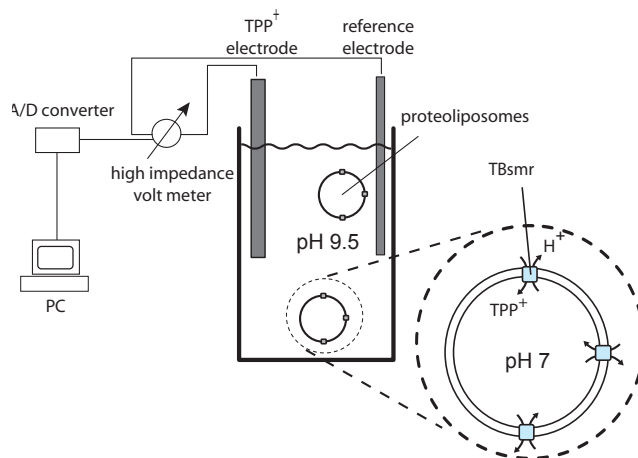


**Figure 4.1:** Schematic layout of the  $TPP^+$  transport assay. Acidic proteoliposomes are diluted in an alkaline buffer, creating a pH gradient. This gradient, acidic inside, is used by the SMR proteins to drive substrate-proton antiport and accumulate  $TPP^+$  inside the liposomes. The decrease of the  $TPP^+$  concentration in the bulk media is detected with an ion selective  $TPP^+$  electrode.

$TPP^+$  with a capacitance slope of 54 mV per decade when fitted with the Nernst equation ( $R=0.999$ ):  $[TPP^+] = 10^{\left(\frac{E-308}{54}\right)}$ . To correctly quantify the  $TPP^+$  concentration, the electrode had to be calibrated directly before each measurement. Therefore, when the electrode was not calibrated, the  $TPP^+$  concentration is given in arbitrary units.

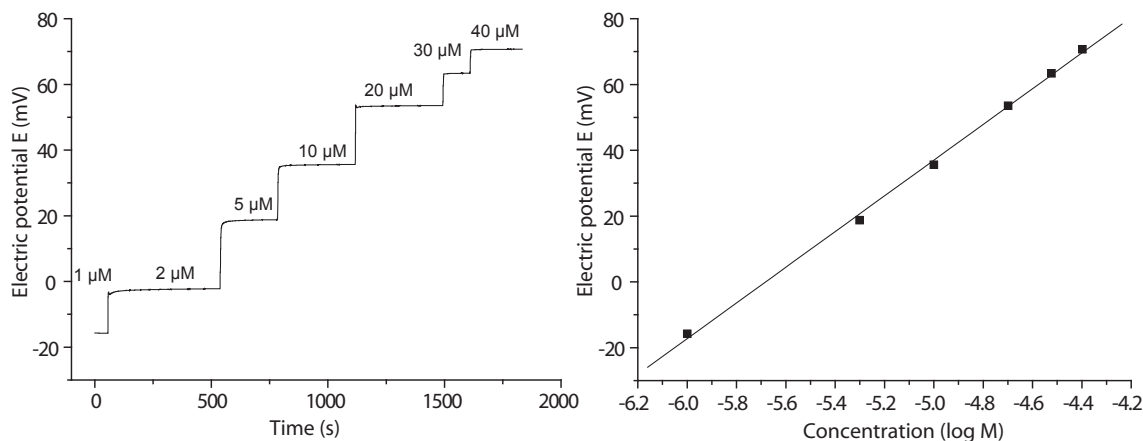


**Figure 4.2:** Calibration of the electrode MI-600. The data was fitted with the Nernst equation ( $R=0.999$ ):  $[TPP^+] = 10^{\left(\frac{E-308}{54}\right)}$ . The capacitance slope was 54 mV per decade.

When acidic TBsmr proteoliposomes are diluted in basic buffer, TBsmr utilizes the preformed proton gradient to actively transport  $TPP^+$  into the *E. coli* liposomes against a concentration gradient. Simultaneously, an electric potential (positive inside) is created by the downward influx of potassium ions which is mediated by valinomycin. Since the

pmf driven transport depends not only on the pH gradient but also on the electric potential, it fulfills two functions: on one hand, it increases the electrogenic transport of the singly charged TPP<sup>+</sup> (Rotem and Schuldiner, 2004). On the other hand, the positive charge inside prevents a passive diffusion of the membrane permeable TPP<sup>+</sup> into the liposomes. Therefore drug influx can only be caused by transport activity of TBsmr. The amount of translocated TPP<sup>+</sup> can be quantified by calibrating the electrode response.

A representative time trace of the transport assay is shown in Fig. 4.3 A. When the TBsmr proteoliposomes at pH 7 were diluted into buffer at pH 9.5 (1), TBsmr used the pH gradient to actively transport TPP<sup>+</sup> from the outside bulk solution into the liposomes which lead to a drop of the measured TPP<sup>+</sup> concentration (2). The diffusion of protons across the membrane caused a breakdown of  $\Delta\text{pH}$  and the system returned to equilibrium (3). The difference (4) in the electric potential between the minimum and the equilibrium corresponds to the translocated TPP<sup>+</sup> ( $\Delta\text{TPP}^+$ ). The lower baseline (5) after transport is due to passive binding of TPP<sup>+</sup> to the lipids and dilution effects. A schematic representation of the TPP<sup>+</sup> transport to illustrate the influence of the proton leakage on the measured transport is shown in Fig. 4.3 B.

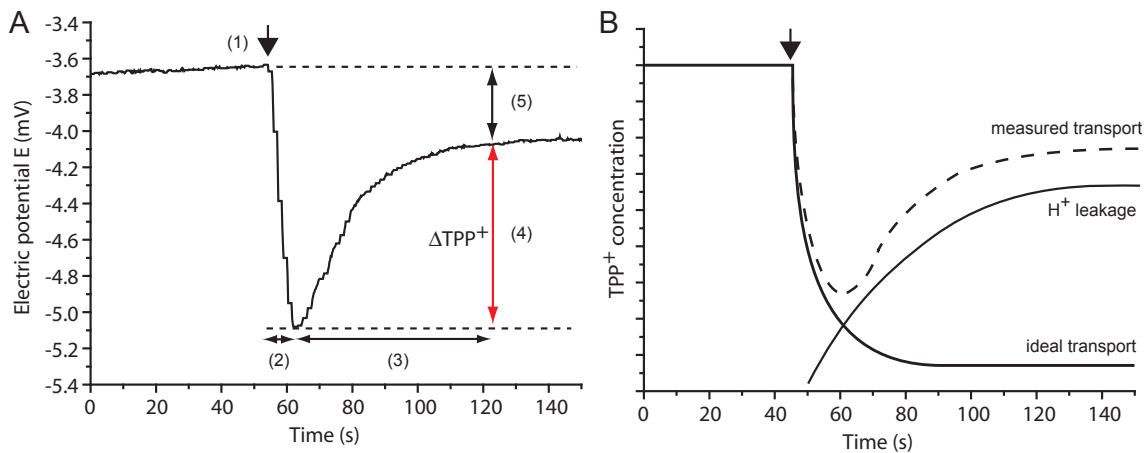


**Figure 4.3:** TPP<sup>+</sup> transport assay. A) Time trace of TPP<sup>+</sup> transport into *E. coli* liposomes by TBsmr: (1) proteoliposomes added, (2) active transport and dilution of TPP<sup>+</sup>, (3) pH gradient collapses, (4) translocated TPP<sup>+</sup> ( $\Delta\text{TPP}^+$ ), (5) TPP<sup>+</sup> concentration change due to dilution and binding to the liposomes (Electrode response not calibrated). B) Schematic representation of the influence of the proton leakage on the TPP<sup>+</sup> transport.

The rapid return of the TPP<sup>+</sup> concentration to an equilibrium (Fig. 4.3 event (3)) did not occur in the measurements of Grinius and Goldberg (1994). The equilibration is likely due to proton leakage as illustrated in Fig. 4.3 B. Without proton leakage, the ideal transport

would lead to a stable, reduced  $\text{TPP}^+$  concentration. However, proton leakage through the membrane collapses the pH gradient and causes the system to return to equilibrium. The collapsing gradient could be caused by residual detergent because Grinius and Goldberg (1994) used the same lipids but a different type of detergent (OG). OG could not be used to reconstitute TBsmr because OG denatured it.

A number of controls were carried out to verify that the observed drop of the  $\text{TPP}^+$  concentration was indeed caused by active transport (Fig. 4.4). No transport was detected either when the ionophore nigericin ( $1 \mu\text{g}/\text{mL}$ ), which dissipates the pH gradient, was added to the outside buffer, or when the essential glutamate E13 of TBsmr was blocked with covalently bound DCCD (Yerushalmi et al., 2001). In addition,  $\text{TPP}^+$  transport was significantly reduced by competitive inhibition in the presence of  $0.5 \text{ mM}$  erythromycin.

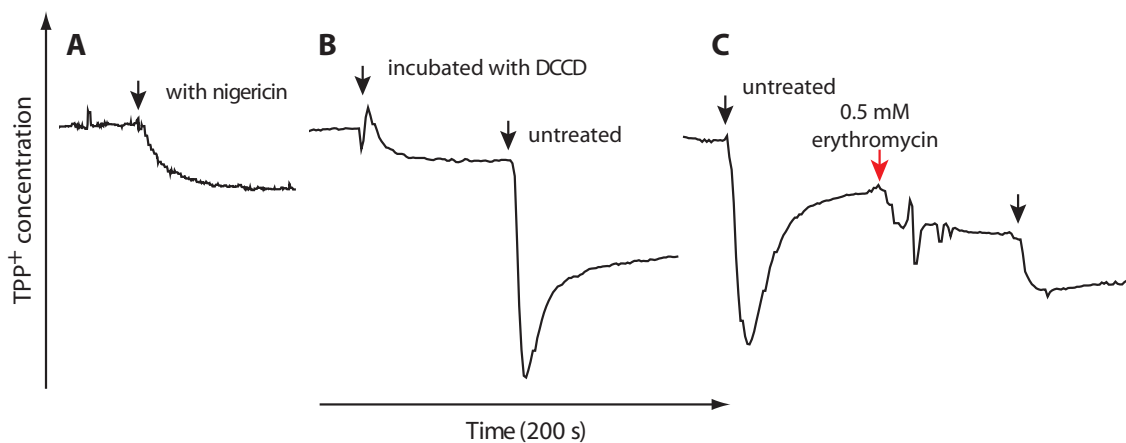


**Figure 4.4:**  $\text{TPP}^+$  transport assay controls. Protein was added as indicated by black arrows. A) The  $\Delta\text{pH}$  was dissipated with  $1 \mu\text{g}/\text{ml}$  nigericin in the outside buffer. B) The TBsmr proteoliposomes were incubated with  $0.5 \text{ mM}$  DCCD which covalently binds to the essential residue E13. C)  $\text{TPP}^+$  transport was competitively inhibited in the presence of  $0.5 \text{ mM}$  erythromycin. (Electrode response not calibrated).

### 4.2.3 Lipids influence $\text{TPP}^+$ transport

TBsmr was reconstituted into different lipids as described previously at a 1:464 mol ratio and assayed for activity (Fig. 4.5 A). TBsmr was functional in *E. coli* total lipids and the synthetic lipid POPC. However, no transport activity was observed in DMPC. A loss of the proton gradient could be excluded as the cause because a high proton permeability was observed for all lipids with the pH sensitive dye pyranine (data not shown). The strong influence of the proton leakage on the transport curve allowed only a qualitative comparison between the different batches of proteoliposomes.

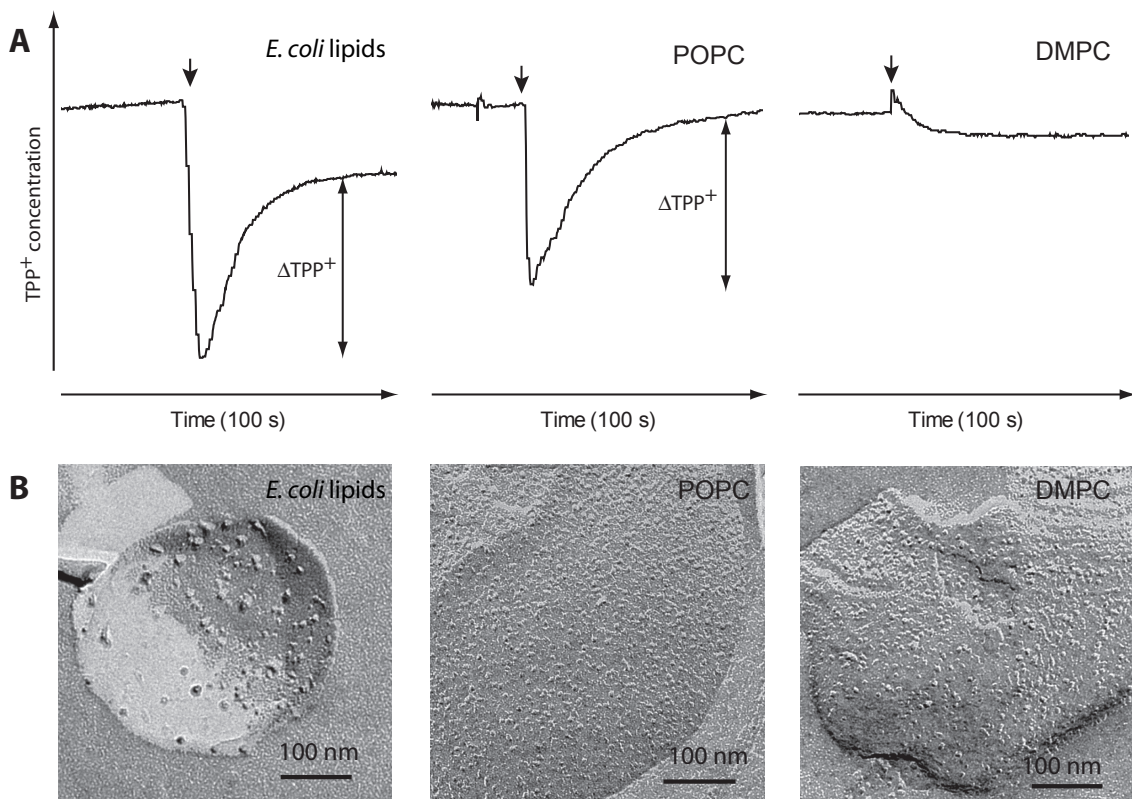


**Figure 4.5:** Influence of lipids on the particle size and TPP<sup>+</sup> transport activity of reconstituted TBsmr. A) The activity of TBsmr reconstituted in different lipids at a 1:500 protein-to-lipid mol ratio was assayed by TPP<sup>+</sup> transport. The addition of TBsmr proteoliposomes is marked with an arrow (Electrode response not calibrated). B) Freeze fracture electron micrographs were taken of TBsmr reconstituted at 1:75 (*E. coli* lipids and DMPC) and 1:50 (POPC) protein-to-lipid mol ratio. (EM micrographs were taken by W. Haase, MPI Biophysics)

The oligomeric state of TBsmr reconstituted in the different lipids was analysed by freeze-fracture electron microscopy. At low resolution, the replicas showed a random distribution of unilamellar and multilamellar vesicles with diameters ranging from 30 to more than 400 nm, displaying intramembrane particles. The form and the size of the liposomes was influenced by the time the liposomes were stored at 4 °C during which liposome fusion can take place, and if and how long the liposomes were sonicated before analysis. Often, small empty vesicles were detectable. When the reconstitution failed or control liposomes without protein were used, no particles were seen. At a higher magnification ( $\geq 16\text{k}$ ), differences in the size of the particles could be observed depending on the type of lipid (Fig. 4.5 B). Compared to DMPC and POPC, the particles were generally larger in *E. coli* total lipids. This increase does not seem to stem from a clustering of the particles, but an increase of the diameter of the particles themselves. Thus, the lipid

composition seems to affect the oligomeric state of TBsmr. The minimal functional unit were the small TBsmr particles in POPC.

The  $\text{TPP}^+$  transport activity of another SMR protein, Smr, has been measured in *E. coli* liposomes by Grinius and Goldberg (1994). To show that TBsmr is fully functional, the rate of transport was also measured in *E. coli* lipids for a better comparison. The electrode response was calibrated by sequential additions of  $\text{TPP}^+$  (0.5 - 50  $\mu\text{M}$ ) and showed a response with a capacitance slope of 54 mV per decade (Fig. 4.2). The initial rates of  $\text{TPP}^+$  uptake were calculated from  $\Delta\text{TPP}^+$  after 9 s with an initial concentration of  $\text{TPP}^+$  in the range of 2-30  $\mu\text{M}$ . The results were analyzed by nonlinear least square fitting (Fig. 4.6). The apparent  $K_M$  of 8  $\mu\text{M}$  and  $V_{\text{max}}$  of 1.9  $\mu\text{mol}/\text{min}$  per mg of TBsmr are similar to a  $K_M$  of 5  $\mu\text{M}$  and  $V_{\text{max}}$  of 2  $\mu\text{mol}/\text{min}$  per mg of Smr. Taking the molecular weight of 14,317 Da into account, TBsmr transports  $\text{TPP}^+$  with a turnover rate of 27  $\text{min}^{-1}$  ( Smr: 26  $\text{min}^{-1}$ ).

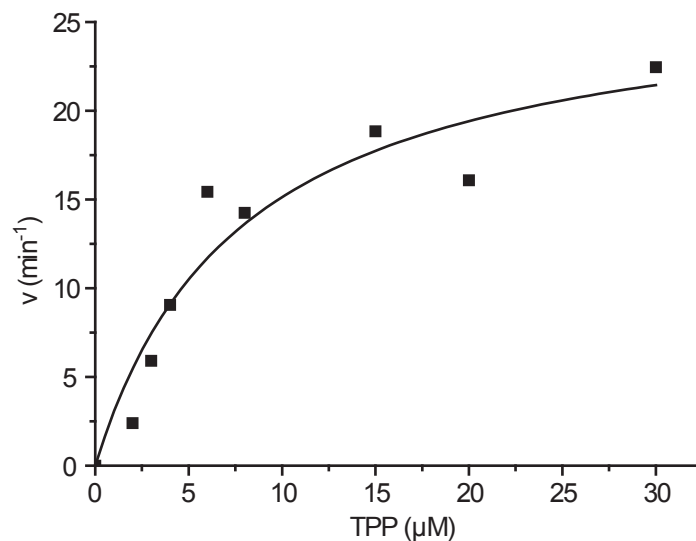


**Figure 4.6:** Transport kinetics,  $V_{\text{max}}$  and  $K_M$ , of TBsmr in *E. coli* liposomes for the substrate  $\text{TPP}^+$ . Initial uptake rates ( $\Delta\text{TPP}^+$  after 9s) of the proteoliposomes were determined in the presence of 2-30  $\mu\text{M}$   $\text{TPP}^+$  with a  $\Delta\text{pH}$  of 2.5 and  $\Delta\psi$  of 136 mV. The apparent  $K_M$  of 8  $\mu\text{M}$  and  $V_{\text{max}}$  of 27  $\text{min}^{-1}$  were determined by nonlinear least square fitting.

#### 4.2.4 Analysis of the freeze-fracture EM images

Freeze-fracture electron microscopy (EM) provides images of integral membrane protein particles embedded in the fractured membrane. This approach involves the analysis of the dimension of the protein particles and thus can yield structural information but at

a low resolution. The method has been used to identify protein species in natural membranes (Park and Biggins, 1964; Wollman et al., 1980) or reconstituted in proteoliposomes (Costello et al., 1984). In addition, it has been shown that the oligomeric state of a protein can be determined from the area of the transmembrane domain which is calculated from the cross-sectional area of freeze-fracture micrographs (Eskandari et al., 1998).

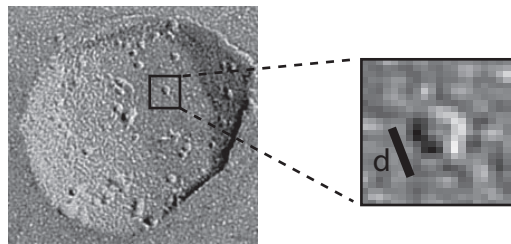


**Figure 4.7:** Measurement of the diameter of protein particles in freeze-fracture images.

To study the size and the oligomeric state of TBsmr in different lipids, the particle diameter were determined by measuring the width of the particle perpendicular to the white shadow (Fig. 4.7). The diameter of the protein complex was calculated by subtracting the platinum - carbon coat (3.8 nm) from the particle diameter (Ruben and Telford, 1980) and plotted as frequency histograms (Goodenough and Staehelin, 1971). The measured particles were binned in frequency histograms according to their diameter (Fig. 4.10 A). A resolution of up to  $\pm 0.5$  nm was determined for freeze-fracture micrographs of gold particles by Eskandari et al. (1998) but a bin size of 1 nm or 0.8 nm was necessary to smoothen the gaps in the histogram caused by the width of individual pixels in the digitized images.

Since the major and minor diameter of the protein ellipsoids do not give a Gaussian distribution (Fig. 4.8), the data could not be fitted with multiple Gaussian functions. Therefore, the diameters were determined by comparing the measured particle distributions to simulated histograms calculated for oligomers with given dimensions. A simulated histogram is generated by binning the diameter of an ellipsoid measured from every direction in  $1^\circ$  steps. Errors in the particle diameter measurement are included in the simulation by assuming a Gaussian distribution for each diameter. For example, the calculated histograms of a particle with  $8 \times 3.1$  nm with and without a standard deviation of 1 nm are shown in Fig. 4.8.

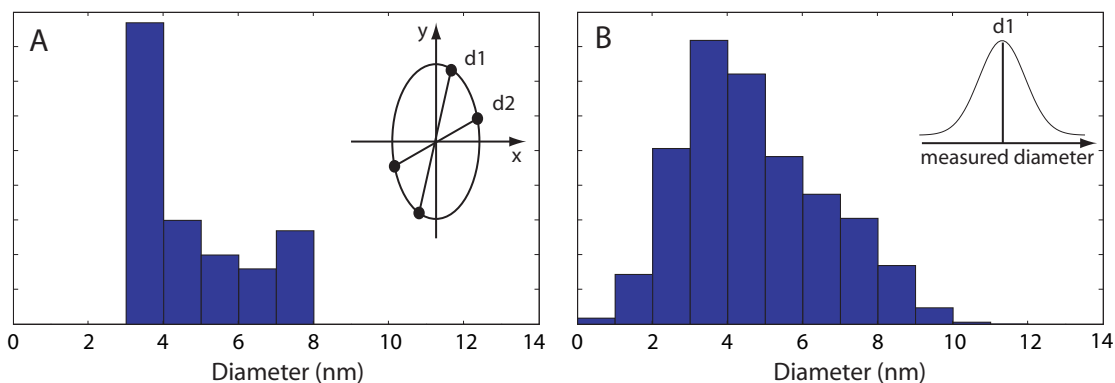


**Figure 4.8:** Simulated histograms for an  $8 \times 3.1$  nm elliptic particle with a 1 nm bin width. A) Calculated histogram without measurement errors. Two arbitrary diameter measurements ( $d_1$  and  $d_2$ ) are shown in the inset. B) Calculated histogram with a standard deviation of 1 nm for each measurement. The inset illustrates that multiple measurements of the diameter ( $d_1$ ) return a Gaussian distribution. The number of particles is 360,000.

The size of a TBsmr dimer with  $3.1 \times 4$  nm is estimated by the dimensions of EmrE in 2D crystals (Tate et al., 2001). Possible arrangements of the tetramer are a side-to-side orientation with  $\sim 6.2 \times 4$  nm, as seen in the crystallographic tetramers of the EM structure (Tate et al., 2001), or an end-to-end tetramer ( $3.1 \times 8$  nm), based on the assumption that the oligomerization takes place at helix 4 (Rath et al., 2006; Elbaz et al., 2004). The simulated histograms were calculated from ellipsoids with a standard deviation of 1 nm for each diameter measurement to account for measurement errors (Fig. 4.8) and are shown in Fig. 4.9.

The measured particle distributions and the best matching simulated histogram are shown in Fig. 4.10. The most probable oligomeric state for DMPC and POPC are dimers. The resolution of the freeze-fracture micrographs are too low to discriminate whether the smaller mean diameter of TBsmr in DMPC compared to POPC, is due to a monomeric state or small structural changes in a dimer. However, the deviation of the TBsmr particle distribution in DMPC from the simulated dimer could explain the lack of transport activity in this type of lipid. In contrast, the broad asymmetric distribution of the TBsmr particles in *E. coli* lipids fitted best to an end-to-end tetramer in agreement with biochemical studies (Elbaz et al., 2004; Rath et al., 2006) because a tetramerization interface at the long side of the dimer could lead to an unchecked, detrimental oligomerization (Rath and Deber, 2007).

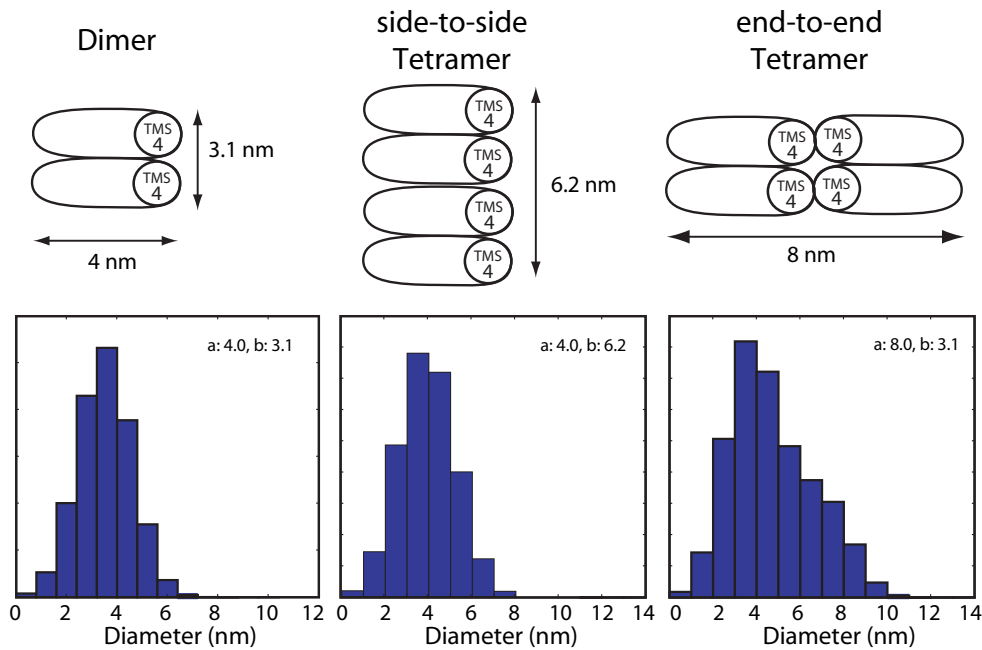


**Figure 4.9:** Schematic model and simulated histograms of possible TBsmr oligomers. A standard deviation of 1 nm was included in each diameter measurement of the simulated histograms. The bin width is 0.8 or 1 nm.

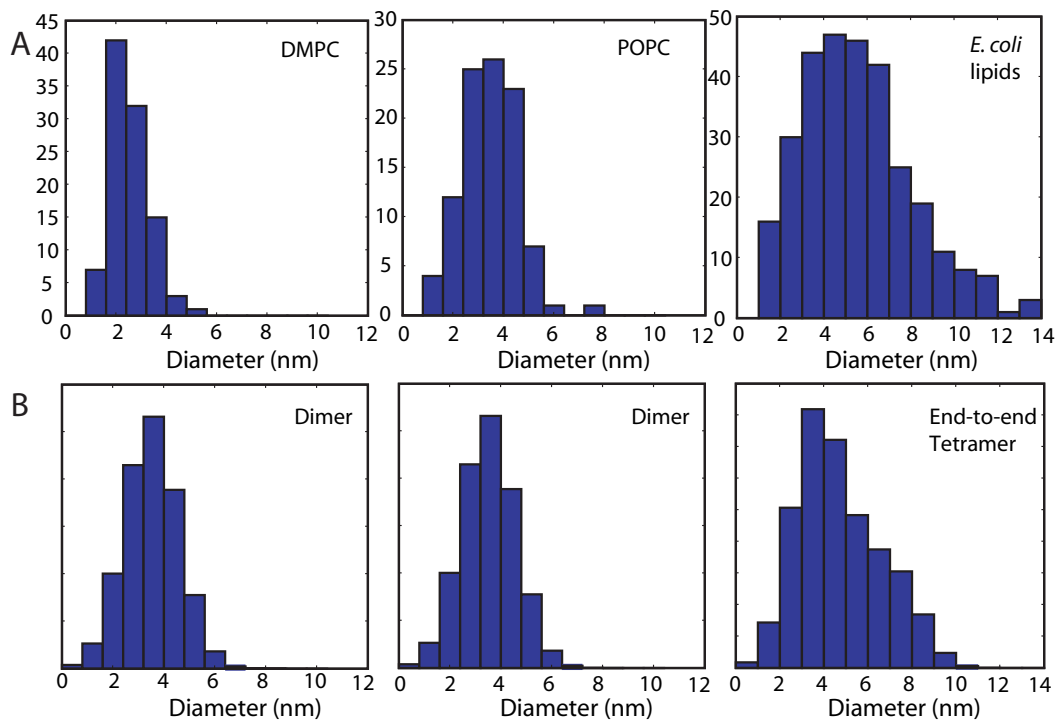


**Figure 4.10:** Determination of the oligomeric state of TBsmr in different lipids. A) Histogram of TBsmr particles in different lipids reconstituted at 1:50 (POPC) and 1:75 (DMPC, *E. coli* total lipids) protein-to-lipid molar ratios. The diameter were corrected for the thickness of the platinum carbon film (3.8 nm). (DMPC, N=100; POPC, N=99; *E. coli* total lipids, N=299). B) Simulated size distribution of a dimer with  $(3.1 \times 4) \pm 1$  nm and end-to-end tetramer with  $(3.1 \times 8) \pm 1$  nm.

## 4.3 Discussion

### TPP assay shows functionality

Integral membrane proteins operate in an environment which is, in part, made of phospholipid molecules in a bilayer. This environment must support the function of the protein in the membrane (Andersen and Koeppe, 2007). Protein activity has been shown to be modulated by physical properties of the lipid molecules such as charges of the head group (Stallkamp et al., 1999), chain length/ hydrophobic thickness (de Lima Santos et al., 2005) and lateral pressure profile (Cantor, 1997), or by specific interactions with non-annular lipids which mediate protein-protein interactions (Nury et al., 2005). Even though the mycobacterial protein TBsmr is functional when heterologously expressed in *E. coli* (Ninio et al., 2001), nothing is known about the influence of lipids on its activity and oligomerization. Therefore a non-radioactive TPP<sup>+</sup> transport assay established for Smr (Grinius and Goldberg, 1994) was used to study the function of TBsmr in liposomes composed of different lipids with an ion selective electrode as illustrated in Fig. 4.1.

TBsmr could be reconstituted independent of the type of lipid (Fig. 4.2) and showed  $\Delta\text{pH}$  dependent TPP<sup>+</sup> transport in *E. coli* lipids (Fig. 4.3). The transport is blocked by incubation with DCCD which binds to the essential residue E13 (Yerushalmi et al., 2001), and by competitive inhibition with the substrate erythromycin (Fig.4.4). Comparing the the measured transport rate of TBsmr in *E. coli* lipids with a  $K_M$  of 8  $\mu\text{M}$  and  $V_{max}$  of 27  $\text{min}^{-1}$  (Fig. 4.6) to Smr in the same lipids with a  $K_M$  of 5  $\mu\text{M}$  and  $V_{max}$  of 26  $\text{min}^{-1}$  gave very similar results (Grinius and Goldberg, 1994). The substrate turnover seems very slow but is consistent with results of TBsmr in a methyl viologen transport assay ( $K_M = 943 \mu\text{M}$ ,  $V_{max} = 316 \text{min}^{-1}$ ) (Ninio et al., 2001). The low affinity of TBsmr for TPP<sup>+</sup> could explain why no TPP<sup>+</sup> binding could be detected in a radioactive binding assay (Ninio et al., 2001) commonly used to assess the activity of EmrE (Gutman et al., 2003)

### Lipids influence the function

With a functional assay at hand, the influence of lipids on the TPP<sup>+</sup> transport was studied. From the plethora of different lipids, POPC and DMPC were chosen for the following reasons: The complex membrane of *M. tuberculosis*, made of the phospholipids phosphatidylinositol mannoside (67%), cardiolipin (20%) and phosphatidylethanolamine (13%), and a high percentage (65%) of tuberculostearic fatty acids (C18:Me) (Sareen and

Khuller, 1990), is very different from the inner membrane of *E. coli* which consists of ~70% PE and ~20% PG, and fatty acid chain lengths between 16 and 18 (43% C16, 33% C16:1, 24% C18:1) (Morein et al., 1996). Nevertheless, heterologously expressed TBsmr is active reconstituted in *E. coli* lipids (Ninio et al., 2001). The bilayer forming synthetic lipid POPC was chosen as a simple mimic of the *E. coli* membrane. The matching chain length of POPC (16:0-18:1) should prevent hydrophobic mismatch while keeping the membrane in the gel phase at room temperature (transition temperature of -3 °C). As a second synthetic lipid, DMPC was chosen because it has been used successfully to study EmrE with bound substrate by ssNMR (Glaubitz et al., 2000) and by electron microscopy (Ubarretxena-Belandia et al., 2003).

TBsmr transported TPP<sup>+</sup> in *E. coli* total lipids and in POPC but not in DMPC (Fig. 4.5). The loss of transport capability was highly reproducible even though it has been shown that EmrE is capable of binding TPP<sup>+</sup> in DMPC (Ubarretxena-Belandia et al., 2003). Since lipids have been shown to mediate the interaction between protein monomers (Nury et al., 2005), changes in the oligomeric state could be responsible for the loss of activity in DMPC.

### Lipids influence the oligomerization

Even though the oligomeric state of EmrE has been extensively studied, mostly in the detergent solubilized state, the oligomeric state of SMR proteins *in vivo* is still unclear (for a complete overview see Bay et al., 2007). Eskandari et al. (1998) determined the oligomeric state of protein species in natural membranes by freeze-fracture EM. The EM replicas give images of protein particles embedded in the fractured membrane, which can be analyzed by plotting the particle diameter as frequency histograms. By comparing the histograms of the TBsmr particles in *E. coli* lipids, POPC and DMPC (Fig. 4.10 A), it is already evident that changes in the oligomeric state are not responsible for the loss of activity of TBsmr in DMPC because the particles in DMPC and POPC are of similar size.

The loss of the transport capability in DMPC could be a consequence of structural changes of TBsmr in the thin DMPC membrane due to a hydrophobic mismatch. Most models assume that the fatty acids in the vicinity of the protein adjust their length to match the hydrophobic core of the protein. While this is true for  $\beta$ -barrel proteins like OmpF, there is evidence that hydrophobic matching of  $\alpha$ -helical membrane proteins also involves tilting of the helices (Lee, 2004) which could affect their function. Alternatively, the lateral pressure profile of DMPC (Cantor, 1999) could stabilize a certain protein con-

formation and change the kinetics and energetics of the transport reaction (Andersen and Koeppe, 2007), similar to a slower folding rate of DGK in the presence of DMPC (Booth et al., 2001). The exact cause for the loss of activity could not be determined from the current data and was attributed to a general “denaturing” effect of DMPC which also has been suggested for the sensor kinase KdpD (Stallkamp et al., 1999) and the lactose permease (Bogdanov et al., 1999).

To determine the exact oligomeric state, the measured particle distributions of TBsmr were compared to simulated histograms of a putative dimer of  $3.1 \times 4$  nm and tetramers of  $3.1 \times 8$  and  $6.2 \times 4$  nm (Fig. 4.9), based on the dimension of the EmrE dimer in the EM structure (Tate et al., 2001) and a possible tetramerization site identified in Hsmr with peptides of helix 4 (Rath et al., 2006). The distribution of the small particles of TBsmr in DMPC and POPC matches best to a dimeric state, whereas the large particles in *E. coli* lipids match end-to-end tetramers (Fig. 4.10).

The combined data from the TPP<sup>+</sup> transport assay and the structural data from freeze-fracture EM show for the first time that an SMR dimer is the minimal unit capable of substrate transport and that tetramers also exist in a membrane environment. The results are consistent with a dimer as the basic functional unit capable of binding substrate and the observed tendency to form higher oligomers in the detergent-solubilized state (Elbaz et al., 2004). A dynamic exchange between the different oligomeric states would also explain the observed smeared bands on the SDS-PAGE gels (Fig. 3.3). Since only TBsmr dimers are necessary for transport, there seems to be no reason for higher oligomers. However, as multidrug efflux pumps are often overexpressed in drug resistant bacteria, the formation of oligomers could be a mechanism to reduced the crowding of proteins in the inner membrane.

## 4.4 Conclusion

It could be shown that reconstituted TBsmr is functional in proteoliposomes and shows the same transport activity as other SMR proteins. It was found that the type of lipid has an influence on the transport activity and oligomeric state of TBsmr. In the membrane TBsmr forms dimers and tetramers depending on the type of lipid. The minimal functional unit was found to be a dimer but TBsmr forms structural tetramers in *E. coli* lipids. Optimal conditions were found for the synthetic lipid POPC, where TBsmr was functional and homogeneous which provides an ideal sample for ssNMR in a native-like environment.

# 5 Transport cycle intermediate in small multidrug resistance protein is revealed by substrate fluorescence<sup>1</sup>

## 5.1 Introduction

It could be shown that reconstituted TBsmr is fully functional. However, a major problem of the TPP<sup>+</sup> transport assay was the rapid collapse of the preformed pH gradient. Therefore a reliable method to create a stable pH gradient was sought to characterize the transport cycle of TBsmr further.

On the basis of cryo electron microscopy data of two-dimensional crystals (Ubarretxena-Belandia et al., 2003), an alternate access model (Fig. 1.7) for the transport mechanism has been proposed (Yerushalmi and Schuldiner, 2000c; Fleishman et al., 2006). In this model, substrate translocation is initiated by substrate binding, which is followed by release of the substrate, triggered by proton binding, and proton antiport. Although the transfer of substrate from a binding to a release site must involve conformational changes within EmrE, no statement could be made about potential intermediate states.

To address this open mechanistic question, EtBr was selected to probe substrate transport across the membrane because of its intrinsic fluorescence. One requirement for *in vitro* transport studies is the generation of a stable and reproducible pH gradient. Here, TBsmr has been co-reconstituted with the light-driven proton pump bacteriorhodopsin (bR) into unilamellar vesicles. On illumination bR generates a stable pH gradient, which TBsmr requires for substrate transport. Co-reconstitution of  $\Delta$ pH-dependant proteins

---

<sup>1</sup>The results of this chapter were published online September 14, 2007 in the FASEB J., doi: 10.1096/fj.07-9162com

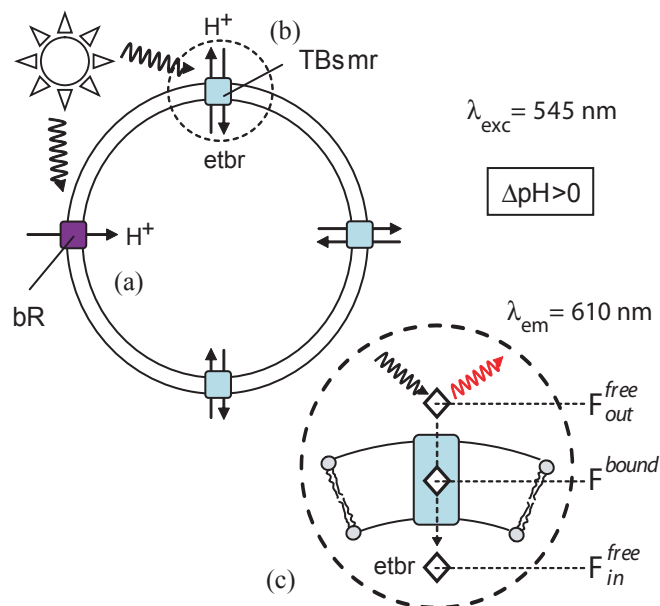


**Figure 5.1:** Principle of the SMR – bR transport assay. Proteoliposomes contain both bR (inside-out) and TBsmr. The assay starts from an equilibrium situation  $[\text{EtBr}]_{\text{in}} = [\text{EtBr}]_{\text{out}}$  with EtBr free in solution contributing to the total fluorescence with  $F_0^{\text{in}}$ . On illumination, bR pumps protons into the liposomes generating a proton gradient (a), which, in turn, is used by TBsmr to transport ethidium bromide to the inside (b). The same light source, which drives bR, is used to excite EtBr fluorescence. The change in environment of the substrate on transport alters its fluorescence properties, which can be monitored (c).

with bR has been extensively used in functional assays for ATPase activity (Racker and Stoeckenius, 1974), sodium channels from eel (Perozo and Hubbell, 1993) and glutamate transporter from rat brain vesicles (Maycox et al., 1990).

The transport process must involve steps for substrate binding, translocation and release. During transport, a substrate such as EtBr could experience a significant change of environment, which would influence its fluorescence properties. Therefore, EtBr itself could report on transient substrate-transporter complexes, which could form during the transport cycle. The fluorescence quantum yield of EtBr is measured, as a proton gradient is formed by bR. As the same light source (545 nm) can be used to activate bR and excite EtBr fluorescence, the experiment can be carried out using a standard fluorescence spectrometer. The basic layout of the experiment is depicted in Fig. 5.1.

In general, the total fluorescence intensity  $F_{\text{total}}$  contains contributions from free EtBr in solution within and outside the liposomes ( $F_{\text{in}}^{\text{free}}, F_{\text{out}}^{\text{free}}$ ), from EtBr non-specifically bound to the liposomes ( $F_{\text{liposome}}^{\text{bound}}$ ), and EtBr bound to TBsmr ( $F^{\text{bound}}$ ):

$$F_{\text{total}} = F_{\text{in}}^{\text{free}} + F_{\text{out}}^{\text{free}} + F_{\text{liposome}}^{\text{bound}} + F^{\text{bound}} \quad (5.1)$$

The experiment starts at equilibrium ( $F_0$ ) with  $\Delta\text{pH}=0$  and the same EtBr concentration inside and outside. On illumination, a pH gradient is generated, and TBsmr starts to transport EtBr into the liposomes. In the following, we will show that this transport process causes an increase in total fluorescence from its equilibrium value  $F_0$  by  $\Delta F$ :

$$F_{total} = F_0 + \Delta F \quad (5.2)$$

where  $\Delta F$  contains mainly fluorescence contributions of EtBr bound to a TBsmr transport cycle intermediate ( $\Delta F = F^{trans}$ ).

## 5.2 Results

### Generation of a stable pH gradient

Proteoliposomes containing both bR and TBsmr were prepared by fusing bR purple membrane patches to TBsmr containing liposomes using the co-reconstitution technique described by Perozo and Hubbell (1993). Light induced proton pumping was tested by trapping the pH sensitive dye pyranine inside TBsmr/bR proteoliposomes (Fig. 5.2). Pyranine has absorption maxima at 405 and 455 nm in its protonated and deprotonated form, respectively. Illuminating the sample caused an increase in fluorescence intensity at 405 nm (protonated population) and a decrease at 455 nm (deprotonated population) which implies an inside-out orientation of bR and acidification of the interior of the liposomes. By comparing the excitation scans to those collected with pyranine loaded proteoliposomes at known pH (data not shown) it was possible to detect a bR induced drop of 0.2 pH units inside the liposomes. This change takes place within 5 min. Once the illumination of bR was stopped, protons leaked back out of the liposomes and equilibrium was reached within a further 5 min. bR orientation and a  $\Delta\text{pH}$  of 0.2 agree well with reported data on reconstituted bR (Perozo and Hubbell, 1993).

### A proton gradient causes a change in EtBr fluorescence in bR/TBsmr proteoliposomes

When the formation of  $\Delta\text{pH}$  is initiated by sample illumination at 545 nm, a time-dependant increase of the EtBr fluorescence at 610 nm is detected. The fluorescence time course  $F_{total}(t)$  starts at equilibrium  $F_0$  where  $[\text{EtBr}]_{in} = [\text{EtBr}]_{out}$  and saturates af-

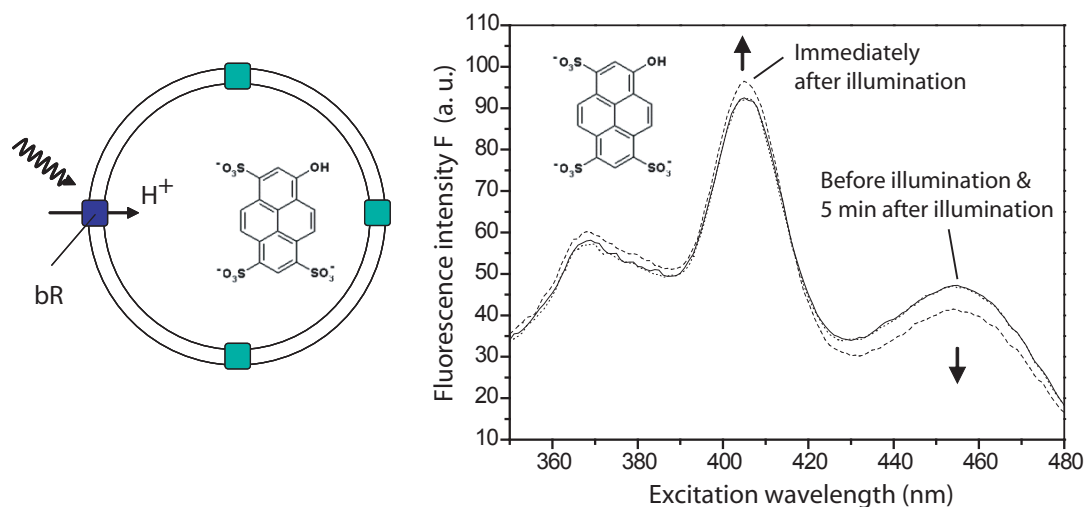


**Figure 5.2:** Directional reconstitution of bR into TBsmr proteoliposomes. Light induced proton pumping was tested by trapping the pH sensitive dye pyranine inside TBsmr/bR proteoliposomes (1  $\mu\text{M}$  TBsmr, 1.4  $\mu\text{M}$  bR,  $\sim 380 \mu\text{M}$  lipids). The sample was illuminated for 5 min at 545 nm using the excitation lamp of the spectrometer (20nm excitation slit width), which causes bR to pump protons across the membrane. After 5 min, the pyranine fluorescence excitation spectrum was monitored at an emission wavelength of 500 nm. The spectra were collected by Dr. Mark Lorch (Prof. Glaubitz, Institute of Biophysical Chemistry, J. W. Goethe-University).

ter  $\sim 100$  s at  $F_0 + \Delta F_{max}$ . Representative time traces are shown in Fig. 5.3 A and are described by:

$$F_{total}(t) = F_0 + \Delta F(t) = F_0 + \Delta F_{max} \times f(t) \quad (5.3)$$

The observed time dependence  $f(t)$  is best described by a sum of at least two exponentials with typical rates of 0.02 and 0.2  $\text{s}^{-1}$ . Processes influencing these rates are the  $\Delta\text{pH}$  generation by bR, EtBr transport into the liposomes, and EtBr and proton leakage out of the liposomes. A detailed kinetic analysis was not necessary for the conclusions drawn from the assay. In the following, I only consider the steady state reached after  $\sim 100$  s and use  $\Delta F_{max}$  as parameter for the change in EtBr fluorescence intensity.

It was found that doubling the amount of TBsmr from 0.5 to 1  $\mu\text{M}$  also causes a doubling of  $\Delta F_{max}$ , as shown by time traces [2] and [1] in Fig. 5.3 A, respectively. Abolishing  $\Delta\text{pH}$  by adding the ionophore nigericin as well as eliminating the proton motive force by adding carbonyl cyanide 3-chlorophenylhydrazone (CCCP) caused a total collapse of  $\Delta F$  (Fig. 5.3 A). This observation supports the notion that the detected fluorescence increase is dependant on a pH gradient. To exclude unspecific binding to bR or the liposomes, the experiment was repeated with TBsmr E13A where the essential residue E13 (in EmrE E14) had been replaced with alanine. No change in EtBr fluorescence could be detected

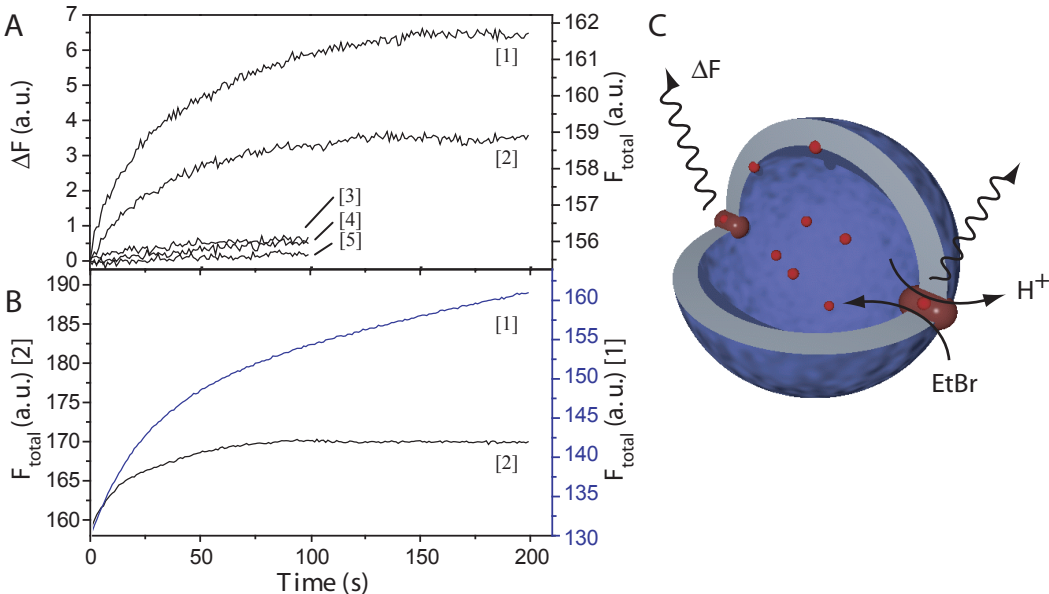


**Figure 5.3:** EtBr fluorescence transport assay. A) Dependence of EtBr fluorescence on  $\Delta pH$  and TBsmr. Representative time traces of EtBr fluorescence ( $\Delta F(t)=F_{total}(t)-F_0$ ) after triggering the generation of  $\Delta pH$  by bR through illumination. Data were collected for 15  $\mu M$  EtBr added to proteoliposomes which contained 1.4  $\mu M$  bR and TBsmr. Doubling the amount of TBsmr from 0.5 [2] to 1  $\mu M$  [1] causes a doubling of  $\Delta F_{max}$ . Adding 5.3  $\mu M$  nigericin [3], or 10  $\mu M$  CCCP [5] to 1  $\mu M$  TBsmr causes the  $\Delta pH$  or  $\Delta pH + \Delta \psi$  to collapse, which results in an almost constant EtBr fluorescence ( $\Delta F(t)=0$ ). Similarly,  $\Delta F(t)=0$  is also observed when using TBsmr E13A (1  $\mu M$ ) [4]. The corresponding molar lipid-to-protein ratios were 380 [1,2,3,4] and 720 [5]. B) EtBr transport can be observed by quenching. After adding KI (0.1 M) to quench the EtBr fluorescence on the outside, an additional linear fluorescence increase is observed upon illumination [1]. In time trace [2] no quencher is added. C) Model of EtBr transport into a vesicle: The fluorescence change is caused by a protein-substrate complex during transport.

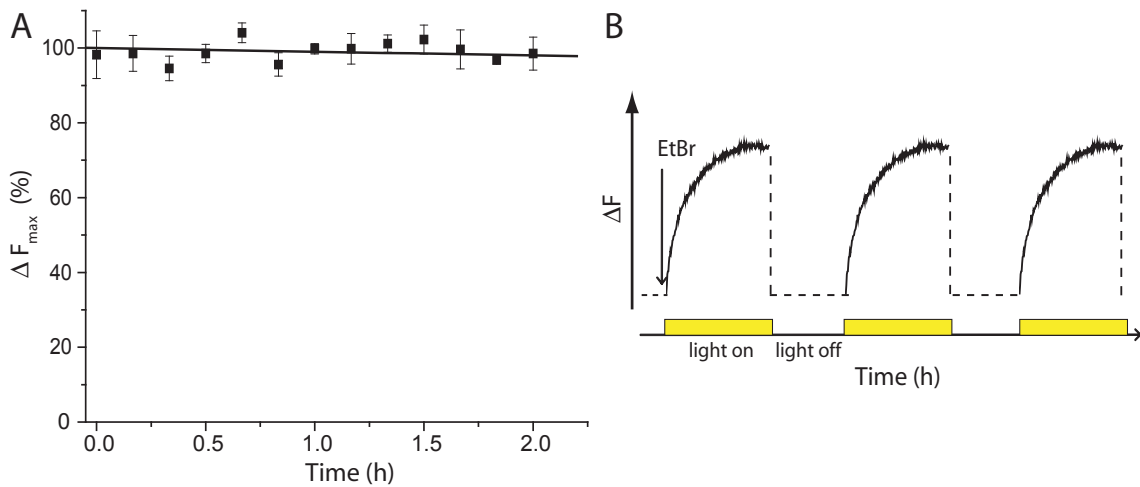


**Figure 5.4:** Long term stability test of the transport assay. A) To test the long term stability of bR and TBsmr in our experimental setup, we have repeatedly illuminated the sample for 5 min followed by a 5 min equilibration period in the dark. The most stable conditions were found for 5 nm excitations slits. Normalized  $\Delta F_{\max}$  is plotted over time and shows a slope of less than  $-1\% \Delta F_{\max}/h$ . B) Scheme of the long term stability assay.

(Fig. 5.3 A) with this inactive mutant. From these observations, we can conclude that the observed fluorescence change  $\Delta F$  is caused by TBsmr, and depends on the pH gradient as well as on the TBsmr concentration.

The TBsmr/bR/lipid molar ratio was screened with respect to largest  $\Delta pH$  and  $\Delta F_{\max}$ . Best results were obtained for 1:1.4:380 (see supplementary Fig. 1 in Basting et al., 2007). The transport assay could be repeated for some hours (Fig. 5.4).

### Detection of ethidium bromide transport into the liposomes

The data suggest  $\Delta pH$ -dependant binding of EtBr to TBsmr. If TBsmr pumps EtBr into the liposomes, the substrate concentration inside should increase while decreasing outside. But the fluorescence of free EtBr inside and outside is indistinguishable and its contribution to  $F_{total}$  does not change ( $F_{in}^{free} + F_{out}^{free} = \text{const.}$ ). To demonstrate that transport actually takes place in our experimental setup, the quencher KI was added to the outside of the liposomes. EtBr is now transported from a quenched environment outside the liposome into a less quenching environment inside and  $F_{in}^{free} + F_{out}^{free}$  is no longer constant. If transport takes place, an increase  $F_{in}^{free}$  of proportional to  $[EtBr]_{in}$  is expected. Indeed, the time trace 1 shown in Fig. 5.3 B is the sum of two components. The first component stems from binding to TBsmr, while the second, linearly increasing component arises

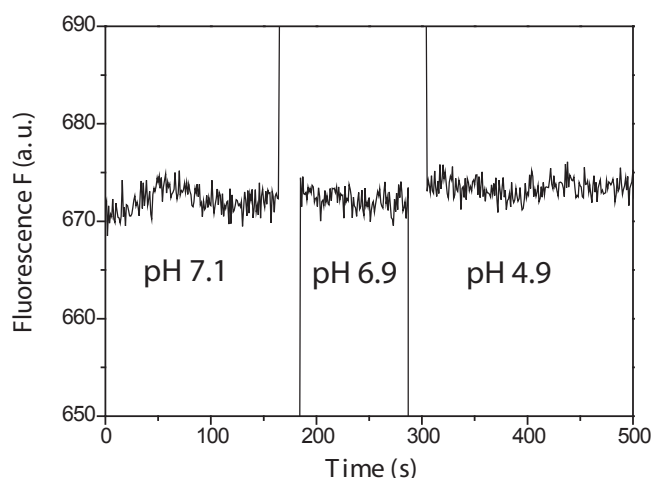


**Figure 5.5:** pH dependence of EtBr fluorescence. Time course of EtBr fluorescence in solution ( $12 \mu\text{M}$ ) remains constant when lowering the pH from 7.1 to 4.9. Excitation and emission slits were set to 3 nm and 10 nm, respectively.

from the accumulation of EtBr inside the liposomes. Without quencher, or with quencher inside and outside, only the first component as in Fig. 5.3 A is observed and saturates after 100 s (trace 2 in Fig. 5.3 B). With quencher,  $F_{total}$  is generally smaller because the contributions from  $F_{out}^{free}$  are reduced. The data show that EtBr is transported by TBsmr in a pH-dependant fashion while  $\Delta F$  arises from the formation of  $\Delta\text{pH}$ -dependant protein substrate complex formed during transport (Fig. 5.3 C).

### Other factors that could influence $\Delta F$ (pH, EtBr concentration, lipids)

Several control experiments were carried out to exclude other factors, which could also potentially contribute to  $\Delta F$ .

As a pH gradient is created by bR, the inside of the liposome is acidified, which could affect the fluorescence of EtBr inside. However, a pH titration of TBsmr in solution revealed no change in fluorescence intensity between pH 5 and pH 7 (Fig. 5.5), which is in agreement with its low  $\text{pK}_a$  values of 0.2 and 2 (Luedtke et al., 2005).

EtBr is hydrophobic (predicted LogP of 0.3, [www.molinspiration.com](http://www.molinspiration.com)) and partitions into the inner and outer membrane leaflet. This more hydrophobic environment could cause an EtBr fluorescence change but when *E. coli* lipids were titrated to a given amount of EtBr in solution (Fig. 5.6 A) no fluorescence increase was observed. When increasing the EtBr concentration in solution, a small fluorescence decay due to the formation of non-fluorescent dimers (Guenza and Cuniberti, 1988) was seen (Fig. 5.6 B). This effect

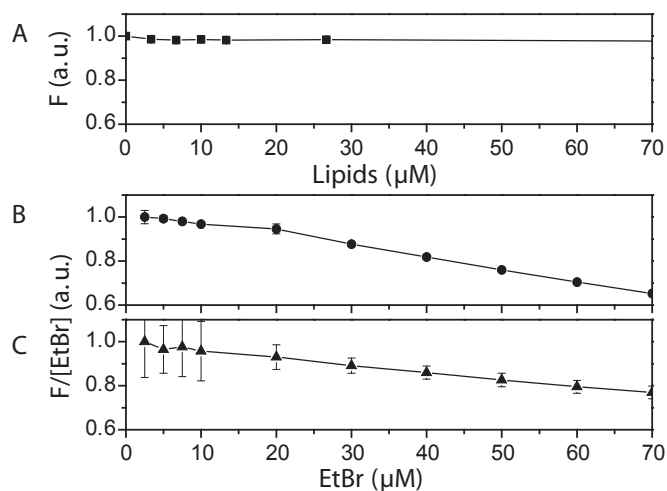


**Figure 5.6:** Fluorescence assay controls. A) Ethidium bromide fluorescence intensity does not increase when adding increasing amounts of *E. coli* lipids to EtBr (10  $\mu\text{M}$ ). B) Increasing the EtBr concentration causes a fluorescence reduction through the formation of non-fluorescent dimers. C) The same trend is observed in the presence of *E. coli* lipids (0.42 mM).

was also observed in the presence of liposomes (Fig. 5.6 C).

These controls show that neither pH nor binding to lipids nor concentration effects influence the EtBr fluorescence intensity in a way relevant for the interpretation of the experimental data in Fig. 5.3.

### Competitive inhibition with $\text{TPP}^+$

To compare the results to established radioactive methyl viologen transport assays, I have selected another substrate,  $\text{TPP}^+$ , for competitive inhibition of EtBr transport.  $\text{TPP}^+$  does not show an intrinsic fluorescence and is highly compatible with the experimental setup. The pH gradient generated by bR is stable over long periods of time, and measurements can be repeated multiple times. Therefore, only a single TBsmr sample per titration curve is required. Because  $\Delta F$  stems from an EtBr-TBsmr complex formed during the transport process,  $\Delta F_{\text{max}}$  can serve as a measure of EtBr transport activity. In Fig. 5.7 A,  $\Delta(\Delta F_{\text{max}})$  is plotted vs.  $[\text{TPP}^+]$ . A sigmoidal model was fitted to the data giving for  $\text{TPP}^+$  an  $\text{IC}_{50}$  of  $10 \pm 2 \mu\text{M}$ , which corresponds to a  $K_i$  of  $1.5 \mu\text{M}$ .

### $\Delta F_{\text{max}}$ depends on $[\text{EtBr}]$ and is described by a single site binding model

If the fluorescence changes observed for EtBr arise from substrate binding to TBsmr during the transport cycle, then it must be possible to determine a  $K_d$  for this substrate protein

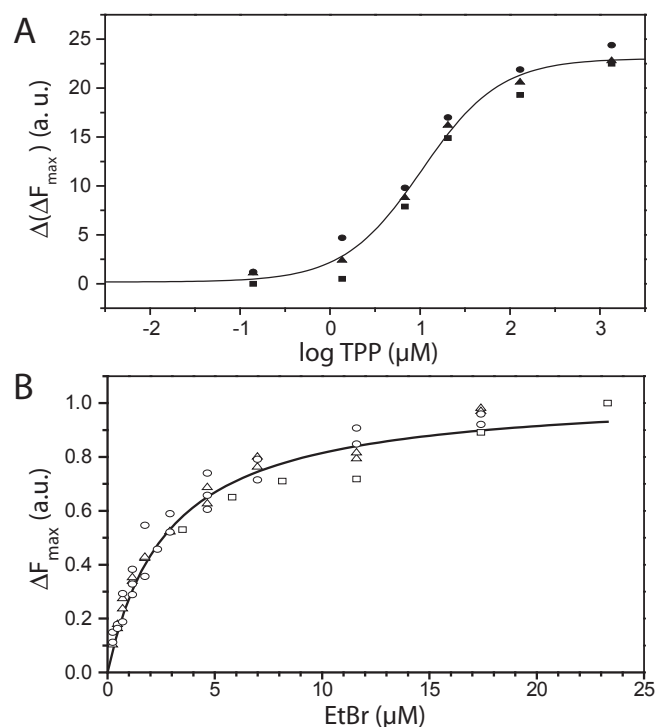


**Figure 5.7:** A) Transport of ethidium bromide is inhibited by  $\text{TPP}^+$ . The fluorescence change was measured in the presence of  $\text{TPP}^+$  and  $15 \mu\text{M}$  EtBr, and plotted as the change of fluorescence  $\Delta(\Delta F_{\max})$  vs  $\text{TPP}^+$ . An  $\text{IC}_{50}$  of  $10 \pm 2 \mu\text{M}$  and a  $K_i$  of  $1.5 \mu\text{M}$  was determined. ( $1 \mu\text{M}$  TBsmr,  $1.4 \mu\text{M}$  bR, triplicates as solid circles, squares and triangles). B) The changes in ethidium bromide fluorescence at different EtBr concentrations fitted to a single binding site model. Data were collected with  $1.4 \mu\text{M}$  bR and  $0.5 \mu\text{M}$  TBsmr (triangles),  $1.4 \mu\text{M}$  bR and  $1 \mu\text{M}$  TBsmr (squares) and  $0.7 \mu\text{M}$  bR and  $1 \mu\text{M}$  TBsmr (circles). Each data set was fitted to a single site weak binding equation and then rescaled so that the maximum predicted amplitude was equal to one. The mean  $K_d$  was  $2.6 \pm 0.2 \mu\text{M}$ . The curve represents a fit to the whole rescaled data set (The data for Fig. B were measured by Dr. M. Lorch).

complex. Fig. 5.7 B shows  $\Delta F_{\max}$  plotted against the EtBr concentration.  $\Delta F_{\max}$  saturates at  $\sim 10 \mu\text{M}$  EtBr. Neither altering the incident light intensity, nor increasing the number of transporters in the vesicles (by changing the TBsmr/lipid ratio) nor altering  $\Delta\text{pH}$  (by changing the bR/lipid ratio) had an effect on the hyperbolic shape of these binding curves. The data fitted well to a single site binding equation yielding a  $K_d$  of  $2.6 \pm 0.2 \mu\text{M}$  (Fig. 5.7 B).

### Anisotropy measurement

To further characterize binding of EtBr to TBsmr during transport, I have performed “steady-state” fluorescence anisotropy measurements. In analogy to Eq. 2.4, the observed average anisotropy  $r_{\text{total}}$  consists of contributions from the equilibrium state at the begin-

ning of the experiment and of contributions from EtBr bound to TBsmr in the presence of  $\Delta\text{pH}$ . The anisotropy is given as:

$$r_{total} = \Delta f \times \Delta r + f_0 \times r_0 \quad (5.4)$$

where  $f_0$ ,  $\Delta f$  stand for the fractional fluorescence intensities and  $r_0$ ,  $\Delta r$  for the corresponding anisotropies without and with  $\Delta\text{pH}$ . Eq. 5.4 is solved for  $\Delta r$  which corresponds to the anisotropy of EtBr bound to TBsmr during the transport cycle:

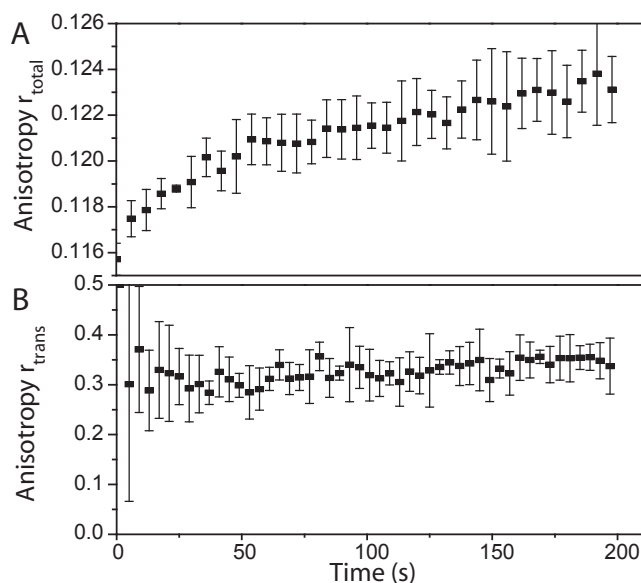
$$r_{trans} = \Delta r = \frac{\Delta F_{\parallel} - \Delta F_{\perp}}{\Delta F_{\parallel} - \Delta F_{\perp}} \quad (5.5)$$

Fig. 5.8 A shows the increase of  $r_{total}$  with time and follows in principle the time course of  $F_{total}$  in Fig. 5.3 A. The total anisotropy starts from its equilibrium value ( $\Delta\text{pH}=0$ ), increases when  $\Delta\text{pH}$  is activated and saturates above 100 s when a steady state is reached. The more EtBr-TBsmr complexes form, the higher will be  $r_{total}$ . The actual anisotropy of EtBr bound to TBsmr was determined by calculating  $r_{trans}$  (Eq. 5.5) which is shown in Fig. 5.8 B. As  $r_{trans}$  does not depend on the number of complexes formed, it remains constant over time with a relatively high value of  $0.33 \pm 0.04$ . The large error of the data points below 25 s is caused by the small signal-to-noise ratio of their fluorescence intensities. They have been ignored for calculating the average value of  $r_{trans}$ .

## 5.3 Discussion

### 5.3.1 Formation of an intermediate substrate-protein complex

Changes of the intrinsic EtBr fluorescence properties were used to report on the proton dependant substrate transport by TBsmr. The creation of a pH gradient causes an increase of the equilibrium fluorescence  $F_0$  by  $\Delta F$  (Fig. 5.3 A, traces 1 and 2). This fluorescence increase disappears when adding nigericin (Fig. 5.3 A, trace 3) or CCCP (Fig. 5.3 A, trace 5), which collapses transmembrane pH gradients or the proton motive force. These controls prove that  $\Delta F$  is  $\Delta\text{pH}$  dependant. Another control experiment has been carried out to exclude  $\Delta\text{pH}$ -dependant unspecific binding: a single, highly conserved Glu residue in the first helix is essential for transport in all SMR proteins (Ninio et al., 2001). Therefore, I have introduced an E13A mutation in TBsmr and found  $\Delta F$  to be 0, which proves that  $\Delta F$  is caused by TBsmr (Fig. 5.3A, trace 4). The observation, that the maximum



**Figure 5.8:** EtBr fluorescence anisotropy. A) The total fluorescence anisotropy is calculated from the measured perpendicular ( $F_{\perp}$ ) and parallel intensities ( $F_{\parallel}$ ). B) Corrected for the fluorescence intensities at time point zero ( $F_{\perp}-F_{\perp}^0, F_{\parallel}-F_{\parallel}^0$ ) the anisotropy of substrate during  $\Delta$ pH is obtained. The anisotropy remained constant over time with mean value of  $r=0.33 \pm 0.04$ .

value  $\Delta F_{max}$  doubles when the number of transport proteins within the liposome is doubled, led me to the conclusion that  $\Delta F$  arises from the  $\Delta$ pH-dependant formation of a substrate-protein complex (Fig. 5.3 A).

During the TBsmr transport cycle, several events such as EtBr binding, translocation, release and accumulation in the membrane and the lumen of the liposomes take place. All of them could involve alterations of the substrate environment, which potentially contribute to changes in total fluorescence intensity  $\Delta F$ . In analogy to Eq. 5.1,  $\Delta F$  can be separated in potential contributions from EtBr free in solution, bound to TBsmr and non-specifically bound to the liposomes, which could all change when  $\Delta$ pH is generated:

$$\Delta F = \Delta F^{free} + \Delta F^{bound} + \Delta F_{liposome}^{bound} \quad (5.6)$$

In the following, these three contributions will be discussed in more detail.

**Contributions from  $\Delta F_{liposome}^{bound}$**  The fluorescence properties of EtBr are not altered when bound to lipids, as demonstrated in Fig. 5.6 A, and therefore, EtBr/liposome binding makes no contribution to  $\Delta F$  and  $\Delta F_{liposome}^{bound}$ . EtBr (LogP=0.3) probably behaves like doxorubicin (LogP=0.6), another multidrug transporter substrate, which has a similar hy-

drophobicity and accumulates in the interface region of the lipids near the charged head groups as shown by solid-state NMR spectroscopy (Siarheyeva et al., 2006). The interface region is much less hydrophobic than the acyl chains (Subczynski et al., 1994) which explains why no fluorescence change is detected on EtBr binding.

**Contributions from  $\Delta F^{free}$**  At the beginning of the experiment without a proton gradient, the EtBr concentration on the inside and outside is equal. During illumination, the liposomes are continuously acidified on the inside, which could create a pH-dependant change of EtBr fluorescence on the inside. It was experimentally verified that EtBr fluorescence is independent of pH in the range of pH 5 - 7 (Fig. 5.5). This is consistent with measurements reported by others, where it was shown that EtBr fluorescence only changes near its pKa of 0.2 and 2 (Luedtke et al., 2005). So the experimental pH differences between the inside and outside of the proteoliposomes have no significant effect onto the fluorescence of free EtBr ( $\Delta F^{free} = 0$ ).

The increasing concentration of EtBr within the lumen could change its fluorescence. However, it will eventually cause a slight fluorescence quenching due to the formation of non-fluorescent dimers (Guenza and Cuniberti, 1988), as shown in Fig. 5.6 B, C. Therefore, EtBr concentration effects can be ruled out as a source of the observed fluorescence increases.

**Contributions from  $\Delta F^{bound}$**  The data clearly show that  $\Delta F$  arises from the  $\Delta$ pH-dependant formation of an EtBr-TBsmr complex. Such a complex could be either the formation of an intermediate state, a TBsmr conformation with an increased binding capacity, or simply arise from binding of EtBr to inversely oriented TBsmr inside the vesicles. In the first case,  $\Delta F$  is caused by a change in environment of EtBr, while in the second and third case, it would be simply the result of a greater capacity to bind substrate.

An increase in binding capacity does not explain the data for two reasons: 1) It could be shown that EtBr is actually transported, which requires more than just a binding step (Fig. 5.3 B). 2) The data in Fig. 5.7 B are well described with a single-site binding model, while an increase in binding capacity would be equivalent with multiple binding sites. This conclusion is consistent with results for LacY, in which no change in binding capacity was found in the presence of an  $H^+$  electrochemical gradient (Guan and Kaback, 2004).

In the experiment, TBsmr is most likely oriented both ways within the membrane. When EtBr is transported into the vesicles, it could bind to inversely oriented transporters

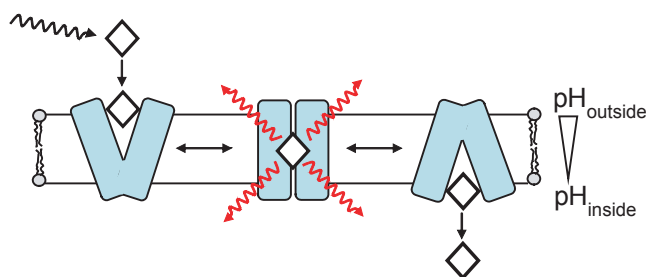


**Figure 5.9:** Intermediate state model. In the presence of a pH gradient, EtBr is translocated across the membrane by TBsmr. A transition between the outward and inward facing binding site involves an intermediate state in which EtBr shows enhanced fluorescence. It is postulated that EtBr is not accessible to water molecules, which quench its fluorescence in solution. EtBr bound to this occluded state is characterized by a  $K_d$  of  $2.6 \pm 0.2 \mu\text{M}$  and a high anisotropy of  $r_{\text{trans}}=0.33 \pm 0.04$ .

and cause a fluorescence increase  $\Delta F_{\text{max}}$ . However, the experiment starts from an equilibrium situation with  $[\text{EtBr}]_{\text{in}}=[\text{EtBr}]_{\text{out}}$ . When increasing this initial substrate concentration,  $\Delta F_{\text{max}}$  should become smaller, as more and more binding sites would be already occupied before  $\Delta\text{pH}$  is activated and transport into the liposomes takes place. However, Fig. 5.7 B shows, that actually the opposite effect is observed.

Since these simple binding models can be ruled out and a conformational change is needed to switch the binding pocket into a release site, an intermediate state is the simplest explanation to explain  $\Delta F$ :

$$\Delta F = \Delta F^{\text{bound}} = \Delta F_{\text{trans}} \quad (5.7)$$

During transport, EtBr experiences within the protein a more hydrophobic environment in form of nonpolar residues and reduced water accessibility. It has been shown by spin labeling (Koteiche et al., 2003) and by chemical cross linking (Soskine et al., 2002) that the equilibrium state binding pocket of EmrE is water accessible. Therefore, the proposed intermediate can be explained by a temporarily occluded state where EtBr is not accessible on either side to water molecules, which strongly quench its fluorescence (Olmsted and Kearns, 1977). A model summarizing the findings is shown in Fig. 5.9: To perform substrate transport, a  $\Delta\text{pH}$ -dependant conformational change takes place, in which EtBr shows enhanced fluorescence because it is shielded from water molecules.

Besides energized uptake, transport can take place by substrate exchange. Since the experiment starts with equal concentrations of EtBr inside the liposomes and in the bulk solution, there should be a continuous exchange of substrate. Since there is no indication

of a second substrate pathway (Yerushalmi and Schuldiner, 2000a), the exchange should also proceed via the proposed occluded state. Therefore, the fluorescence increase can only be observed if the active transport is faster than substrate exchange. This has been shown for EmrE where energized transport of methyl viologen is up to 15 times faster than substrate exchange (Yerushalmi and Schuldiner, 2000b).

### 5.3.2 Characterization of an intermediate substrate-protein complex

Several experiments were carried out to further strengthen the conclusions and to characterize the TBsmr transport cycle intermediate state. In analogy to methyl viologen transport assays, it is possible to inhibit the transport by TBsmr by another substrate such as TPP<sup>+</sup> (Fig. 5.7 A). The resulting IC<sub>50</sub> (10 μM) and K<sub>i</sub> (1.5 μM) seem rather high compared to a K<sub>i</sub> of 30 nM and IC<sub>50</sub> of 35 nM known for EmrE but are consistent with previous results of TBsmr in a methyl viologen transport assays (IC<sub>50</sub>= 4.5 μM, K<sub>i</sub>=4.3 μM) (Ninio et al., 2001). For this comparison, the K<sub>i</sub> values were calculated by us from the data reported by Schuldiner and co-workers (Ninio et al., 2001; Yerushalmi et al., 1995).

The observed hyperbolic increase in  $\Delta F_{max}$  with increasing EtBr concentration can be analyzed in terms of a single site binding equation (Fig. 5.7 B). This suggests that  $\Delta F$  arises from a single intermediate state and not from multiple binding events. The determined K<sub>d</sub> of 2.6 μM corresponds to a steady state between EtBr free and bound to the intermediate state.

The formation of this intermediate complex is also supported by fluorescence anisotropy measurements. Although the total anisotropy of free and bound ethidium increases slightly (Fig. 5.8 A), the fluorescence anisotropy of the substrate-protein complex does not change during the experiment, supporting a single state with immobile substrate (Fig. 5.8 B). The high anisotropy  $r_{trans}=0.33\pm 0.04$  of ethidium in the complex is consistent with a tightly bound, rigid substrate. I compare EtBr intercalated in DNA, which has been well studied: At a high viscosity of  $\eta=16$  mPa·s, EtBr has a similarly high anisotropy of  $\sim 0.3$ . Depending on the DNA length, the anisotropy decreases to  $\sim 0.2$  (97 bp) and  $\sim 0.1$  (32 bp) at a viscosity of  $\eta=1$  mPa·s, which is attributed to internal motions for the larger DNA and helix tumbling for the shorter DNA (Genest et al., 1985). Considering the size of the protein in comparison to the DNA, the decrease of the anisotropy compared to a theoret-

ical value of  $r=0.4$  is attributed to wobbling of the drug in the binding site and to internal motions of the protein and the whole liposome.

### 5.3.3 Relevance for transport models

I have presented experimental data on changes of the intrinsic fluorescence properties of ethidium bromide while being transported through the membrane by TBsmr. The combination of bacteriorhodopsin to create a stable pH gradient over a long period of time with EtBr is especially convenient, as only a standard fluorescence spectrometer is needed. Experiments can be repeated many times on the same sample, enabling time-efficient titration studies as shown in Fig. 5.7. It is a useful complement to radioactive measurements for non-fluorescent substrates.

The data suggest that TBsmr and also EmrE are undergoing conformational changes in the presence of a pH gradient, as monitored indirectly by changes of the EtBr environment. In a preliminary report of this experimental setup (Lorch et al., 2005b), EmrE did behave similar to TBsmr with an intermediate state  $K_d$  of  $4.2 \mu\text{M}$ . These findings show the existence of a transport cycle intermediate in the SMR proteins, which only forms in the presence of  $\Delta\text{pH}$ .

The occluded substrate-protein complex found here represents an intermediate state in the alternating access model proposed for EmrE (Fleishman et al., 2006) in which the protein switches between conformations with alternate access to the inside or the outside (Fig. 5.10). It is similar to the alternating access model proposed for another secondary transporter, LacY (Kaback et al., 2007), where a release of water molecules and a closing of the binding pocket has been observed in molecular dynamics (MD) simulations (Yin et al., 2006b). A transport intermediate state between open conformations accessible to either side has also been found for the  $\text{Na}^+ \text{-K}^+$  ATPase, in which potassium ions temporarily become occluded (Beauge and Glynn, 1979). Therefore, the transport cycle based on the published alternate-access model (Fleishman et al., 2006) (Fig. 1.7) should include an additional intermediate state (Fig. 5.9).

## 5.4 Conclusion

The EmrE homologue TBsmr has been co-reconstituted with the light-driven proton pump bacteriorhodopsin. The generation of a stable pH gradient and simultaneous excitation

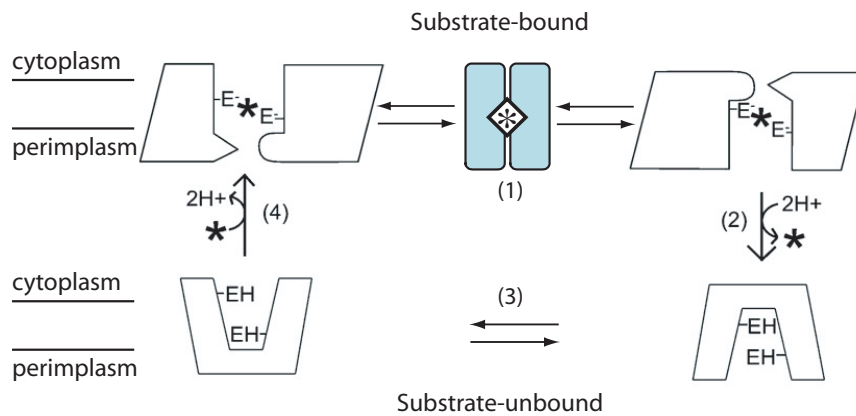


**Figure 5.10:** Proposed alternate-access mechanism for proton-coupled translocation of substrates by SMR proteins including the occluded substrate-protein complex in blue. (1) Two substrate-bound forms of the protein interconvert between conformations, in which the substrate, marked by an asterisk (\*), faces the cytoplasm or the periplasm due to conformational changes through an occluded intermediate state (blue). (2) In the periplasmic-facing conformation, the substrate is supplanted by the binding of two protons to the Glu14 positions (marked by E-) on both monomers, thus driving the equilibrium towards substrate translocation. (3) A conformational change reorients the binding site towards the cytoplasm. (4) Substrate binding on the cytoplasmic side forces the protons out of the translocation chamber into the cytoplasm (adapted from Fleishman et al., 2006).

of EtBr fluorescence did reveal the formation of a transient, occluded substrate-protein complex during the transport cycle.

The application of NMR, FTIR or electron paramagnetic resonance (EPR) methods with sample illumination to SMR proteins co-reconstituted with bacteriorhodopsin will allow steady-state investigations of this transport cycle intermediate in more detail. The kinetics of its formation could be followed by time-resolved fluorescence spectroscopy in which a pH gradient is generated using caged protons (Barth and Corrie, 2002).

# 6 Liquid-state NMR study on detergent-solubilized TBsmr

## 6.1 Introduction

The previous chapter described how a new transport cycle intermediate could be found and was characterized by fluorescence changes of the substrate. It should be possible to identify and observe changes in key amino acids in the protein as they interact with the substrate EtBr. Liquid-state NMR is an ideal technique to monitor such protein-ligand interactions by chemical shift mapping (Shuker et al., 1996). Spectral changes provide residue-specific information, for example about the binding of a ligand. Even though detergent-solubilized TBsmr is not able to complete the full transport cycle, it could still bind EtBr. The bound ligand will perturb the environment of the neighbouring amino acids and thus change the chemical shift of those nuclei. An assignment of the resonances is needed to correlate the changes in the HSQC spectrum to specific residues in the protein. High quality spectra and a stability of the protein in detergent for  $\sim 1$  week are necessary for the 3D experiments (Salzmann et al., 1999) used for the assignment of the signals in the HSQC spectrum. The promising stability of TBsmr in the detergent Fos-12 and well resolved spectra of the homologue Smr in that detergent Krueger-Koplin et al. (2004) prompted me to study the detergent-solubilized TBsmr by liquid-state NMR.

## 6.2 Results and discussion

### 6.2.1 NMR sample optimization

For membrane proteins, it has been shown that the choice of the detergent is critical for the quality of the spectrum (Krueger-Koplin et al., 2004). For example, the detergents Fos-12 and LPPG have been shown to give well resolved spectra (Krueger-Koplin et al.,

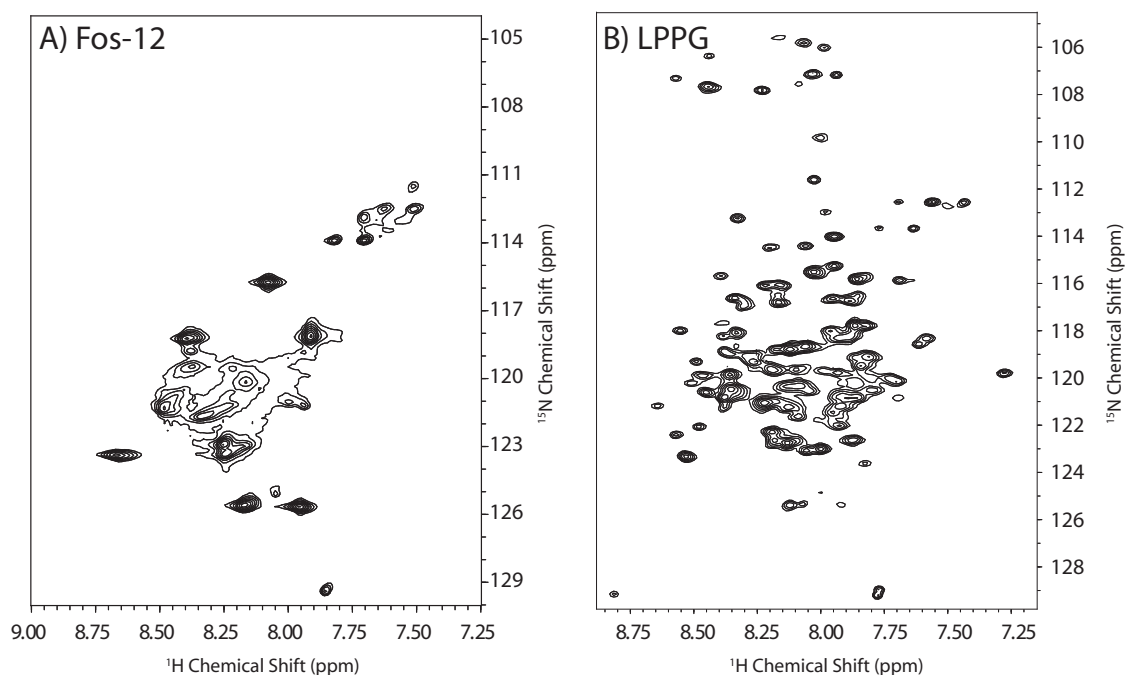


**Figure 6.1:** 2D  $^1\text{H}$ - $^{15}\text{N}$  HSQC NMR spectra of uniformly  $^{13}\text{C}$ ,  $^{15}\text{N}$  labeled TBsmr in different detergents. Shown are A) 0.35 mM TBsmr, 15 mM Tris pH 7.5, 0.1% (w/v) Fos-12, 23 °C and B) 0.8 mM TBsmr, 15 mM Hepes pH 7.5, 100 mM NaCl, 2 mM TCEP, 10% (w/v) LPPG.

2004), leading to a complete assignment of Smr in LPPG (Poget et al., 2006).

Since TBsmr was stable in the detergent Fos-12 for  $\geq 2$  weeks (Fig. 3.6), 2D  $^1\text{H}$ - $^{15}\text{N}$  TROSY-HSQC NMR spectra of TBsmr in Fos-12 and LPPG were recorded to assess the influence of those detergents on the sample properties. The resulting spectra are shown in Fig. 6.1. The TBsmr construct including the tag should give rise to 141 cross peaks in these spectra. In the spectrum with LPPG, 73% of the expected cross peaks could be resolved. Most of them were uniform in intensity but several cross peaks had the shape or intensity of multiple overlaid resonances.

The protein-detergent complexes in Fos-12 and LPPG were larger than 100 kDa as determined by gelfiltration and being able to concentrate the protein with a MWCO of 100 kDa. The remarkable high quality of the NMR spectrum of the TBsmr in the detergent LPPG implied slower relaxation rate as expected for such large protein-detergent complexes. This behaviour was also observed for Smr in LPPG and, based on rotation correlation time measurements, was attributed to the free rotation of the small 15 kDa protein within the micelle (Krueger-Koplin et al., 2004).

In agreement with the observations of Krueger-Koplin et al., the spectra quality in-

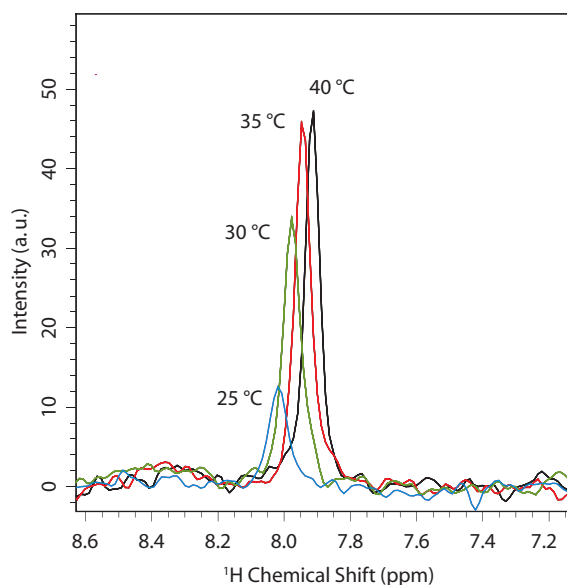


**Figure 6.2:** Influence of the temperature on the amide proton signal intensity of TBsmr in a liquid-state NMR experiment. 1D slice at 110 ppm in the  $^{15}\text{N}$  dimension of 2D  $^1\text{H}$ - $^{15}\text{N}$  TROSY-HSQC NMR experiment.

creased with the detergent concentration and reached a maximum at 10% (w/v). The final detergent concentration corresponds to a  $\sim 1.2$  mM micellar concentration, which suggests that a 1:1 protein - detergent micelle ratio enhanced the spectrum quality. The estimate of the LPPG micellar concentration is based on the assumption that LPPG has the same aggregation number, 160 detergent molecules per micelle, as 1-myristoyl-2-hydroxy-sn-glycero-3-[phospho-RAC-(1-glycerol)] (LMPG) (Rankin et al., 1999).

Attempts to improve the sensitivity of the NMR experiments by increasing the measurement temperature were not successful. The temperature had a significant influence on the spectral quality and lifetime of TBsmr in LPPG. The intensity and line width of an amide proton resonance in a slice at 110 ppm in the  $^{15}\text{N}$  dimension of 2D  $^1\text{H}$ - $^{15}\text{N}$  TROSY-HSQC NMR spectra was used as an indicator of this influence. As seen in Fig. 6.2, both the signal intensity and proton line width improved with temperature and an optimum was found at 40 °C. However, the stability of TBsmr was compromised at temperatures above 30 °C. To evaluate the sample stability at different temperatures, 2D  $^1\text{H}$ - $^{15}\text{N}$  TROSY-HSQC NMR spectra were recorded of TBsmr before and after incubating the sample for 5 days at 25, 30, 35 and 40 °C. At 25 and 30 °C, only small changes in the chemical shift and intensity of the resonances were observed after 5 days. However, at higher temperatures, the position of many resonances changed. In general, the signal in-

tensity decreased and some resonances disappeared completely. Therefore, the 3D NMR experiments for assignment were recorded at 30 °C. Compared to the Smr protein which was stable without salt at 47 °C (Krueger-Koplin et al., 2004), the optimum condition to keep TBsmr stable was a salt concentration of 100 mM NaCl and 30 °C. The reduced stability of TBsmr is probably caused by its high tendency to aggregate.

Even though the spectrum of TBsmr were much better resolved in LPPG compared to Fos-12, the narrow distribution of the cross peaks in the proton dimension of the HSQC spectra are an indication of a non-natively folded TBsmr in LPPG. The dispersion of the cross peaks in the NMR spectra are similar to the ones of non-functional Smr in LPPG (Poget et al., 2006, 2007). Just recently, an NMR study of Smr capable of binding substrate was published (Poget and Girvin, 2007). There a significantly improved dispersion of the proton chemical shifts could be correlated to functional Smr. However, these information were published after the experiments on TBsmr.

### 6.2.2 Backbone resonance assignment

To assign the backbone of the protein, the following 3D experiments, TROSY-HNCO/TROSY-HN(CA)CO, TROSY-HNCA/TROSY-HN(CO)CA and TROSY-HNCACB were measured. On the basis of these experiment, 42% (56 out of 134) of the amide and  $C\alpha$  atoms could be assigned tentatively (Fig. 6.3) and are summarized in Tab. A.5. The assigned nuclei are dispersed throughout the protein sequence, covering most of TMS 1 and parts of TMS 2–4. The main problem with the remaining unassigned resonances was the ambiguity of the sequential peaks in the HNCA spectrum. The HNCACB experiment helped to resolve some ambiguities but in general the sensitivity of this experiment was too low to detect most  $C\beta$  peaks. A representative strip plot of the HNCA used for the sequential assignment is given in Fig. 6.5. The assignment of connected resonances to residues in the protein sequence was based on the probability of a correct match between the probable amino acids of these sequential peaks and the protein sequence (Tab. A.4). The probability for a correct alignment was calculated by the software CARA based on statistical distribution of the chemical shifts (Keller, 2004). For a 100% certain assignment, anchor point in the sequence would be necessary which could be obtained e.g. by a combinatorial isotope labeling scheme (Trbovic et al., 2005). Even though a complete backbone assignment was possible for Smr (Poget et al., 2006), only a partial assignment could be achieved for TBsmr (Fig. 6.4) due to the high overlap of the resonances even in the 3D experiments and the reduced stability of TBsmr compared to Smr.

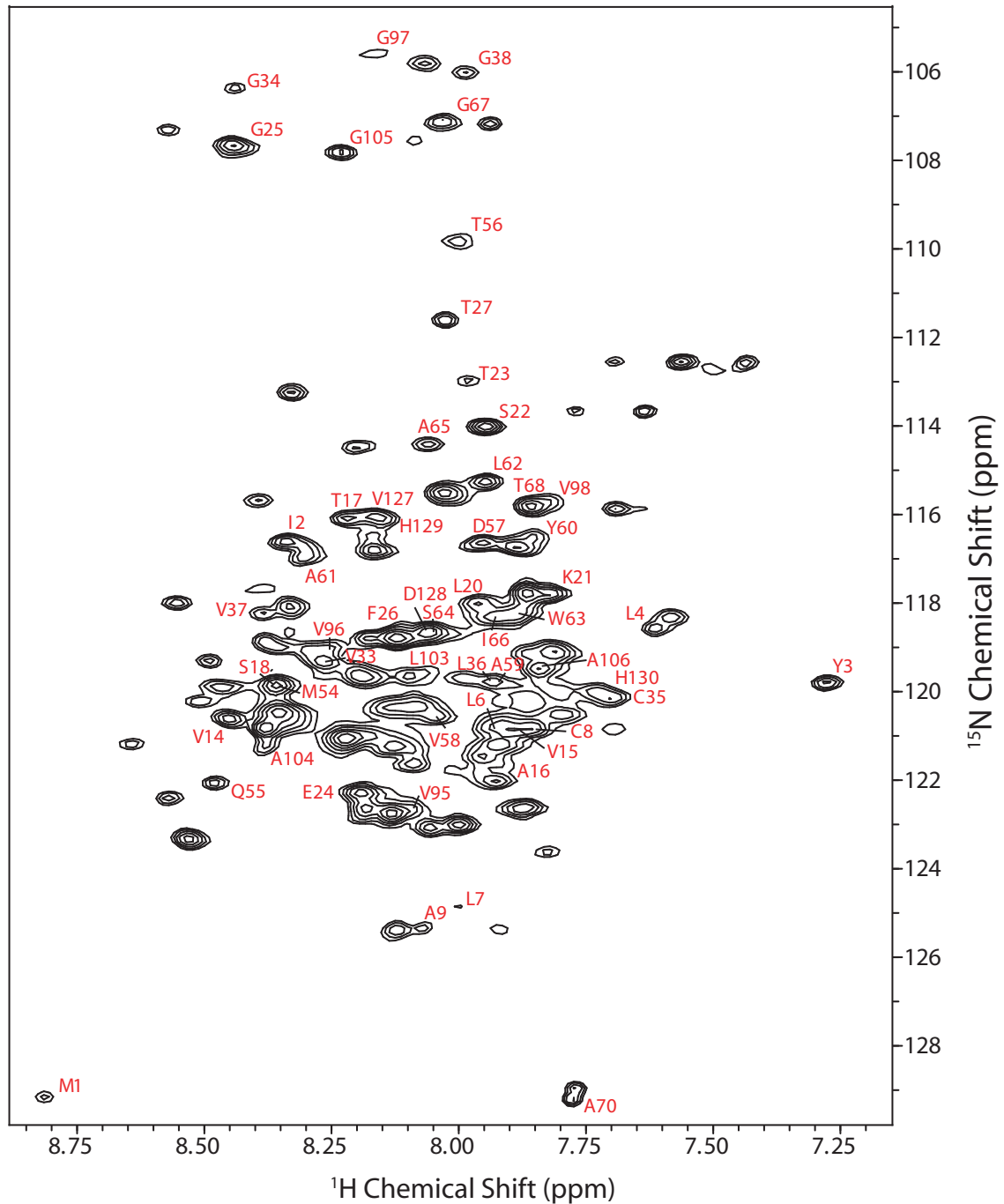


**Figure 6.3:**  $^1\text{H}$ - $^{15}\text{N}$  TROSY HSQC spectrum of 0.8 mM uniformly  $^{13}\text{C}$ ,  $^{15}\text{N}$  labeled TBsmr in 15 mM HEPES pH 7.5, 100 mM NaCl, 2 mM TCEP, 10% LPPG (w/v). The spectrum was recorded at 30 °C on an Avance 700 MHz spectrometer with 8 scans per increments and 512 complex points in the indirect dimension. Backbone resonance assignments are indicated by the amino acid type and the sequence number.

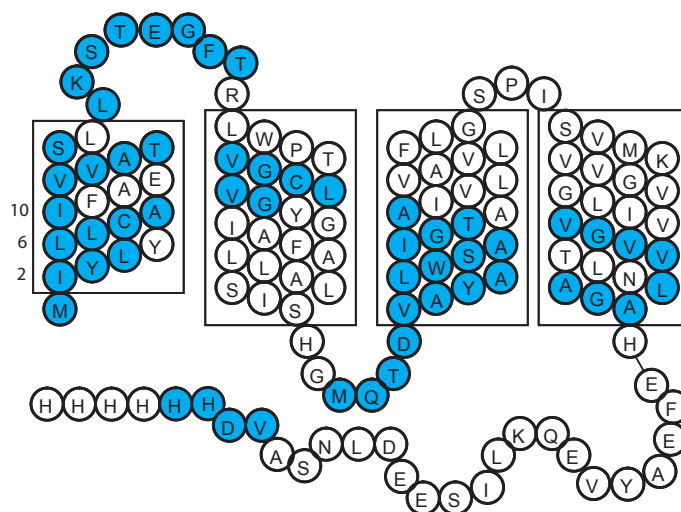


**Figure 6.4:** Topology model of TBsmr with tentatively assigned residues in blue.

### 6.2.3 EtBr interacts non-specifically with TBsmr in detergent

Based on the tentative assignment of 42% of the backbone resonances, 2D  $^1\text{H}$  - $^{15}\text{N}$  TROSY-HSQC NMR spectra of  $^{15}\text{N}$  labeled TBsmr in the presence and absence of the substrate EtBr were recorded to map the chemical shift changes on the protein sequence (Fig. 6.6). The shifts were dispersed through the whole protein in the transmembrane regions and the loops (M1, N-terminus; T23, TMS 1; G25, loop 1; T56, loop 2; Y60, TMS 3; G97, TMS 4) indicating that the induced chemical shifts are not caused by specific binding. Due to the hydrophobic nature of EtBr (predicted LogP of 0.3, [www.molinspiration.com](http://www.molinspiration.com)), it is likely that EtBr will partition into the micelles and thereby induces changes in the protein. This conclusion is supported by the shifts of both sidechain tryptophan W30 and W63 N $\epsilon$  residues, even though only W63 is implicated in substrate binding (Elbaz et al., 2005).

### 6.2.4 TBsmr is monomeric in LPPG

The oligomeric state of TBsmr in LPPG was analysed by laser induced liquid beam ionization/desorption mass spectrometry (LILBID-MS) under soft desorption condition (Morgner et al., 2007) and found to be mainly monomeric (Fig. 6.7). Since the SMR proteins have to be dimers to bind substrate with high affinity (Rotem et al., 2001), it is likely that TBsmr is not functional. An additional binding assay could be used as an independent control for the activity of TBsmr in LPPG. However, the standard radioactive

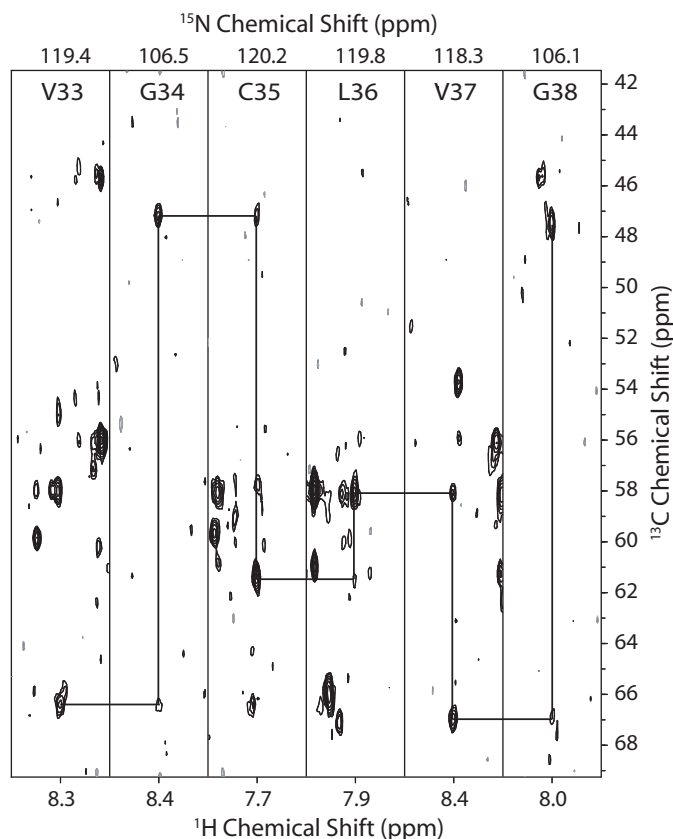


**Figure 6.5:** Representative strip plot of the TROSY-HNCA experiment. The intra-residue connectivities from the  $C\alpha^{(i)}$  to the  $\alpha^{(i-1)}$ , and inter-residue connectivities to  $C\alpha^{(i)}$  in the preceding residue's strip are indicated.

TPP<sup>+</sup> binding assay, used to assess the activity of EmrE (Muth and Schuldiner, 2000), did not work for TBsmr (Ninio et al., 2001) and thus could not be used. Even though Smr forms functional dimers in LPPG (Poget et al., 2006), it is also not functional because it has a strongly reduced binding affinity for TPP<sup>+</sup> in LPPG compared to Smr in the better membrane mimetic bicelles (Poget et al., 2007). The strong influence of the membrane mimetic on the conformation of SMR proteins was also seen in changes of the backbone chemical shifts of Smr and TBsmr when moving to different membrane mimetic environments (Tab. 7.1). Such conformational changes in detergent have also been detected in fluorescence quenching experiments (Federkeil et al., 2003). Therefore it can be concluded, that LPPG is suitable for high resolution NMR spectra but seems not to be able to keep the SMR proteins in a functional state. Due to these results a further assignment of TBsmr in LPPG was not pursued.

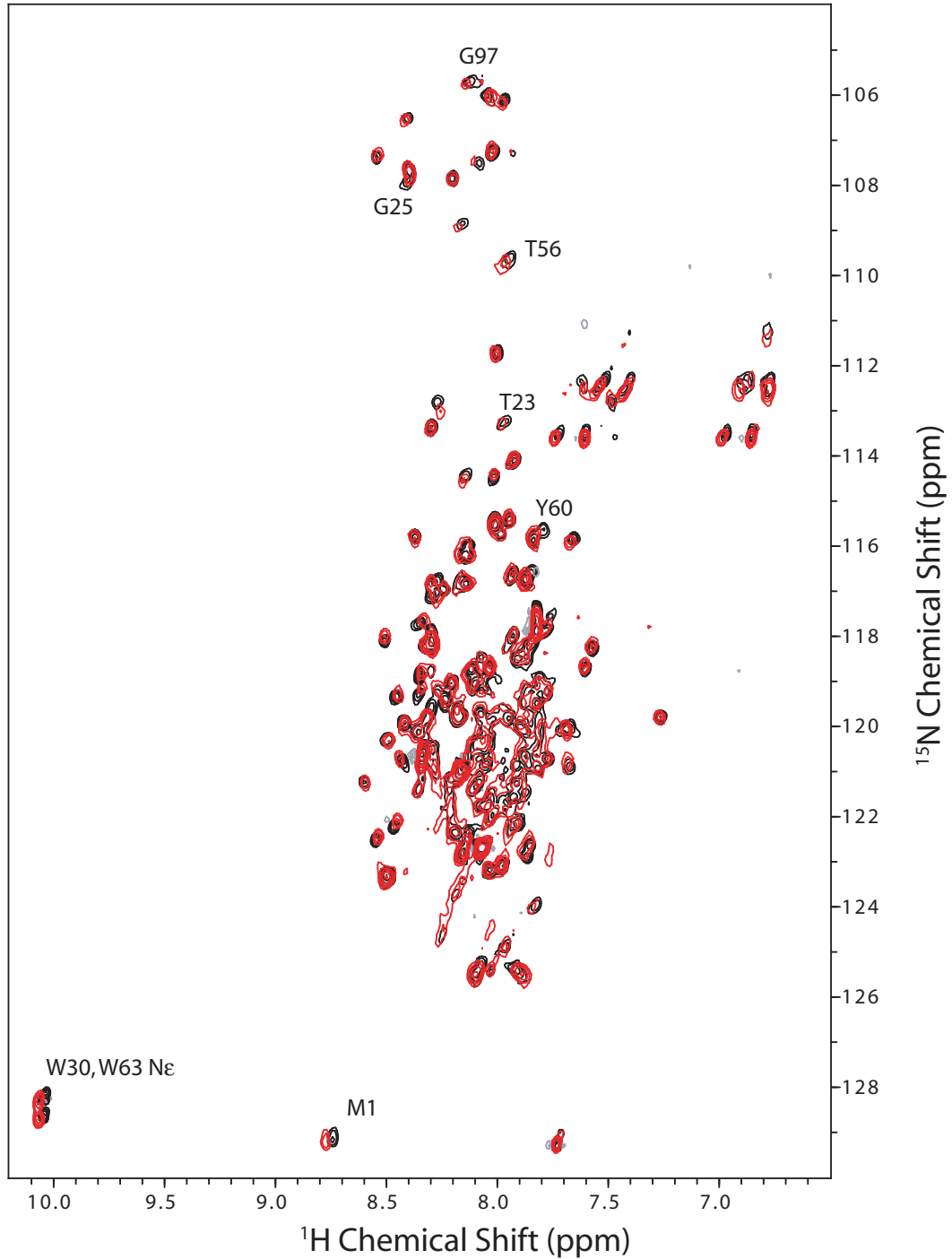


**Figure 6.6:** 2D  $^1\text{H}$ - $^{15}\text{N}$  HSQC spectrum of TBsmr with and without EtBr. Shown in black: 0.3 mM TBsmr, 15 mM potassium phosphate buffer pH 7.5, 2% (w/v) LPPG, 40 °C, and in red: +1 mM EtBr.

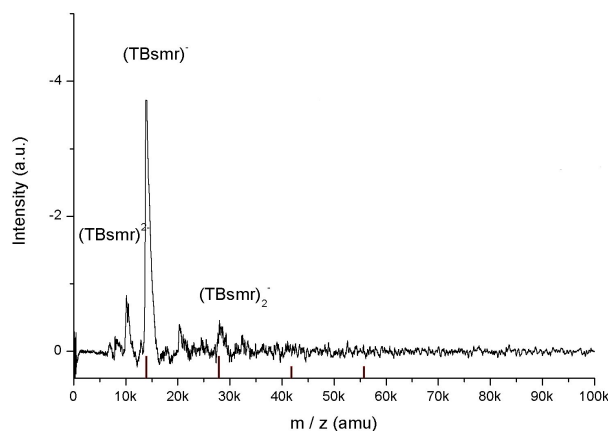


**Figure 6.7:** LILBID mass spectroscopy of TBsmr in LPPG. The spectrum is consistent with doubly (7 kDa) and singly charged (14 kDa) ions of monomeric TBsmr, and singly ionized dimers (28 kDa). Before the measurement, the sample was diluted 1:10 with water to a final concentration of 2.8  $\mu\text{M}$  (1 mM Tris pH 7.5, 0.8% LPPG). The spectrum was measured by Nina Morgner (Prof. Brutschy, Institute of Physical and Theoretical Chemistry, J. W. Goethe-University Frankfurt).

### 6.3 Conclusion

In agreement with previous studies (Krueger-Koplin et al., 2004; Poget et al., 2006), the detergent LPPG was found to be highly suitable for liquid-state NMR experiments on the membrane protein TBsmr and 42% of the residues could be assigned tentatively. However, the detergent was not able to keep neither TBsmr nor Smr (Poget and Girvin, 2007) natively folded and thus no specific interaction between TBsmr and the substrate EtBr could be determined. These observations were confirmed by LILBID mass spectrometry which found TBsmr to be mainly in the non-functional monomeric state in the detergent LPPG. The strong influence of the membrane mimetic on the protein function, prompted me to conduct further studies on protein-substrate interactions with solid-state NMR on TBsmr in proteoliposomes.

# 7 Solid-state NMR study on TBsmr proteoliposomes

## 7.1 Introduction

Instead of looking at the whole protein, it is often useful to focus on specific molecular segments. Even the conformation of a single residue may bear functionally relevant information. Besides the essential E14 in EmrE, the aromatic residues W63, Y40, and Y60 have been shown to be directly involved in drug binding and transport (Rotem et al., 2006; Elbaz et al., 2005). As TBsmr only contains two tryptophans, it offers the possibility to study their role in substrate binding by solid-state NMR.

The aim of the work presented in this chapter was to gain information about specific amino acids involved in the drug recognition mechanism of TBsmr. To this end, different isotope labeling schemes for solid-state NMR experiments were tested to improve the quality the spectra to identify and characterize key residues in the binding pocket of TBsmr. Selective isotope labeling of the conserved W63, which is located near the binding pocket, was used to probe the chemical environment of that residue with and without substrate.

## 7.2 Results

### 7.2.1 $^{15}\text{N}$ solid-state NMR experiments

TBsmr was expressed in auxotrophic *E. coli* CT19 cells (Waugh, 1996) which are auxotrophs for leucine, tyrosine and tryptophan (for the genotype see Tab. A.3) in defined media (Muchmore et al., 1989), supplemented with  $^{15}\text{N}$  isotope labeled leucine, tyrosine or tryptophan, to obtain TBsmr in which a single type of amino acid is selectively labeled. The protein was found in the membrane fraction, solubilized with detergent and puri-

fied by Ni affinity chromatography. The detergent-solubilized TBsmr was reconstituted in DOPC or *E. coli* total lipids by rapid dilution or detergent removal with polystyrene beads.

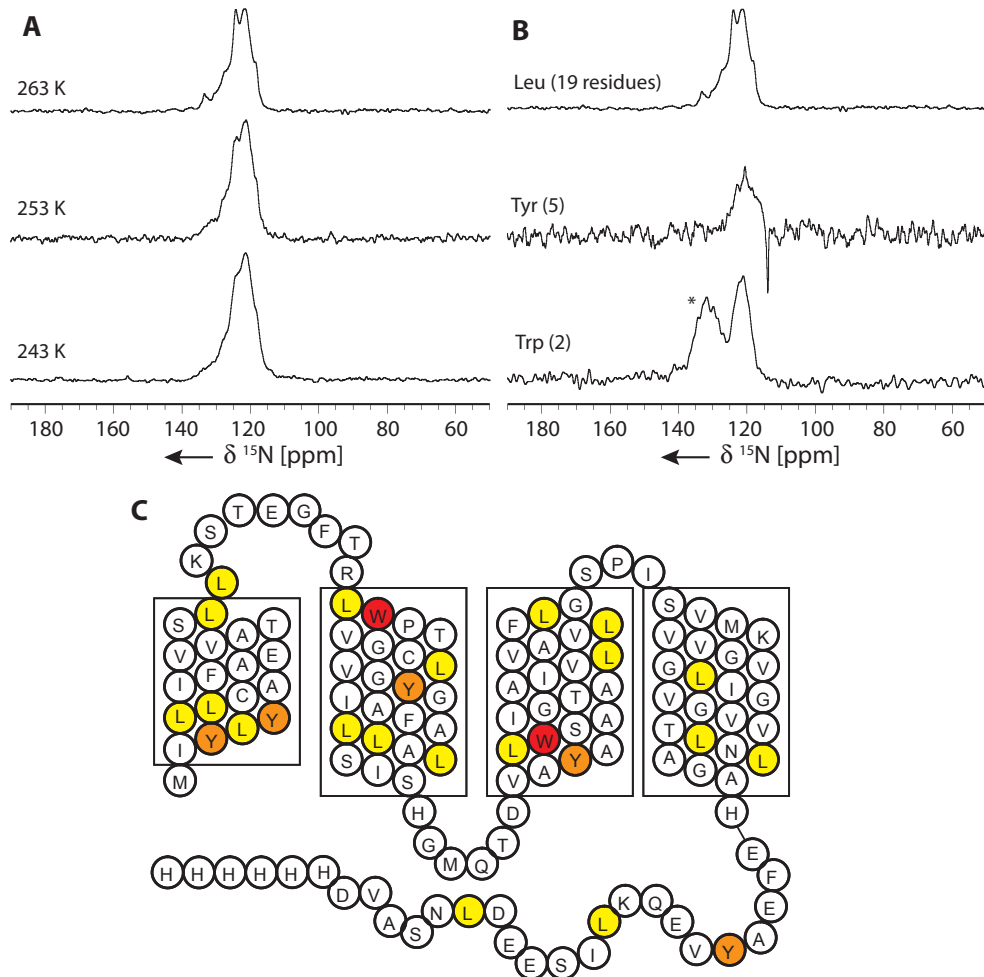


**Figure 7.1:** 1D  $^{15}\text{N}$  CPMAS NMR spectra of TBsmr proteoliposomes: A)  $^{15}\text{N}$  Leu labeled TBsmr spectra were recorded at different temperatures. The rotor contained 5 mg TBsmr in 15 mg DOPC (MAS=8 kHz, 30k scans). B)  $^{15}\text{N}$  labeling of different types of amino acid with a decreasing number of labeled residues. Leu sample: 5 mg TBsmr, 15 mg DOPC, 30k scans, 263 K; Tyr: 10 mg TBsmr, 34 mg *E. coli* lipids, 3k scans, 260 K; Trp: 5 mg TBsmr, 27 mg *E. coli* lipids, 56k scans, 220 K. Side chain  $^{15}\text{N}$ -Trp are marked with an asterisk (\*). C) Topology plot of TBsmr in which the position of  $^{15}\text{N}$  isotope labeled residues are color coded.

Figure 7.1 A) shows a 1D cross polarization magic angle spinning (CPMAS) NMR experiment of  $^{15}\text{N}$  leucine labeled TBsmr recorded on a DMX-400 at temperatures ranging from 243-263 K. At 243 K, the spectrum exhibits a single, broad signal between 120-130 ppm. At higher temperatures, the resolution increased and additional resonances

could be resolved. Since the spectra were too crowded to resolve all resonances, less abundant amino acids were labeled. Spectra of tyrosine and tryptophan labeled proteoliposomes, recorded under similar conditions, are shown in Fig. 7.1 B. Even though the number of labeled residues was decreased significantly by different labeling schemes from 19 to two, no individual residues could be resolved. The large line width of the  $^{15}\text{N}$  resonances with e.g.  $\sim 240$  Hz for the two tryptophan residues could be due to a restricted motional averaging of the residues inside the membrane.

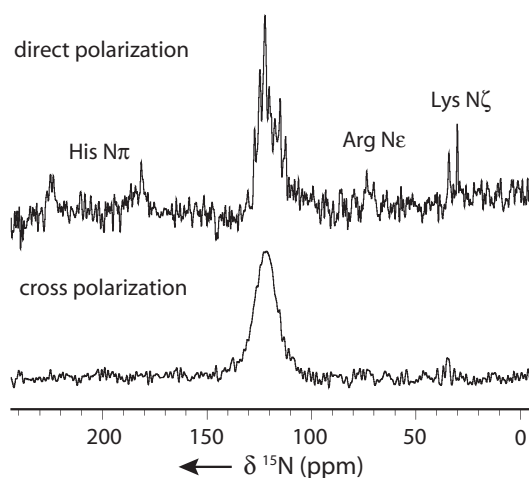


**Figure 7.2:** Direct polarization (DP) and cross polarization (CP) spectra of uniformly  $^{15}\text{N}$  labeled TBsmr in the non-frozen state. The backbone nitrogens resonate at 110-130 ppm. The arginine  $\text{N}\zeta$ , lysine  $\text{N}\epsilon$  and histidine sidechain nitrogens ( $\text{N}\pi$ ) give rise to signals at 80, 30 and 170-250 ppm, respectively. For the DP experiment, 20k scans were acquired at 277 K. The CP experiment was run for 5k scans with a non-frozen sample at 270 K.

To verify that the residues which give broad signals are buried within the membrane, direct polarization and cross polarization experiments of uniform  $^{15}\text{N}$  labeled TBsmr were recorded in the non-frozen state (Fig. 7.2). The DP spectrum shows amide backbone signals at 110-130 ppm and sidechain signals from the arginines, lysines and histidines at 90, 30 and 180 ppm, respectively. The atoms of the mobile sidechains give rise to narrow resonances whereas the amide region is a combination of narrow and broad signals. The mobility of residues outside the membrane attenuates the dipolar coupling and thus decreases the cross polarization efficiency. Therefore signals that do not appear in the CP spectrum due to their high mobility should appear in a direct polarization (DP) experiment independent of their motion. Based on that reasoning, the narrow signals in the amide region can be assigned to mobile residues which are located outside the membrane in the tag and in the loops because the signals disappeared in the CP spectrum.

### 7.2.2 Attempt to identify conserved Glu-13

Uniform  $^{13}\text{C}$  labeling was used to observe all amino acids at once to identify possible outliers. Glycines and leucines were selectively unlabeled (Hong and Jakes, 1999; Atreya and Chary, 2000) to reduce spectral crowding. The C-terminal myc/his-tag was removed at position F109 or Y112 by chymotrypsin digestion to further simplify the spectra, after confirming with the TPP<sup>+</sup> transport assay that the function of the protein is not affected. The same enzyme has been used successfully to remove the tag of EmrE without affecting its activity (Prof. S. Schuldiner, personal communication).

In initial experiments, the RFDR sequence (Bennett et al., 1998) was used for recoupling as it showed faster cross peak build-up rates for single bonds than long range interactions compared to PDSB which would reduce the number of cross peaks signals. However, the cross peak intensities in the RFDR experiment, which depend on the differences in chemical shift or CSA tensor orientations, performs best when the isotropic chemical shift difference  $|\Omega_1 - \Omega_2|$  matches a multiple of the MAS spinning frequency (Baldus et al., 1998). This requirement leads to reduced  $\text{C}\alpha\text{-C}\beta$  cross peaks in the RFDR experiment compared to the PDSB sequence (McDermott et al., 2000).

Therefore, 2D  $^{13}\text{C}\text{-}^{13}\text{C}$  homonuclear correlation spectra of TBsmr proteoliposomes were recorded using the PDSB sequence. Fig. 7.3 shows a PDSB spectrum of TBsmr measured at 250 K with 100 ms mixing time. The strong diagonal signals arise from isotope labeled TBsmr and natural abundance  $^{13}\text{C}$  carbons of the lipids. The observed cross peaks were caused by intra-residual correlations. Overlapping residues give rise to large peaks that could only be assigned to the type of amino acid. The distribution of  $\text{C}\alpha$  chemical shifts can be used to determine the secondary structure of these amino acids and thereby draw a conclusion about the correct fold of the protein (Frericks et al., 2006). For example, the average  $\text{C}\alpha$  chemical shift of the isoleucines in TBsmr is 63.3 ppm and thus falls into the range of  $64.7 \pm 1.7$  ppm (Wang and Jardetzky, 2002) expected for an  $\alpha$ -helical protein, which is distinct from the random coil chemical shift ( $60.6 \pm 2$  ppm). Similarly, alanine resonances appear at 53.2 ppm and match the average  $\alpha$ -helical shift ( $54.8 \pm 0.9$  ppm) in the data base. The 21 isoleucines and alanines are spread out over all four transmembrane helices and thus show that the protein in general is folded correctly.

1D  $^{13}\text{C}$  CP and DP experiments in the frozen and non-frozen state indicate that the signal intensities for residues outside the transmembrane domain are significantly reduced at 250 K with CP. The well resolved outlier at 182/34 ppm in the spectrum of TBsmr (Fig. 7.3) was tentatively assigned to the  $\text{C}\delta\text{-C}\gamma$  cross peak of the essential glutamate E13

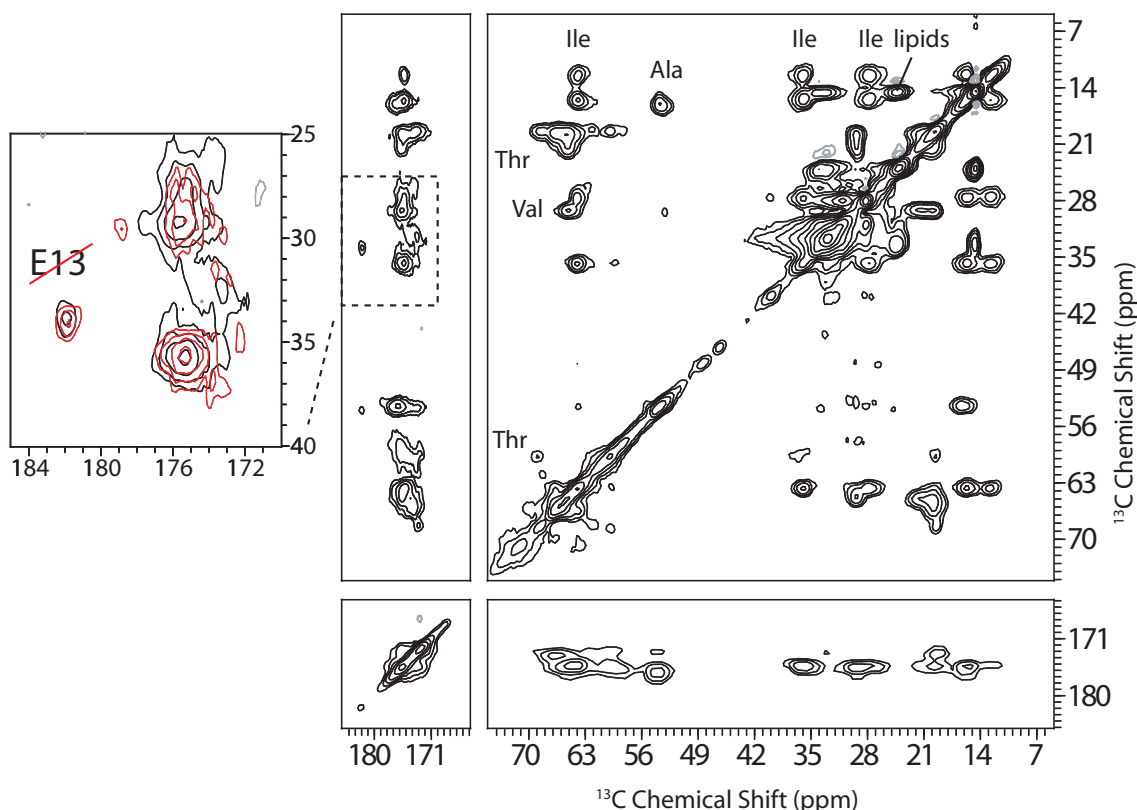


**Figure 7.3:** 2D  $^{13}\text{C}$ - $^{13}\text{C}$  PDSD spectra of  $^{13}\text{C}$  selectively unlabeled TBsmr E13A (black) and TBsmr wt (red). All amino acids but glycine and leucine were uniformly  $^{13}\text{C}$  isotope labeled. The myc/his-tag was removed by chymotrypsin cleavage. Some larger peaks consisting of multiple residues are labeled by the amino acid type. The enlarged region contains the peak that could correspond to E13  $\text{C}\delta$ - $\text{C}\gamma$ . However, as the peak at 182/34 ppm did not vanish in the mutant E13A (black vs. red), the residue E13 cannot be assigned to that particular peak. Both spectra were recorded with 100 ms mixing time at 250 K on a 600 MHz spectrometer with 320 scans, and 320 increments in the indirect dimension and a spinning speed of 10 kHz. Both samples contained 12 mg TBsmr in 32 mg POPC (1:50 protein-to-lipid molar ratio) in 50 mM Tris pH 9, 150 mM KCl.

because it is the only glutamate residue buried in the transmembrane region. However, the observed cross peak is not the essential glutamate E13 because the signal is still visible on mutation of the residue (E13A). The result is consistent with measurements on glutamate labeled EmrE E25C, where the  $\text{C}\delta$  chemical shift of E14 resonates at 179 ppm (Lehner et al., 2007).

### 7.2.3 $^{19}\text{F}$ solid-state NMR experiments

TBsmr contains two tryptophans, a non-essential W30 and a conserved W63, which is necessary for substrate binding (Elbaz et al., 2005). Substrate binding has been studied

in liquid-state NMR with  $^{19}\text{F}$  labeled tryptophan (Luck and Falke, 1991), which is very sensitive to the environment with a chemical shift range of up to 17 ppm (Pearson et al., 1993). Even though *E. coli* can tolerate up to 80%  $^{19}\text{F}$ -5-W labeling of all tryptophans in the cell without affecting growth seriously (Kim et al., 1990), the incorporation of fluorinated tryptophan can affect ligand binding (Dougherty, 2007). After the activity of TBsmr was tested in the bR/ SMR assay and confirmed that  $^{19}\text{F}$ -5-W TBsmr labeled is capable of EtBr transport (Fig. 7.4 B), CPMAS experiments of 5-fluoro-tryptophan labeled TBsmr were carried out to detect substrate binding by chemical shift changes of the conserved W63. Figure 7.4 shows spectra of frozen TBsmr proteoliposomes with and without the substrates EtBr at pH 8.5. At 12 kHz spinning speed, the spectra exhibited multiple spinning sidebands due to the large chemical shift anisotropy of fluorine. The isotropic shift of 5-fluoro-tryptophan TBsmr resonates at -46 ppm. The measured linewidth of 1000 Hz is in the same range as previous  $^{19}\text{F}$  measurements (Grage et al., 2002). Compared to the linewidth, the chemical shift dispersion of the two tryptophan was too small to resolve the two tryptophan residues. No chemical shift changes of the conserved W63 were observed upon the addition of substrate.

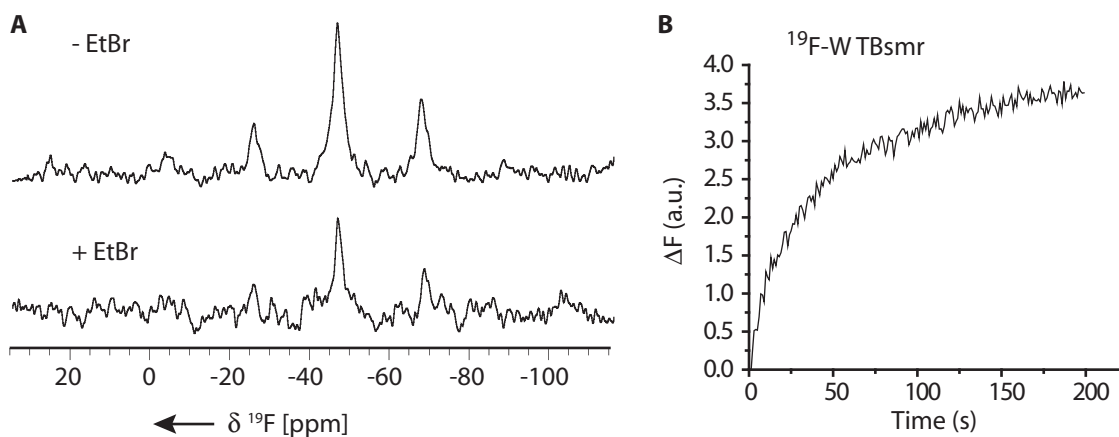


**Figure 7.4:** A) 1D  $^{19}\text{F}$  DP-MAS NMR spectra of TBsmr proteoliposomes in the absence and presence of EtBr. The EtBr sample was measured with 4mg TBsmr in 20 mg *E. coli* lipids at pH 8.5. No chemical shift change was observed in the presence of substrate. Both spectra were recorded at 253 K on a 600 MHz spectrometer with direct polarization for 4 k and 2 k scans with and without EtBr, respectively. The spinning rate was set to 12 kHz. B) bR-SMR transport assay of  $^{19}\text{F}$ -W TBsmr (15  $\mu\text{M}$  EtBr; 1  $\mu\text{M}$  TBsmr; 1.4  $\mu\text{M}$  bR).

### 7.2.4 Trp 63 labeling (Involvement of W63 in substrate binding)

A single tryptophan mutant of TBsmr was cloned (TBsmr W30A) and confirmed to be active with the bR/SMR assay (Fig. 7.5). TBsmr W30A was uniform- $^{13}\text{C}$ -W labeled selectively at W63. 2D  $^{13}\text{C}$ - $^{13}\text{C}$  homonuclear correlation DARR spectra of TBsmr W30A were acquired to study chemical shift changes of the key residue on EtBr binding. Compared to the PDSM sequence, the polarization transfer between  $^{13}\text{C}$  spins in the DARR experiment is enhanced by recovering the  $^{13}\text{C}$ - $^1\text{H}$  dipolar interaction by continuous wave irradiation on  $^1\text{H}$  which leads to faster buildup rates for the cross peaks (Crocker et al., 2004). Fig 7.6 shows a DARR spectrum of TBsmr proteoliposomes recorded at 230 K and 25 ms mixing time with and without substrate at pH 8.

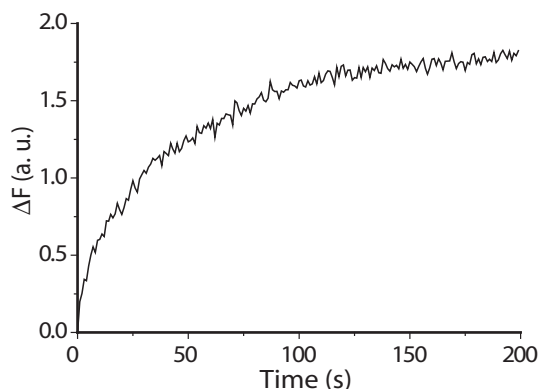


**Figure 7.5:** bR-SMR transport assay of TBsmr W30A.

Without substrate, there was a single peak for every nuclei with a line width of 1.7 – 4 ppm, values comparable to those found for EmrE (Lehner et al., 2007). Large line widths are commonly encountered in solid-state NMR of biological materials and are considered native for unaligned and non-crystalline proteins between 1 and 4 ppm for  $^{13}\text{C}$  (Kobayashi et al., 2006; Hong et al., 2003). A single set of cross peaks indicates that the two W63 residues in the TBsmr dimer are equivalent (Fig. 7.6). However, multiple distinct molecular environments in the presence of the substrate EtBr are suggested by the broadening of  $\text{C}'$ ,  $\text{C}\alpha$  and  $\text{C}\beta$  cross peaks in the  $^{13}\text{C}$  spectrum of TBsmr (Fig. 7.6 B, C). To obtain a more quantitative picture, a line shape analysis was carried out for the cross peaks of those resonances. The  $\text{C}'$ ,  $\text{C}\alpha$  and  $\text{C}\beta$  cross peak resonances can be best described by two resonances with similar integral intensities ( $\text{C}'$ - $\text{C}\beta$  cross peak: 60% to 40%; W63  $\text{C}'$ - $\text{C}\alpha$ : 56% to 44%; W63  $\text{C}\alpha$ - $\text{C}\beta$  57% to 43%) and linewidths ranging from

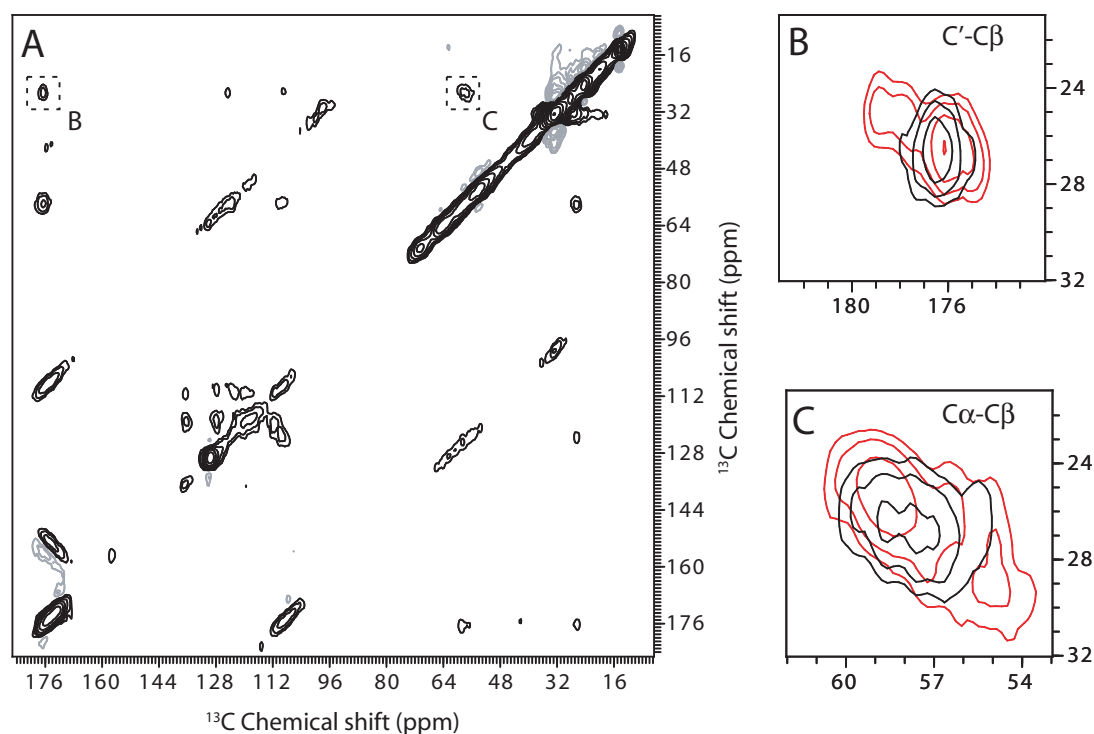


**Figure 7.6:** DARR experiment of  $^{13}\text{C}$  tryptophan labeled TBsmr W30A recorded with 25 ms mixing time. The complete 2D  $^{13}\text{C}$ - $^{13}\text{C}$  spectrum of the apo protein is shown in black (A). Fig. (B) and (C) show an overlay of TBsmr W30A with (red) and without (black) EtBr. The addition of EtBr lead to a peak splitting of the  $\text{C}'$  (B),  $\text{C}\alpha$  (C) and  $\text{C}\beta$  signals. The chemical shifts are summarized in Tab. 7.1. Both spectra were recorded at 230 K on a 600 MHz spectrometer with 1k scans per increment, and 96 increments in the indirect dimension. The rotor contained 10.5 mg TBsmr in 18.4 mg POPC (1:33 protein-to-lipid molar ratio) in the absence or presence of EtBr (300  $\mu\text{g}$ ; >1:1 EtBr-to-protein molar ratio; >1000 $\times K_d$ ) at pH 8.0 (Tris pH 8.0; 50 mM NaCl). The spinning speed was set to 10 kHz.

2-3.3 ppm (Fig. 7.7). The different chemical shifts of these resonances are indicative of two inequivalent TBsmr W30A populations because the shifts of these atoms strongly depend on the torsion angles of the peptide (Neal et al., 2003) and therefore report changes of the backbone structure. The line width indicates a limited amount of heterogeneity.

The chemical shift data of all atoms of W63 are summarized in Table 7.1. The chemical shifts of Smr in detergent (Poget et al., 2006) and in bicelles (Poget et al., 2007), the soluble tripeptide KWK (Oh and Markley, 1989) and TBsmr in LPPG are given as a reference. The backbone chemical shifts of reconstituted TBsmr differ from TBsmr in detergent by values reaching 1 ppm. Even more pronounced are the differences in the  $\text{C}\alpha$  chemical shifts of Smr by 2 ppm in different environments (LPPG and bicelles). These results suggest that the backbone chemical shifts of W63 are very sensitive to the environment, and that the membrane mimetic has to be chosen carefully. If the protein

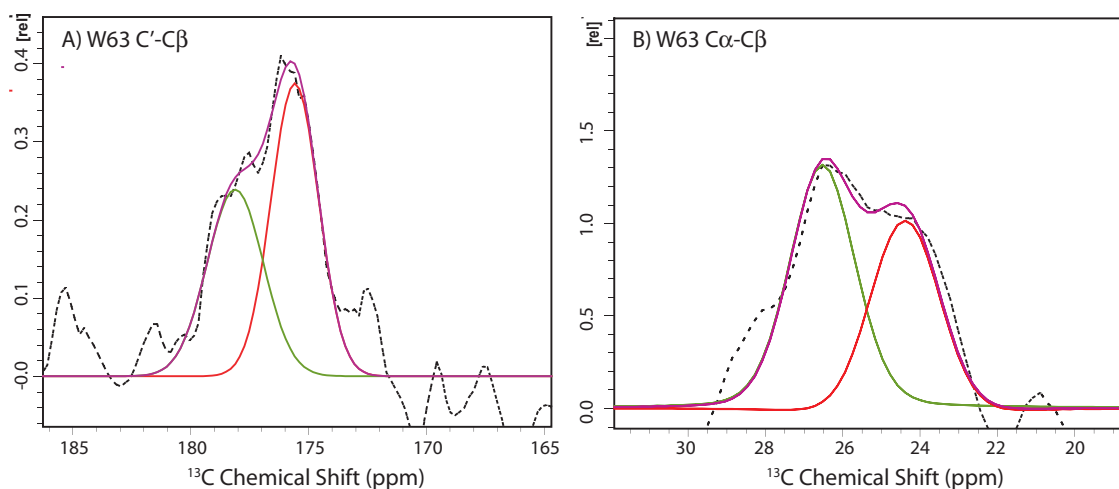


**Figure 7.7:** Solid-state NMR line shape analysis of the W63 peak of TBsmr W30A. A) Sum of the W63 C'-C $\beta$  cross peak. B) Sum of the W63 C $\alpha$ -C $\beta$  cross peak.

keeps the same structure in a lipid bilayer as in detergent, the liquid-state NMR data can be used for assignment in the solid-state (Werner et al., 2007). However, based on the narrow dispersion of the cross peaks in the liquid-state NMR spectra of TBsmr in LPPG (Fig. 6.3), which indicates a non-natively folded protein (Poget and Girvin, 2007), and the mainly monomeric, non-functional TBsmr in LPPG, as shown by LILBID-MS (Fig. 6.7), this is not true for TBsmr.

While the differences in the C', C $\alpha$  and C $\beta$  chemical shifts revealed changes in the backbone structure, the chemical shifts of the sidechain atoms varied between 0 – 1.1 ppm and did not give a conclusive answer about a direct interaction between EtBr and the aromatic ring of W63. Not only bound ligands can cause chemical shift changes of the tryptophan side chain resonances, but also different orientations of the ring trapped in the frozen state. An evidence for the inhomogeneous structure of the aromatic rings are the single broad  $^{15}\text{N}$  tryptophan sidechain signals of TBsmr with a line width of 7.8 ppm (Fig. 7.1), which were also seen in spectra of frozen rhodopsin with a line width of  $\sim 7.3$  ppm for five tryptophans (Werner et al., 2007). Therefore, an interpretation of the  $^{13}\text{C}$  side chain chemical shifts of TBsmr is not possible. In contrast, 2D crystals of proteorhodopsin measured in the non-frozen state gave narrow  $^{15}\text{N}$  tryptophan sidechain signals with line widths in the range of 0.8 ppm indicating a highly ordered side chains (Shastri et al., 2007).

**Table 7.1:** Assignments of  $^{13}\text{C}$  chemical shifts (ppm) of W63 in TBsmr with and without EtBr to obtain  $\Delta_{+\text{EtBr}}$ . Chemical shifts of molecules determined by liquid-state NMR are given for reference.

|                         | C'              | C $\alpha$   | C $\beta$     | C $\gamma$ | C $\delta$ 1 | C $\delta$ 2 | C $\epsilon$ 2 | C $\epsilon$ 3 | C $\zeta$ 1 | C $\zeta$ 2 | C $\eta$ 2 |
|-------------------------|-----------------|--------------|---------------|------------|--------------|--------------|----------------|----------------|-------------|-------------|------------|
| TBsmr                   | 176.6           | 57.7         | 26.4          | 108.6      | 124.8        | 127.8        | 136.7          | 117.9          | 111.1       | 120.2       | 122.7      |
| TBsmr <sup>a</sup>      | 176.1,<br>178.5 | 55,<br>58.6  | 26.7,<br>24.7 | 108.7      | 124          | 127.8        | 136.5          | 116.8          | 111.8       | 119.8       | 121.6      |
| $\Delta_{+\text{EtBr}}$ | -0.5,<br>1.9    | -2.7,<br>0.9 | 0.3,<br>-1.7  | 0.1        | -0.8         | 0            | -0.2           | -1.1           | 0.7         | -0.4        | -1.1       |
| KWK <sup>b</sup>        | 172.3           | 54.6         | 27.5          | 109.1      | 124.7        | 127          | 136.3          | 118.6          | 112.1       | 119.5       | 176.6      |
| Smr <sup>c</sup>        | 177.9           | 58.9         | 29            |            |              |              |                |                |             |             |            |
| Smr <sup>d</sup>        |                 | 60.9         |               |            |              |              |                |                |             |             |            |
| TBsmr <sup>e</sup>      | 175.4           | 58.2         |               |            |              |              |                |                |             |             |            |

<sup>a</sup> +EtBr (two shifts are due to a peak splitting)<sup>b</sup> L-Lysyl-L-tryptophyl-L-lysine in  $^2\text{H}_2\text{O}$  (Oh and Markley 1989)<sup>c</sup> Smr in LPPG (data from Poget et al., 2006)<sup>d</sup> Smr in bicelles (data from Poget et al., 2007)<sup>e</sup> TBsmr in LPPG (this work)

## 7.3 Discussion

### Assignment of key residues

The assignment of individual residues is the starting point for all NMR studies of a protein. Mason et al. have shown an elegant way to circumvent the problems of resolving individual residues in the large membrane protein bacteriorhodopsin by selectively  $^{15}\text{N}$  labeling methionine residues and assigning them by rotational-echo double-resonance (REDOR) NMR experiments with multiple  $^{15}\text{N}$ - $^{13}\text{C}$  pair labeled samples (Mason et al., 2005).

While the same strategy was applied to rhodopsin (Werner et al., 2007), all attempts to obtain well resolved  $^{15}\text{N}$  spectra of TBsmr in the frozen state failed due to a large linewidth of the signals (Fig. 7.1). However, in contrast to 2D crystals of proteorhodopsin (Shastri et al., 2007), the CP efficiency for TBsmr decreased rapidly in the non-frozen state and thus spectra with a sufficient signal-to-noise ratio could only be obtained in the frozen state. Decreasing the number of labeled residues did not improve the spectrum quality and proved that the lack of resolution is not caused by signal overlap but by line broadening. Even though well resolved solid-state NMR spectra of some proteins have been obtained at low temperature (Mason et al., 2005; Werner et al., 2007), a significant decrease in resolution upon freezing the sample has been observed for others (Shastri

et al., 2007; Agarwal et al., 2007; Martin and Zilm, 2003), which could be due to freeze trapping thermal motions of the protein (Agarwal et al., 2007; Chevelkov et al., 2007; Lehner et al., 2007).

The resolution in the  $^{15}\text{N}$  dimension is generally worse than in the  $^{13}\text{C}$  dimension because of the narrow shift dispersion and often larger line widths of  $^{15}\text{N}$  nuclei. Consequently, well resolved  $^{13}\text{C}$  spectra proved to be critical to achieve the complete assignment of the globular SH3 domain by solid-state NMR (Castellani et al., 2002). However, the resolution of  $^{13}\text{C}$  spectra of uniformly labeled TBsmr was not good enough for an assignment. Alternatively, single residues can be assigned by mutagenesis. An individual cross peak (182/34 ppm) in the 2D  $^{13}\text{C}$  -  $^{13}\text{C}$  dipolar correlation spectrum of TBsmr (Fig. 7.3) was tentatively assigned as the  $\text{C}_\delta$ - $\text{C}_\beta$  cross peak of the E13 based on its chemical shift and low mobility. The presence of the cross-peak in the spectrum of the TBsmr E13A mutant indicates that the residue is not the conserved E13, in agreement with similar experiment for EmrE (Agarwal et al., 2007).

### Substrate binding – W63 sidechain interactions with EtBr

A successful strategy in solid-state NMR is to focus on specific residues/co-factors to gain information about key elements of a protein that is too large to study as a whole. This approach relies on the fact that only the atoms of interest are isotope labeled and give rise to signals in the spectrum, while all other amino acids are not visible in the spectrum. Either an isotope labeled ligand is inserted into the unlabeled protein (Verdegem et al., 1999), or a single amino acid is labeled (Lehner et al., 2007). Besides the conserved E13, some of the aromatic residues in TBsmr are essential for the function of the protein (Yerushalmi et al., 1996; Rotem et al., 2006). The conserved W63 (corresponding to W61 in EmrE) is implicated in substrate binding (Elbaz et al., 2005), and was chosen as a target because there is only one other tryptophan in TBsmr. The tryptophan W30 is not conserved and could be mutated to alanine without the loss of activity. Transport activity of the mutant TBsmr W30A could be shown in the coupled bR-SMR assay for the substrate EtBr (Fig. 7.5).

Tryptophan residues can interact with a ligand by different mechanisms. They can participate in pi-pi stacking (Vazquez-Ibar et al., 2003) or pi-cation interaction (Zacharias and Dougherty, 2002) with the substrate. For example, in the crystal structure of BmrR, the ligand  $\text{TPP}^+$  is stabilized by pi-pi stacking with two tyrosines (Zheleznova et al., 1999). In contrast to the other aromatic residues, tryptophans tend to cluster near the

membrane surface due to their amphipathic nature (Arkin and Brunger, 1998). Near the membrane surface, the aromatic residues could draw a cationic substrate or proton out of the aqueous environment into the hydrophobic core of the protein (Dougherty, 1996). A bound substrate would then induce chemical shift changes in the tryptophan side chain atoms. However, significant chemical shift changes of the  $^{13}\text{C}$  or  $^{19}\text{F}$  labeled tryptophan sidechain, indicative of a direct interaction of the W63 aromatic side chain with bound substrate, could not be observed in the presence of substrate (Tab. 7.1 and Fig. 7.4).

### Asymmetric W63 in the TBsmr dimer

While a direct interaction between the aromatic ring of W63 and EtBr could be not be proven, the addition of EtBr caused a significant splitting of the backbone  $\text{C}'$ ,  $\text{C}\alpha$  and  $\text{C}\beta$  resonances (Fig. 7.6), which indicate changes in the backbone structure e.g. due to bound ligand (Bertini et al., 2006). Indeed, a recent ssNMR study of ligand bound Bcl-xL showed large chemical shift changes in the sidechain region of some amino acids while the  $\text{C}\alpha$  and  $\text{C}\beta$  atoms of these residues were unaffected (Zech et al., 2004).

Before one can draw further conclusions, it has to be ensured that the observed splitting into approximately two equal populations is biological relevant: Membrane proteins are prone to aggregation. To be the underlying cause for the splitting, roughly half of the protein would need to be aggregated. However, no aggregation was detected using freeze-fracture electron microscopy. The splitting of  $\text{C}'$ ,  $\text{C}\alpha$  and  $\text{C}\beta$  could also be caused by an incomplete saturation of the binding site. This is unlikely for two reasons: First, the EtBr concentration was more than  $1000 \times K_d$  ( $K_d = 2.6 \mu\text{M}$ ) which makes 40-50% saturation improbable. Second, the non binding fraction should exhibit no chemical shift changes in the spectrum. This is not the case, as the chemical shifts of both peak populations in the split resonances were shifted.

Since aggregation and incomplete binding can be excluded as a cause for the doublets, the best explanation is an “asymmetric” arrangement of W63 in two different backbone conformations. Such an asymmetry has recently been shown for the homodimeric EmrE by ssNMR, where two sets of chemical shifts were observed for the conserved E14 (Lehner et al., 2007). A similar observation has been made for the residue W63 of EmrE (Sharoni et al., 2005), where it could be shown that the function of an inactive EmrE W63C mutant is partially recovered in mixed oligomers. Asymmetry has also been reported for a subgroup of EmrE-like SMR proteins (YdgE/F (Nishino and Yamaguchi, 2001; Jack et al., 2000), YvdR/S, YkkC/D (Jack et al., 2000), EbrA/EbrB

(Masaoka et al., 2000; Kikukawa et al., 2006; Zhang et al., 2007)), which have been found to act as hetero oligomers with a defined topology for each molecule.

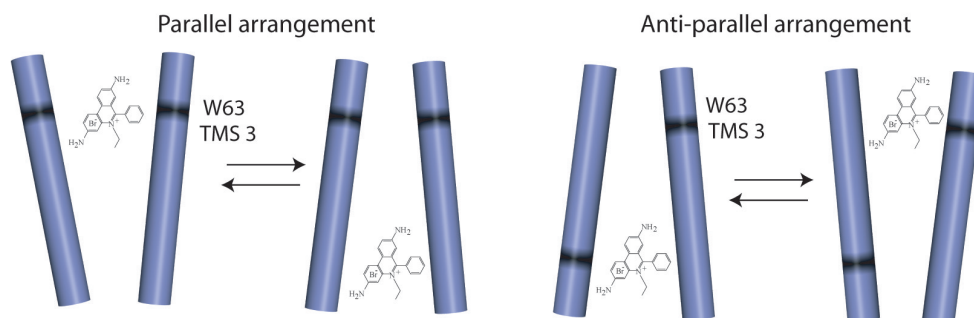


**Figure 7.8:** Model of a parallel and anti-parallel arrangement of TMS 3 in the TBsmr dimer. The two observed W63 populations can be explained by an asymmetric binding and release site in a parallel dimer or two asymmetric W63 populations in a anti-parallel dimer with a similar binding and release site.

Currently, there is a strong debate about the topology of EmrE with arguments for a parallel and an anti-parallel orientation (Schuldiner, 2007). However, none can be excluded based on the asymmetric backbone arrangement of W63 in the presence of substrate: In an anti-parallel arrangement, substrate binding would probably lead to two different backbone conformations of W63 with two distinct chemical shifts. But without a pH gradient present, TBsmr can still exchange substrate (Yerushalmi and Schuldiner, 2000b). EtBr bound to a binding- and release site in different molecules of a parallel TBsmr dimer, where the tryptophans are symmetric in each conformation, would also agree with the NMR data. Even without two separate binding sites, a substrate induced asymmetry in a single, parallel conformation could cause the observed splitting of the W63 resonances, too. The two models are depicted in Fig. 7.8.

Although it was not possible to identify the exact topology of the TBsmr dimer, the published x-ray and EM structures of EmrE (Fleishman et al., 2006; Chen et al., 2007) strongly suggest an anti-parallel arrangement of the purified construct. However, the main question that remains is, if EmrE *in vivo* also forms an anti-parallel arrangement, or if the observed dual topology is an artifact of the purification process induced e.g. by the detergent.

## 7.4 Conclusion and outlook

It could be shown that solid-state NMR can provide additional, site-specific information about key residues in TBsmr. Even though the resolution of the ssNMR spectra of TBsmr

was low, the problem could be circumvented by selective  $^{13}\text{C}$  labeling of a single amino acid. 2D  $^{13}\text{C}$ - $^{13}\text{C}$  correlation spectroscopy revealed two populations of the conserved W63 residue with distinct backbone structures in the presence of substrate. This structural asymmetry is consistent with both an antiparallel and parallel dimer topology.

Even though a 3D x-ray crystal structure of EmrE has been determined recently (Chen et al., 2007), with 4 Å, the resolution is too low to determine the position of the side chains. In light of the current controversy about the parallel or anti-parallel topology of the homo dimeric SMR proteins (Schuldiner, 2007), a detailed understanding about the equivalence of important residues in the binding pocket would be useful for the understanding of the substrate recognition and transport mechanism of those proteins. A systematic study of the local environment of the amino acids in TMS1 and 2 by solid-state NMR could help to characterize the binding pocket further. An isotope labeling strategy such as segment labeling (Yamazaki et al., 1998) of the first transmembrane helix will probably be necessary to achieve well resolved solid-state NMR spectra of the critical amino acids. To prevent the problem of structural changes induced by the purification process, it could be necessary to study the protein directly in the native membrane (Spooner et al., 1994).

## 8 Summary

Antibiotic resistance of pathogenic bacteria is a major worldwide problem. Bacteria can resist antibiotics by active efflux due to multidrug efflux pumps. The focus of this study has been the mycobacterial multidrug transporter TBsmr because it belongs to the small multidrug resistance (SMR) family whose members are a paradigm to study multidrug efflux due to their small size. SMR proteins are typically 11-12 kDa in size and have a four-transmembrane helix topology. They bind cationic, lipophilic antibiotics such as ethidium bromide (EtBr) and TPP<sup>+</sup>, and transport them across the membrane in exchange for protons. To understand the molecular mechanism of multidrug resistance, we have to gain information about the structure and function of these proteins. The research described in this thesis aimed to deduce details about the topology, transport cycle and key residues of TBsmr using biophysical techniques.

Solid-state NMR (ssNMR) can provide detailed insight into structural organization and dynamical properties of these systems. However, a major bottleneck is the preparation of mg amounts of isotope labeled protein. In case of proteoliposomes, the problem is compounded by the presence of lipids which have to fit into the small active volume of the ssNMR rotor. In **Chapter 3**, an enhanced protein preparation is described which yields large amounts of TBsmr reconstituted in a native lipid environment suitable for further functional and structural studies. The achieved high protein-to-lipid ratios made a further characterization by ssNMR feasible.

The transport activity and oligomeric state of the reconstituted protein in different types of lipid was studied as shown in **Chapter 4**. The exact oligomeric state of native SMR proteins is still uncertain but a number of biochemical and biophysical studies in detergent suggest that the minimal functional unit capable of binding substrate is a dimer. However, binding assays are not ideal since a protein may bind substrate without completing the transport cycle which can only be shown for reconstituted protein in transport assays. By combining functional data of a TPP<sup>+</sup> transport assay with information about the oligomeric state of reconstituted TBsmr obtained by freeze-fracture electron microscopy,

it could be shown that lipids affect the function and the oligomeric state of the protein, and that the TBsmr dimer is the minimal functional unit necessary for transport.

The transport cycle must involve various conformational states of the protein needed for substrate binding, translocation and release. A fluorescent substrate will therefore experience a significant change of environment while being transported, which influences its fluorescence properties. Thus the substrate itself can report intermediate states that form during the transport cycle. In **Chapter 5**, the existence of such a substrate-transporter complex for the TBsmr and its substrate EtBr could be shown. The pH gradient needed for antiport has been generated by co-reconstituting TBsmr with bacteriorhodopsin. The measurements have shown the formation of a pH-dependant, transient substrate-protein complex between binding and release of EtBr. This state was further characterized by determining the  $K_d$ , by inhibiting EtBr transport through titration with non-fluorescent substrate and by fluorescence anisotropy measurements. The findings support a model with a single occluded intermediate state in which the substrate is highly immobile.

Liquid-state NMR is a useful tool to monitor protein-ligand interactions by chemical shift mapping and thus identify and characterize important residues in the protein which are involved in substrate binding. In agreement with previous studies (Krueger-Koplin et al., 2004), the detergent LPPG was found to be highly suitable for liquid-state NMR studies of the membrane protein TBsmr and 42% of the residues could be assigned, as reported in **Chapter 6**. However, no specific interactions with EtBr were found. This observation was confirmed by LILBID mass spectrometry which showed that TBsmr was predominantly in the non-functional monomeric state.

Functional protein was prepared in proteoliposomes which can be investigated by solid-state NMR (**Chapter 7**). Besides the essential E13, the aromatic residues W63, Y40, and Y60 have been shown to be directly involved in drug binding and transport. Different isotope labeling strategies were evaluated to improve the quality of the NMR spectra to identify and characterize these key residues. In a single tryptophan mutant of reconstituted TBsmr W30A, the binding of ethidium bromide could be detected by  $^{13}\text{C}$  solid-state NMR. The measurements have revealed two populations of the conserved W63 residue with distinct backbone structures in the presence of substrate. There is a controversy about the parallel or anti-parallel arrangement of the protomers in the EmrE dimer (Schuldiner, 2007) but this structural asymmetry is consistent with both a parallel and anti-parallel topology.

## 9 Zusammenfassung

Das Phänomen der Multidrug-Resistenz (Multiwirkstoff-Resistenz) wurde erstmals 1976 als Korrelation von abnehmender Wirkstoffpermeabilität und zunehmender Expression des membranständigen P-Glycoproteins beschrieben (Juliano and Ling, 1976). Mittlerweile ist die Antibiotikaresistenz pathogener Bakterien ein Problem für die Gesundheit von Menschen weltweit. Zum Beispiel sind ungefähr ein Drittel der Weltbevölkerung mit dem Erreger *Mycobacterium tuberculosis* infiziert. Davon erkrankten etwa 5-10% an Tuberkulose, woran im Jahr 2005 allein ca. 1,6 Millionen Menschen gestorben sind. In Zukunft werden diese Infektionskrankheiten durch die Ausbreitung von Stämmen wie multiresistenter Tuberkulose (MDR-TB), die gegen mehr als ein Antibiotikum unempfindlich sind, noch schwieriger zu behandeln sein. Die Resistenz kann eine intrinsische Fähigkeit aller Spezies eines Stamms, oder eine erworbene Fähigkeit z.B. durch den Austausch von Plasmiden sein. Bakterien besitzen verschiedene Mechanismen zum Schutz vor Antibiotika wie die Inaktivierung des Antibiotikums durch Blockieren der enzymatischen Reaktion der Prosubstanz zum aktiven Wirkstoff, oder die Mutation des Wirkstoffziels. Ein weiterer Schutz ist die Reduzierung der Konzentration der toxischen Substanz innerhalb der Zelle, indem die Durchlässigkeit der Zellwand für Antibiotika gesenkt wird, oder indem Antibiotika durch so genannte Multidrug-Transportproteine in der Zellmembran aktiv aus der Zelle heraus transportiert werden.

Zusätzlich sind diese Transporter als Modellsysteme auch von großem generellem Interesse. Deren erstaunliche Fähigkeit eine Vielzahl sehr diverser Wirkstoffe spezifisch zu binden, scheint den verbreiteten Ansichten über Substrat-Protein-Wechselwirkung zu widersprechen. Es gibt zurzeit zwei mögliche Paradigmen um die Existenz von Multidrug-Transportern zu erklären. Einerseits kann man annehmen, dass sie im Laufe der Evolution entstanden sind um Zellen mit einem Schutzmechanismus gegen toxische Stoffe auszustatten. Andererseits wäre es auch möglich, dass ihre eigentliche Funktion der Transport eines bestimmten Substrates ist und Multidrug-Transport nur als opportunistischer Nebeneffekt auftritt, wenn der Organismus in einer experimentellen Situation verschiede-

nen Wirkstoffen ausgesetzt ist. Beide Hypothesen werden von den gegenwärtigen experimentellen Fakten gleichermaßen unterstützt. Daher ist es notwendig Struktur-Funktions-Informationen zu erhalten, um die Mechanismen von Substraterkennung und Transport zu verstehen. Dies könnte auch die Entwicklung wirksamerer Wirkstoffe für bestehende Therapien unterstützen.

Aus bioenergetischer und struktureller Sicht können Multidrug-Transporter in zwei Klassen eingeteilt werden. Bei den sekundären Transportern ist der Stoffaustausch mit einem Ionen-transport gekoppelt, während ABC (ATP binding cassette) Transporter die für den Stofftransport benötigte Energie aus der ATP-Hydrolyse gewinnen. Die meisten bakteriellen MDR-Transporter sind sekundäre Transporter und gehören zu einer von vier unterschiedlichen Transporterfamilien: Major facilitator superfamily (MFS), resistance nodulation division family (RND), multidrug and toxic compound extrusion family (MATE) und die small multidrug resistance family (SMR). Die MFS-Familie enthält z.B. Transporter wie Bmr, LmrP, QacA und QacB.

Zur Untersuchung des Multidrug-Transports befasst sich die vorliegende Arbeit mit der SMR-Familie, deren Mitglieder sich auf Grund ihrer kleinen Größe hervorragend als Modellsysteme eignen. Ziel dieser Arbeit ist es, ein besseres Verständnis von der Oligomerisierung, dem Transportzyklus und wichtigen, konservierten Aminosäuren der SMR-Familie durch Untersuchungen mit biophysikalischen Methoden zu bekommen. Das am besten untersuchte SMR-Protein ist EmrE aus *Escherichia coli*. Es hat durch eine kontroverse Diskussion über seine dreidimensionale Struktur und die parallele oder anti-parallele Anordnung der Protomere im Dimer viel Aufmerksamkeit auf sich gezogen (Rapp et al., 2007; Schuldiner, 2007). EmrE transportiert eine Reihe unterschiedlicher aromatischer und positiv geladener Substrate im Austausch gegen Protonen durch die Membran (Rotem and Schuldiner, 2004). Andere SMR-Proteine haben überlappende, aber auch signifikant andere Substratspezifitäten mit gemessenen Bindungsaffinitäten im nano- bis mikromolaren Bereich (Muth and Schuldiner, 2000; Ninio and Schuldiner, 2003; Sikora and Turner, 2005b). Die SMR-Proteine sind typischerweise 11-12 kDa schwer, bestehen aus vier transmembran  $\alpha$ - Helizes, und einem hoch konserviertem Glutamat 14 (Muth and Schuldiner, 2000). Die Vier-Helix Topologie von EmrE wurde auf Grund einer Hydrophobizitätsanalyse vorhergesagt und später mit Fourier-Transformations-Infrarot- (FTIR) und Lösungs-Kernspinresonanz- (NMR) Spektroskopie nachgewiesen (Arkin et al., 1996; Schwaiger et al., 1998).

Um offene strukturelle und mechanistische Fragen zu beantworten, wurde TBsmr von

*M. tuberculosis* als ein typisches SMR Protein ausgewählt, da es sich sehr gut exprimieren ließ. TBsmr (Genzugangsnummer Rv3065, auch bekannt als mmr) hat 70% Ähnlichkeit und 43% Identität zu EmrE. Beide Proteine verleihen Resistenz gegen TPP<sup>+</sup>, Acriflavin, Ethidium Bromid, Benzalkonium und Methyl Viologen, während TBsmr zusätzlich noch vor Safranin O, Pyronin Y und Erythromycin schützt (De Rossi et al., 1998b).

Zusätzlich zu funktionellen Untersuchungen und der Kristallisation zur Strukturbestimmung von Multidrug-Transportern eignet sich vor allem die Festkörper-NMR-Spektroskopie, um Informationen über die Struktur und Dynamik dieser Systeme zu bekommen. Die Möglichkeit, eine Vielzahl fester Zustände wie 3D-Kristalle oder Proteine in Lipidmembranen zu untersuchen, ist ein großer Vorteil der Festkörper-NMR gegenüber anderen Methoden. Andererseits ist die Notwendigkeit von mg-Mengen Isotopen markierter Proteine ein großer Engpass bei der Umsetzung. Vorteilhaft sind NMR-Messungen an Proteoliposomen, da sich das Protein dann in seiner nativen Membranumgebung befindet. Der Nachteil dieser Proben ist das zusätzliche Volumen durch Lipide, da die Festkörper-NMR-Rotoren nur ein geringes Probenvolumen fassen. In **Kapitel 3** wird eine verbesserte Probenpräparation beschrieben, mit der sich große Mengen isotopenmarkiertes TBsmr gewinnen und mit einem hohen Protein-zu-Lipid Verhältnis in Liposomen rekonstituieren lassen. Während bei der Optimierung der Expression die meisten Parameter wie z. B. die Art der Induktion einen geringen Einfluss auf die Proteinmenge hatte, waren zwei Techniken besonders zielführend: Das Antibiotikum Rifampicin (Lee et al., 1995; Arkin et al., 1996), welches selektiv an die *E. coli* Ribonukleinsäure-Polymerase bindet und die Expression von *E. coli* eigenen Proteinen unterdrückt, sowie die "Spin Down"-Technik bei der die Bakterien in unmarkiertem Medium wachsen und vor der Induktion in einem geringeren Volumen an frischem, isotopenmarkiertem Medium resuspendiert werden (Almeida et al., 2001). Durch Kombination beider Methoden konnte die Menge des Proteins bezogen auf das isotopenmarkierte Medium, im Vergleich zur normalen Expression vervielfacht werden. Es wurden verschiedene Detergenzien zur Solubilisierung von TBsmr getestet (DDM, OG, Triton X-100, Fos-12). Die besten Ergebnisse hinsichtlich Monodispersität und Langzeitstabilität wurde mit Fos-12 erreicht.

Basierend auf den Erfahrungen mit DGK (Lorch et al., 2005a), wurde versucht, 3D-Kristalle für eine Röntgenstrukturanalyse herzustellen, die ebenso für Festkörper-NMR genutzt werden können. Kristallisationsbedingungen wurden im pH Bereich 7-10 für verschiedenste Detergenzien getestet (DDM, DTM, DM, Cymal-6, Fos-12). Allerdings konnten nur in Fos-12 Bedingungen gefunden werden, unter denen keine Aggregation

zu beobachten war. Es wurden hauptsächlich kleine Kristalle erhalten, die nicht für eine Röntgenstrukturanalyse geeignet waren.  $^{15}\text{N}$ -MAS NMR-Spektren dieser Kristalle waren nicht wesentlich besser aufgelöst als die Spektren von rekonstituierten Proben. Daher wurde dieser Ansatz zunächst nicht weiterverfolgt.

Zur Rekonstitution von TBsmr wurden zwei wichtige Faktoren identifiziert: die Art der Rekonstitution wie z. B. Dialyse (Allen et al., 1980) oder Verdünnung (Yerushalmi et al., 2001), sowie die Wahl des Detergenz. Die besten Ergebnisse wurde mit der "Bio-beads" Methode (Levy et al., 1990) und dem Detergenz Dodecylmaltosid (DDM) erzielt und ermöglichten eine Rekonstitution in *E. coli* Lipide unabhängig von dem Protein-zu-Lipid Verhältnis. Diese Verbesserungen ermöglichten die nachfolgenden Messungen zur Charakterisierung von TBsmr.

Angesichts der erfolgreichen Rekonstitution des mykobakteriellen Proteins TBsmr in *E. coli* Lipidvesikel wurde der Einfluß von verschiedenen Lipiden auf die Funktion und den Oligomerisierungszustand von TBsmr untersucht (**Kapitel 4**). Da Proteine anderer Transporterfamilien wie die MFS typischerweise 10 bis 14  $\alpha$ -Helizes enthalten, ist es unwahrscheinlich das einzelne SMR-Monomere Substrat transportieren können. Der Oligomerisierungszustand der nativen SMR-Proteine ist noch nicht sicher bestimmt. Es gibt zwar Hinweise auf Monomere und Tetramere (Winstone et al., 2005; Elbaz et al., 2004), aber die meisten biochemischen und biophysikalischen Untersuchungen in Detergenz gelösten Proteins deuten aber darauf hin, dass ein Dimer die minimale funktionelle Einheit ist, die Substrat binden kann (Soskine et al., 2002; Koteiche et al., 2003; Ubarretxena-Belandia et al., 2003; Butler et al., 2004). Die Existenz von gepaarten SMR-Proteinen, die gleichzeitig exprimiert werden müssen, um einen Resistenzphänotyp zu verursachen, unterstützt diese Vermutung (Jack et al., 2000). Alle Funktionstests von in Detergenz gelöstem Protein basieren jedoch auf Bindungsstudien. Ligand-Bindungs Experimente haben aber den Nachteil, dass eventuell Substrat an das Protein bindet, es aber trotzdem nicht transportiert werden kann (Smirnova and Kaback, 2003). Um dieses Problem zu umgehen, muß die Funktion und Struktur von TBsmr in Lipidmembranen untersucht werden. Wie in Kapitel 4 beschrieben, wurde die Transportaktivität von Tetraphenylphosphonium ( $\text{TPP}^+$ ), welches ein typisches Multidrugtransporter-Substrat ist, in verschiedenen Lipiden untersucht. Die Messungen erfolgten mit Hilfe von pH-Sprüngen und einer  $\text{TPP}^+$ -sensitiven Elektrode. Dabei wurde ein Einfluß der Lipidsorte auf die Aktivität und der Oligomerisierungszustand von TBsmr festgestellt. In *E. coli* Lipiden und POPC war Transport messbar, in DMPC jedoch nicht. Ein Grund hierfür

könnte in den recht kurzen Kohlenwasserstoffketten in DMPC liegen, die möglicherweise TBsmr in eine nichtaktive Konformation zwingen. Durch Kombination mit Informationen über den Oligomerisierungsgrad des rekonstituierten Proteins aus Gefrierbruch-Elektronenmikroskopie Untersuchungen, konnte die Existenz von funktionalen Dimeren, die Substrat transportieren, in POPC nachgewiesen werden. In Übereinstimmung mit bisherigen Untersuchungen, die auf die Existenz höherer Oligomere hindeuten, wurden in *E. coli* Lipiden Tetramere gefunden.

Obwohl gezeigt werden konnte, das rekonstituiertes TBsmr voll funktional war, stellte der schnelle Kollaps der pH-Gradienten durch pH-Sprünge ein Problem bei den Aktivitätsmessungen dar. Daher war ein neuer Assay mit einem stabilen pH-Gradienten notwendig, um den Transportzyklus weiter zu untersuchen (**Kapitel 5**). Auf Basis von Cryo-Elektronenmikroskopie-Daten zweidimensionaler EmrE-Kristalle wurde von anderen Forschergruppen ein Strukturmodell entwickelt und ein Transportmechanismus mit alternierendem Zugang vorgeschlagen (Ubarretxena-Belandia et al., 2003; Yerushalmi and Schuldiner, 2000c; Fleishman et al., 2006). In diesem Modell wird der Transportvorgang durch das Binden von Substrat induziert. Die Freisetzung des Substrates wird durch eine anschließende Protonenbindung und Antiport ausgelöst. Obwohl der Transport des Substrats von der Bindungs- zur Freisetzungstelle konformationelle Änderungen in EmrE beinhalten muss, konnte keine Aussage über mögliche Übergangszustände getroffen werden. Der Transportzyklus muss aber eine Reihe von verschiedenen Konformationen für die Bindung, den Transport und die Freisetzung des Substrats enthalten. Ein fluoreszierende Substanz wird sich beim Transport durch die starken Änderungen der Umgebung in ihren Fluoreszenzeigenschaften verändern. Deshalb könnte das Substrat selbst als Reporter für Zwischenzustände im Transportzyklus benutzt werden. Wie in Kapitel 5 beschrieben, konnte die Existenz eines solchen Substrat-Transporter-Komplexes für TBsmr und das Substrat Ethidiumbromid mit einem neu entwickelten Assay nachgewiesen werden. Die Möglichkeit einen pH-Gradient zu generieren, der für den Transport notwendig ist, wurde durch die Korekonstitution von TBsmr mit Bakteriorhodopsin geschaffen. Bei Beleuchtung der Probe entstand ein pH-Gradient. Darüber hinaus konnte eine Intensitätszunahme der Ethidiumbromid Fluoreszenz beobachtet werden, es sein denn, die Ausbildung von  $\Delta\text{pH}$  oder  $\Delta\psi$  wurden durch Zugabe von Ionophoren verhindert, oder die essenzielle Aminosäure Glutamat-13 in TBsmr wurde gegen Alanin ausgetauscht. Die Fluoreszenzänderung wurde durch einen pH-abhängigen, transienten Substrat-Protein-Komplex zwischen der Bindung und der Freisetzung von Ethidium verursacht. Zusätzlich

wurde dieser Zustand durch die Bestimmung eines  $K_{ds}$ , der Hemmung des Ethidiumtransports durch die Titration mit einem nicht fluoreszierendem Substrats und durch Fluoreszenzanisotropiemessungen genauer charakterisiert. Die Ergebnisse deuten auf einen einzelnen, verdeckten Übergangszustand hin, in dem das Substrat unbeweglich ist.

Aufgrund der beobachteten Langzeitstabilität von TBsmr in Fos-12 wurden Lösungs-NMR-Experimente durchgeführt, um zu evaluieren, ob Substrat-Protein-Interaktionen gemessen werden können (**Kapitel 6**). Die Qualität der NMR-Spektren in Fos-12 war zu gering, konnte aber durch einen Wechsel zu 10% LPPG wesentlich verbessert werden. Durch eine Reihe von 3D TROSY-HNCO/HN(CA)CO, HN(CO)CA/HNCACB-Experimenten war es möglich, 42% aller Resonanzen des Protein-Rückgrates vorläufig zuzuordnen. Die restlichen Resonanzen konnten wegen zu starker spektraler Überlappung nicht zugeordnet werden. Variationen von Temperatur, Pufferzusammensetzung und pH-Wert führten zu keiner Verbesserung des Ergebnisses. Die Titration von Ethidiumbromid führte zu leichter Verschiebung fast aller Resonanzen, was auf eine unspezifische Wechselwirkung deutet die vermutlich durch eine Veränderung der Detergenzmizellen durch die Partition von Ethidiumbromid in die Mizellen verursacht wird. Der oligomere Zustand von TBsmr in LPPG Mizellen wurde mittels Laser Induced Liquid Beam Ionization/Desorption (LILBID) Massenspektrometrie studiert. Dieses neuartige Verfahren (Morgner et al., 2007) wies eindeutig auf Monomere hin. Eine Vielzahl biochemischer Studien legt jedoch eine Dimer-Struktur für SMR Proteine nahe. Es war daher fraglich, ob in Mizellen eine funktionale Präparation gegeben ist.

Das Problem einer funktionalen Präparation ließ sich durch Aktivität in Lipidmembranen lösen, wo Membranproteine sehr gut mittels Festkörper-NMR untersucht werden können (**Kapitel 7**). Neben dem essentiellen Glutamat 14 in EmrE (E13 in TBsmr) wurden einige weitere, aromatische Aminosäuren (Y40, Y60, W63) über Mutationsstudien identifiziert (Elbaz et al., 2005; Rotem et al., 2006), die für den Transportzyklus wichtig sind. Die genaue Funktion dieser Aminosäuren für die Bindung und den Transport ist noch nicht bekannt, sie sind aber vermutlich für den hohen pKa des konservierten Glutamat 14 in EmrE verantwortlich (Yerushalmi and Schuldiner, 2000c). Da die aromatischen Aminosäuren in der Bindung von Substrat involviert sind, enthalten sie strukturelle Informationen über die Bindungstasche von TBsmr. Aufbauend auf den NMR-Studien in Detergenzmizellen und den Aktivitätsmessungen in Lipiddoppelschichten wurden Festkörper-NMR-Messungen an vollständig und selektiv markierten Proben durchgeführt. Wie in Kapitel 7 beschrieben, wurden verschiedene Isotopenmarkierungs-Schema-

ta getestet um die Qualität der NMR-Spektren soweit zu verbessern, dass einzelne Aminosäuren identifiziert und charakterisiert werden können. Versuche in vollständig markiertem TBsmr rekonstituiert in POPC die wichtigste Aminosäure in der Bindungstasche, E13, spektroskopisch sowie mit einer E13A Mutante zuzuordnen, war wegen des unzureichenden Signal-zu-Rausch Verhältnisses und überlappender Linien nicht möglich. Stattdessen konnte in der Mutante TBsmr W30A, in der ein einzelnes Tryptophan vollständig mit  $^{13}\text{C}$  Isotopen markiert war, die Bindung von Ethidiumbromid detektiert werden. Die Messungen offenbarten zwei Populationen der konservierten Aminosäure W63 mit verschiedenen Konformationen des Peptidrückgrats in Gegenwart von Substrat. Die beobachtete strukturelle Asymmetrie von W63 ist sowohl in einer parallelen wie auch anti-parallelen Topologie der Dimere möglich.

# Appendix

**Table A.1:** Defined media for selective isotope labeling (Muchmore et al., 1989).

| Compound      | Unlabeled (g/l) | Labeled (g/l) |
|---------------|-----------------|---------------|
| alanine       | 0.5             | 0.6 (DL)      |
| arginine      | 0.4             |               |
| aspartic acid | 0.4             | 0.1           |
| cystein       | 0.05            |               |
| glutamine     | 0.4             |               |
| glutamic acid | 0.65            | 0.55          |
| glycine       | 0.55            | 0.5           |
| histidine     | 0.1             |               |
| isoleucine    | 0.23            | 0.05          |
| leucine       | 0.23            | 0.06          |
| lysine        | 0.42            | 0.06          |
| methionine    | 0.25            | 0.15          |
| phenylalanine | 0.13            | 0.075         |
| proline       | 0.1             |               |
| serine        | 2.1             | 0.5           |
| threonine     | 0.23            | 0.15          |
| valine        | 0.23            | 0.1           |

After autoclaving, 50 ml 40% (w/v) glucose, 4 ml 1 M MgSO<sub>4</sub>, and 10 ml filter sterilized trace metals (2 mg CaCl<sub>2</sub>\* 2 H<sub>2</sub>O, 2 mg ZnSO<sub>4</sub>\* 7 H<sub>2</sub>O, 2 mg MnSO<sub>4</sub>\* H<sub>2</sub>O, 50 mg L-tryptophane, 50 mg thiamine, 50 mg niacin, 1 mg biotin) were added under steril conditions. The final pH is 7.2.

**Table A.5:** NMR resonance assignments of TBsmr in 10% LPPG at pH 7.5

| Residue | $\delta N$ (ppm) | $\delta H^N$ (ppm) | $\delta C'$ (ppm) | $\delta C^\alpha$ (ppm) | $\delta C^\beta$ (ppm) |
|---------|------------------|--------------------|-------------------|-------------------------|------------------------|
| Met 1   | 129.1            | 8.8                |                   | 56.4                    |                        |

---

| Residue | $\delta N$ (ppm) | $\delta H^N$ (ppm) | $\delta C'$ (ppm) | $\delta C^\alpha$ (ppm) | $\delta C^\beta$ (ppm) |
|---------|------------------|--------------------|-------------------|-------------------------|------------------------|
| Ile 2   | 116.7            | 8.3                |                   | 63.3                    |                        |
| Tyr 3   | 119.9            | 7.3                |                   | 61.0                    | 37.7                   |
| Leu 4   | 118.6            | 7.6                |                   | 58.1                    |                        |
| Leu 6   | 120.9            | 7.9                | 175.5             | 58.1                    | 38.4                   |
| Leu 7   | 124.9            | 8.0                | 177.1             | 52.3                    |                        |
| Cys 8   | 120.9            | 7.9                | 176.9             | 55.0                    | 42.4                   |
| Ala 9   | 125.3            | 8.1                | 176.1             | 52.2                    |                        |
| Ile 10  | 124.2            | 7.6                | 180.4             | 58.9                    | 39.4                   |
| Val 14  | 120.7            | 8.5                |                   | 56.5                    |                        |
| Val 15  | 121.0            | 7.9                |                   | 65.5                    |                        |
| Ala 16  | 122.0            | 8.0                |                   | 55.4                    |                        |
| Thr 17  | 116.2            | 8.2                |                   | 60.9                    |                        |
| Ser 18  | 120.1            | 8.4                | 174.6             | 57.9                    | 64.0                   |
| Leu 20  | 118.1            | 8.0                | 178.1             | 56.8                    |                        |
| Lys 21  | 117.9            | 7.8                |                   | 57.7                    |                        |
| Ser 22  | 114.1            | 7.9                | 175.2             | 59.6                    | 63.8                   |
| Thr 23  | 113.1            | 8.0                |                   | 63.3                    |                        |
| Glu 24  | 122.3            | 8.2                |                   | 58.3                    |                        |
| Gly 25  | 107.7            | 8.4                |                   | 46.3                    |                        |
| Phe 26  | 118.9            | 8.1                |                   | 59.6                    | 38.6                   |
| Thr 27  | 111.7            | 8.0                |                   | 65.1                    |                        |
| Val 33  | 119.4            | 8.2                |                   | 66.4                    |                        |
| Gly 34  | 106.4            | 8.4                |                   | 47.2                    |                        |
| Cys 35  | 120.2            | 7.7                |                   | 61.4                    |                        |
| Val 36  | 119.8            | 7.9                |                   | 58.1                    |                        |
| Val 37  | 118.3            | 8.4                |                   | 67.1                    |                        |
| Gly 38  | 106.1            | 8.0                |                   | 47.4                    |                        |
| Met 54  | 119.7            | 8.3                |                   | 58.0                    | 32.7                   |
| Gln 55  | 122.1            | 8.5                |                   | 55.3                    |                        |
| Thr 56  | 109.8            | 8.0                |                   | 65.0                    |                        |

| Residue | $\delta N$ (ppm) | $\delta H^N$ (ppm) | $\delta C'$ (ppm) | $\delta C^\alpha$ (ppm) | $\delta C^\beta$ (ppm) |
|---------|------------------|--------------------|-------------------|-------------------------|------------------------|
| Asp 57  | 116.8            | 8.0                |                   | 61.4                    |                        |
| Val 58  | 120.7            | 8.1                |                   | 63.4                    |                        |
| Ala 59  | 119.6            | 7.9                |                   | 57.2                    |                        |
| Tyr 60  | 116.5            | 7.8                |                   | 55.3                    |                        |
| Ala 61  | 117.0            | 8.3                |                   | 57.5                    |                        |
| Leu 62  | 115.4            | 8.0                |                   | 61.4                    |                        |
| Trp 63  | 118.3            | 7.9                |                   | 58.2                    |                        |
| Ser 64  | 118.7            | 8.1                |                   | 57.3                    |                        |
| Ala 65  | 114.4            | 8.1                |                   | 59.4                    |                        |
| Ile 66  | 118.4            | 7.9                |                   | 56.1                    |                        |
| Gly 67  | 107.1            | 8.0                |                   | 45.6                    |                        |
| Thr 68  | 115.9            | 7.9                |                   | 56.4                    | 63.7                   |
| Ala 70  | 129.3            | 7.8                | 182.4             | 53.7                    | 20.2                   |
| Val 95  | 122.6            | 8.1                | 177.6             |                         |                        |
| Val 96  | 119.1            | 8.2                |                   | 66.6                    |                        |
| Gly 97  | 105.7            | 8.2                |                   | 47.4                    |                        |
| Val 98  | 115.7            | 7.8                |                   | 66.3                    |                        |
| Leu 103 | 119.2            | 8.1                |                   | 54.4                    |                        |
| Ala 104 | 121.3            | 8.4                | 176.3             | 57.0                    |                        |
| Gly 105 | 107.8            | 8.2                |                   | 45.6                    |                        |
| Ala 106 | 119.5            | 7.8                |                   | 56.0                    |                        |
| Val 127 | 116.0            | 8.2                |                   | 65.5                    |                        |
| Asp 128 | 118.7            | 8.1                |                   | 58.2                    | 41.8                   |
| His 129 | 116.2            | 8.1                |                   | 64.2                    |                        |
| His 130 | 120.1            | 7.7                |                   | 66.4                    |                        |

**Table A.2:** Minimal media for uniform  $^{13}\text{C}/^{15}\text{N}$  isotope labeling.

| Compound                     | g/l  |
|------------------------------|------|
| $\text{K}_2\text{HPO}_4$     | 10.5 |
| $\text{KH}_2\text{PO}_4$     | 4.5  |
| $(\text{NH}_4)_2\text{SO}_4$ | 1    |

After autoclaving, 10 ml 40% (w/v) glucose, 1 ml 1 M  $\text{MgSO}_4$ , 1 ml 2.5 mg/ml thiamine (steril filtered) and 1 ml 100 mg/ml ampicillin (steril filtered) were added under sterile conditions.

**Table A.3:** *E. coli* strains used to express TBsmr

| Strain     | Genotype   | auxotrophic                            | Literature              |
|------------|--|--|-------------------------|
| CT19       | BL21(DE3) + <i>aspC, ilvE, trpB, tyrB, avtA</i>  | Leu, Val, Ile, Tyr, Trp, Phe, Asp, Ala | (Fiaux et al., 2004)    |
| BL21(DE3)  | <i>F- ompT gal dcm lon hsdSB(rB- mB-) λ(DE3 [lacI lacUV5-T7 gene 1 ind1 sam7 nin5])</i>  | no                                     | (Studier et al., 1990)  |
| T7 Express | <i>fhuA2 lacZ::T7 gene1 [lon] ompT gal sulA11 R(mcr-73::miniTn10-- TetS)2 [dcm] R(zgb-210::Tn10-- TetS) endA1 Δ(mcrC-mrr)114::IS10</i> | no                                     | (Biolabs N. E.)         |
| TA15       | <i>Mel BLid nhaA 1 nhaB 1 lacZY</i>  | no                                     | (Goldberg et al., 1998) |

**Table A.4:** Alignment probability of assigned spin systems of TBsmr calculated by the software CARA.

| Sequence  | Alignment probability |
|-----------|-----------------------|
| M1-L4     | 62 %                  |
| L6-I10    | 63 %                  |
| V14-S18   | 48 %                  |
| L20-T27   | 56%                   |
| V33-G38   | 71%                   |
| M54-T68   | 51 %                  |
| A70       | 62 %                  |
| V95-V98   | 65 %                  |
| L103-A106 | 54 %                  |
| V127-H120 | 45 %                  |

# List of Tables

|     |   |     |
|-----|---|-----|
| 1.1 | Putative mycobacterial drug efflux pumps associated with reduced susceptibility to antibacterial agents . . . . . | 20  |
| 2.1 | PCR reaction mix . . . . .  | 22  |
| 2.2 | Schägger gel components . . . . .   | 25  |
| 3.1 | Expression screen of TBsmr for optimum expression conditions. . . . .   | 41  |
| 3.2 | Detergent reconstitution screen . . . . .   | 49  |
| 4.1 | Summary of experimental evidence for the oligomeric states of EmrE. . . . .                                       | 55  |
| 4.2 | Lipid reconstitution screen. . . . .  | 56  |
| 7.1 | Assignments of $^{13}\text{C}$ chemical shifts of W63 in TBsmr with and without EtBr. . . . .                     | 102 |
| A.1 | Defined media for selective isotope labeling . . . . .  | 116 |
| A.5 | NMR resonance assignments . . . . .   | 116 |
| A.2 | Minimal media for uniform $^{13}\text{C}/^{15}\text{N}$ isotope labeling. . . . .                                 | 119 |
| A.3 | <i>E. coli</i> strains used to express TBsmr . . . . .  | 119 |
| A.4 | Alignment probability of assigned spin systems of TBsmr calculated by the software CARA. . . . .                  | 119 |

# List of Figures

|      |  |    |
|------|--|----|
| 1.1  | Distribution of multidrug-resistant tuberculosis rates among previously treated cases. . . . .                         | 4  |
| 1.2  | Multidrug resistance mechanisms. . . . .   | 5  |
| 1.3  | Schematic comparison of the five families of multidrug-resistant efflux pumps. . . . .                                 | 6  |
| 1.4  | A phylogenetic tree of the SMR protein family. . . . .   | 8  |
| 1.5  | Sequence alignment of SMR proteins. . . . .  | 9  |
| 1.6  | Backbone model of the transmembrane region of EmrE. . . . .  | 11 |
| 1.7  | Alternate-access mechanism for proton-coupled translocation of substrates by the SMR family of proteins. . . . .       | 13 |
| 1.8  | <sup>13</sup> C solid-state NMR spectra of glycine (A). Schematic view of rotor with magic angle spinning (B). . . . . | 15 |
| 1.9  | Topology model of the TBsmr construct. . . . .   | 17 |
| 1.10 | Substrates of TBsmr. . . . .   | 18 |
| 1.11 | Biophysical techniques used to study TBsmr. . . . .  | 19 |
| 2.1  | Plasmid map of pT7-7 vector . . . . .  | 22 |
| 2.2  | DNA and protein sequence of the TBsmr (Rv3065) construct with myc/his-tag. . . . .                                     | 23 |
| 2.3  | Stern-Volmer plot of ethidium bromide. . . . .   | 33 |
| 2.4  | Pulse sequences of the cross polarization (A) and direct polarization (B) solid-state NMR experiments. . . . .         | 35 |
| 2.5  | Pulse sequence for the PDSO (A) and DARR (B) experiments. . . . .  | 37 |
| 3.1  | Schematic flowchart of the TBsmr sample preparation and the techniques used. . . . .                                   | 39 |
| 3.2  | Dot blot analysis of TBsmr expression yields in different <i>E. coli</i> strains. . . . .                              | 40 |
| 3.3  | SDS-PAGE and western blot of TBsmr. . . . .  | 42 |

|      |  |    |
|------|--|----|
| 3.4  | Mass spectrometry MALDI-TOF spectrum of purified TBsmr. . . . .  | 43 |
| 3.5  | Monodispersity of TBsmr in different detergents assessed by gel filtration.  | 44 |
| 3.6  | Long term stability of TBsmr in Fos-12 determined by gelfiltration. . . .  | 45 |
| 3.7  | Crystals of TBsmr. . . . .   | 46 |
| 3.8  | <sup>15</sup> N CPMAS NMR spectrum of TBsmr microcrystals and proteoliposomes.   | 47 |
| 3.9  | Freeze fracture electron micrographs of reconstituted TBsmr . . . . .  | 48 |
| 4.1  | Schematic layout of the TPP <sup>+</sup> transport assay. . . . .  | 57 |
| 4.2  | Calibration of the electrode MI-600. . . . .   | 57 |
| 4.3  | TPP <sup>+</sup> transport assay. . . . .  | 58 |
| 4.4  | TPP <sup>+</sup> transport assay controls. . . . .   | 59 |
| 4.5  | Influence of lipids on the particle size and TPP <sup>+</sup> transport activity of re-<br>constituted TBsmr. . . . .  | 60 |
| 4.6  | Transport kinetics, V <sub>max</sub> and K, of TBsmr in E. coli liposomes for the<br>substrate TPP <sup>+</sup> . . . . .  | 61 |
| 4.7  | Measurement of the diameter of protein particles in freeze-fracture images.  | 62 |
| 4.8  | Simulated histograms for an elliptic particle. . . . .   | 63 |
| 4.9  | Schematic model and simulated histograms of possible TBsmr oligomers.  | 64 |
| 4.10 | Determination of the oligomeric state of TBsmr in different lipids. . . . .  | 64 |
| 5.1  | Principle of the SMR – bR transport assay. . . . .   | 69 |
| 5.2  | Directional reconstitution of bR into TBsmr proteoliposomes. . . . .   | 71 |
| 5.3  | EtBr fluorescence transport assay . . . . .  | 72 |
| 5.4  | Long term stability test of the transport assay. . . . .   | 73 |
| 5.5  | pH dependance of EtBr fluorescence. . . . .  | 74 |
| 5.6  | Fluorescence assay controls. . . . .   | 75 |
| 5.7  | Transport of ethidium bromide is inhibited by TPP <sup>+</sup> (A). EtBr binding<br>curve (B). . . . .   | 76 |
| 5.8  | EtBr fluorescence anisotropy. . . . .  | 78 |
| 5.9  | Intermediate state model. . . . .  | 80 |
| 5.10 | Proposed alternate-access mechanism for proton-coupled translocation of<br>substrates by SMR proteins including the occluded substrate-protein com-<br>plex. . . . . | 83 |

---

|     |  |     |
|-----|--|-----|
| 6.1 | $^1\text{H}$ - $^{15}\text{N}$ HSQC spectrum of uniformly $^{13}\text{C}$ , $^{15}\text{N}$ labeled TBsmr in different detergents. . . . . | 85  |
| 6.2 | Influence of the temperature on the amide proton signal intensity of TBsmr in a liquid-state NMR experiment. . . . .                       | 86  |
| 6.3 | $^1\text{H}$ - $^{15}\text{N}$ TROSY HSQC spectrum of uniformly $^{13}\text{C}$ , $^{15}\text{N}$ labeled TBsmr. . . . .                   | 88  |
| 6.4 | Topology model of TBsmr with tentatively assigned residues in blue. . . . .  | 89  |
| 6.5 | Representative strip plot of the TROSY-HNCA experiment. . . . .  | 90  |
| 6.6 | 2D $^1\text{H}$ - $^{15}\text{N}$ HSQC spectrum of TBsmr with and without EtBr. . . . .  | 91  |
| 6.7 | LILBID mass spectroscopy of TBsmr in LPPG. . . . .   | 92  |
| 7.1 | 1D $^{15}\text{N}$ CPMAS NMR spectra of TBsmr proteoliposomes. . . . .   | 94  |
| 7.2 | DP and CP spectra of uniformly $^{15}\text{N}$ labeled TBsmr in the non-frozen state. . . . .  | 95  |
| 7.3 | 2D $^{13}\text{C}$ - $^{13}\text{C}$ PDSO spectra of $^{13}\text{C}$ selectively unlabeled TBsmr E13A and TBsmr wt. . . . .                | 97  |
| 7.4 | 1D $^{19}\text{F}$ DP-MAS NMR spectra of TBsmr proteoliposomes in the absence and presence of EtBr. . . . .                                | 98  |
| 7.5 | bR-SMR transport assay of TBsmr W30A. . . . .  | 99  |
| 7.6 | DARR experiment of $^{13}\text{C}$ tryptophan labeled TBsmr W30A. . . . .  | 100 |
| 7.7 | Solid-state NMR line shape analysis of the W63 crosspeaks of TBsmr W30A. . . . .   | 101 |
| 7.8 | Model of a parallel and anti-parallel arrangement of TMS 3 in the TBsmr dimer. . . . .   | 105 |

# Abbreviations

|                    |  |
|--------------------|--|
| aa                 | amino acids  |
| BC                 | benzalkonium chloride  |
| bR                 | bacteriorhodopsin  |
| CCCP               | carbonyl cyanide 3-chlorophenylhydrazone                     |
| CIL                | Cambridge Isotope Laboratories                               |
| cmc                | critical micelle concentration                               |
| CP                 | cross polarization   |
| cymal-6            | 6-cyclohexyl-1-hexyl-D-maltoside                             |
| DARR               | dipolar assisted rotational resonance                        |
| DCCD               | N,N'-dicyclohexylcarbodiimide                                |
| ddH <sub>2</sub> O | double deionized water                                       |
| DDM                | n-dodecyl- $\beta$ -D-maltoside                              |
| DGK                | diacylglycerol kinase  |
| DHB                | 2,5-dihydroxy benzoic acid:2-hydroxy-5-methoxy benzoic acid  |
| DM                 | decyl- $\beta$ -D-maltoside                                  |
| DMPC               | 1,2-dimyristoyl- <i>sn</i> -glycero-3-phosphocholine         |
| DOPC               | 1,2-dioleoyl- <i>sn</i> -glycero-3-phosphocholine            |
| DPOPE              | 1,2-dipalmitoleoyl- <i>sn</i> -glycero-3-phosphoethanolamine |

---

|           |   |
|-----------|---|
| DSS       | 2,2-dimethyl-2-silapentane-5-sulfonic acid                    |
| DTM       | n-decyl- $\beta$ -D-thiomaltoside                             |
| DTT       | 1,4-dithio-DL-threitol  |
| EM        | electron microscopy   |
| EPR       | electron paramagnetic resonance                               |
| ESI       | electrospray ionization                                       |
| EtBr      | ethidium bromide  |
| FID       | free induction decay  |
| Fos-12    | n-dodecylphosphocholine                                       |
| FTIR      | fourier transform infrared                                    |
| GRAVY     | grand average of hydrophobicity                               |
| HPLC      | high pressure liquid chromatography                           |
| HSQC      | heteronuclear single quantum correlation                      |
| IPTG      | isopropyl $\beta$ -D-thiogalactoside                          |
| ITC       | isothermal titration calorimetry                              |
| LB        | Luria-Bertani   |
| lb        | line broadening   |
| LILBID    | laser induced liquid beam ionization/desorption               |
| LMPG      | 1-myristoyl-2-hydroxy-sn-glycero-3-[phospho-RAC-(1-glycerol)] |
| LPPG      | 1-palmitoyl-2-hydroxy-sn-glycero-3-[phospho-RAC-(1-glycerol)] |
| MALDI-TOF | matrix assisted laser desorption/ionization - time-of-flight  |
| MAS       | magic angle spinning  |

---

|                  |   |
|------------------|---|
| MD               | molecular dynamics  |
| MDR              | multidrug resistance  |
| MS               | mass spectrometry   |
| MV <sup>2+</sup> | methyl viologen   |
| MWCO             | molecular weight cut-off                                      |
| Ni-NTA           | nickel-nitrilotriacetic acid                                  |
| NMR              | nuclear magnetic resonance                                    |
| OG               | octylglucoside  |
| PCR              | polymerase chain reaction                                     |
| PDSD             | proton-driven spin diffusion                                  |
| pmf              | proton motif force  |
| POPC             | 1-palmitoyl-2-oleoy- <i>sn</i> -glycero-3-phosphocholine      |
| POPE             | 1-palmitoyl-2-oleoy- <i>sn</i> -glycero-3-phosphoethanolamine |
| POPG             | 1-palmitoyl-2-oleoy- <i>sn</i> -glycero-3-phosphoglycerol     |
| QAC              | quarterny ammonium compounds                                  |
| REDOR            | rotational-echo double-resonance                              |
| RNA              | ribonucleic acid  |
| SDS-PAGE         | sodium dodecylsulfate polyacrylamide gel electrophoresis      |
| SEC              | size exclusion chromatography                                 |
| SMR              | small multidrug resistance                                    |
| Smr              | staphylococcal multidrug resistance                           |
| S/N              | signal-to-noise ratio   |

|                  |  |
|------------------|--|
| SPINAL           | small phase incremental alternation          |
| ssNMR            | solid-state NMR                              |
| TCEP             | Tris(2-Carboxyethyl) phosphine               |
| TEMED            | N,N,N',N'-Tetramethylethylenediamine         |
| TMS              | transmembrane segment                        |
| TOCL             | 1,1',2,2'-tetraoleoyl-cardiolipin            |
| TPP <sup>+</sup> | tetraphenyl phosphonium                      |
| TPPM             | two-pulse phase modulation                   |
| triton X-100     | t-octylphenoxypolyethoxyethanol              |
| TROSY            | transverse relaxation optimized spectroscopy |

# Acknowledgements

At this place I would like to thank all the people who contributed to this work and made my stay at the J. W. Goethe University a memorable time.

First of all, I wish to thank Prof. Clemens Glaubitz for the opportunity to work in his young and motivated group. I am very grateful for his continuing optimism and support throughout the project, and I enjoyed our numerous discussions about the ins and outs of SMR proteins which proved to be very fruitful. Also, I thank him for organizing the funding (SFB628 and Proamp).

Furthermore, I would like to thank, Dr. Mark Lorch and Dr. Jakob Lopez, the best Post-Docs in the world but also friends.

Special thanks go to my SMR - team colleague Ines Lehner, who walked the same path as me.

I am thankful to Gregor Madej, Horng der Ou and Christian Klammt, with whom I have spend a lot of time drinking beer and talking business.

The remaining present group members of AK Glaubitz are thanked.

Outside the group, I would like to thank Dr. Winfried Haase of the MPI of Biophysics for the numerous freeze-fracture EM pictures, and Björn Meyer from the Karas group for the MS spectra.

The liquid-state NMR was performed in collaboration with Frank Löhr from the Dötsch group. My thanks goes to Frank Löhr, Prof. Volker Dötsch and the other members of the group with whom we did so many things that it felt like we were part of the same group.

If your research is going to be one long emergeny, it is a good idea to have some friends: Theofanis Manolikas, Max Stadler, Sebastian Richers, Fuensanta Martinez, Sina Reckel, Lucia Cenacchi, Sachin Surade, Rob Dempski, Andrea Sauerwein and Ulrike Wedemeyer.

Finally, I would like to thank Nora Willian and my parents for their love and support throught the years.

## References

- Agarwal V, Fink U, Schuldiner S, Reif B (2007) MAS solid-state NMR studies on the multidrug transporter EmrE. *Biochim Biophys Acta Biomembr* : advanced online publication doi:10.1016/j.bbamem.2007.09.012
- Allen TM, Romans AY, Kercret H, Segrest JP (1980) Detergent removal during membrane reconstitution. *Biochim Biophys Acta* **601**: 328–342
- Almeida FC, Amorim GC, Moreau VH, Sousa VO, Creazola AT, Americo TA, Pais AP, Leite A, Netto LE, Giordano RJ, Valente AP (2001) Selectively labeling the heterologous protein in *Escherichia coli* for NMR studies: a strategy to speed up NMR spectroscopy. *J Magn Reson* **148**: 142–146. doi:10.1006/jmre.2000.2213
- Andersen OS, Koeppe RE (2007) Bilayer thickness and membrane protein function: an energetic perspective. *Annu Rev Biophys Biomol Struct* **36**: 107–130. doi:10.1146/annurev.biophys.36.040306.132643
- Andronesi OC, Becker S, Seidel K, Heise H, Young HS, Baldus M (2005) Determination of membrane protein structure and dynamics by magic-angle-spinning solid-state NMR spectroscopy. *J Am Chem Soc* **127**: 12965–12974. doi:10.1021/ja0530164
- Arkin IT, Brunger AT (1998) Statistical analysis of predicted transmembrane alpha-helices. *Biochim Biophys Acta* **1429**: 113–128
- Arkin IT, Russ WP, Lebendiker M, Schuldiner S (1996) Determining the secondary structure and orientation of EmrE, a multi-drug transporter, indicates a transmembrane four-helix bundle. *Biochemistry* **35**: 7233–7238. doi:10.1021/bi960094i
- Atreya HS, Chary KVR (2000) Amino acid selective "unlabelling" for residue specific NMR assignments in proteins. *Curr Sci* **79**: 504–507

- Auer M, Kim MJ, Lemieux MJ, Villa A, Song J, Li XD, Wang DN (2001) High-yield expression and functional analysis of Escherichia coli glycerol-3-phosphate transporter. *Biochemistry* **40**: 6628–6635
- Baldus M, Geurts DG, Meier BH (1998) Broadband dipolar recoupling in rotating solids: a numerical comparison of some pulse schemes. *Solid State Nucl Magn Reson* **11**: 157–168
- Barth A, Corrie JE (2002) Characterization of a new caged proton capable of inducing large pH jumps. *Biophys J* **83**: 2864–2871
- Basting D, Lehner I, Lorch M, Glaubitz C (2006) Investigating transport proteins by solid state NMR. *Naunyn Schmiedebergs Arch Pharmacol* **372**: 451–464. doi: 10.1007/s00210-006-0039-4
- Basting D, Lorch M, Lehner I, Glaubitz C (2007) Transport cycle intermediate in small multidrug resistance protein is revealed by substrate fluorescence. *FASEB J* : advance online publication doi:10.1096/fj.07-9162com
- Bay DC, Rommens KL, Turner RJ (2007) Small multidrug resistance proteins: A multidrug transporter family that continues to grow. *Biochim Biophys Acta Biomembr* : advanced online publication doi:10.1016/j.bbamem.2007.08.015
- Beauge LA, Glynn IM (1979) Occlusion of K ions in the unphosphorylated sodium pump. *Nature* **280**: 510–512
- Bennett AE, Rienstra CM, Auger M, Lakshmi KV, Griffin RG (1995) Heteronuclear decoupling in rotating solids. *J Chem Phys* **103**: 6951–6958. doi:10.1063/1.470372
- Bennett AE, Rienstra CM, Griffiths JM, Zhen W, Jr, Griffin RG (1998) Homonuclear radio frequency-driven recoupling in rotating solids. *J Chem Phys* **108**: 9463–9479
- Bertini I, Felli IC, Gonnelli L, Pierattelli R, Spyranzi Z, Spyroulias GA (2006) Mapping protein-protein interaction by <sup>13</sup>C'-detected heteronuclear NMR spectroscopy. *J Biomol NMR* **36**: 111–122. doi:10.1007/s10858-006-9068-z
- Biolabs NE (2007) T7 Express : cited 28.11.07 from <http://www.neb.uk.com>
- Bloch F (1956) Dynamical Theory of Nuclear Induction. II. *Phys Rev* **102**: 104+. doi: 10.1103/PhysRev.102.104

- Bogdanov M, Umeda M, Dowhan W (1999) Phospholipid-assisted refolding of an integral membrane protein. Minimum structural features for phosphatidylethanolamine to act as a molecular chaperone. *J Biol Chem* **274**: 12339–12345
- Booth PJ, Templer RH, Curran AR, Allen SJ (2001) Can we identify the forces that drive the folding of integral membrane proteins? *Biochem Soc Trans* **29**: 408–413
- Boulter JM, Wang DN (2001) Purification and characterization of human erythrocyte glucose transporter in decylmaltoside detergent solution. *Protein Expr Purif* **22**: 337–348. doi:10.1006/prev.2001.1440
- Brennan PJ, Nikaido H (1995) The envelope of mycobacteria. *Annu Rev Biochem* **64**: 29–63. doi:10.1146/annurev.bi.64.070195.000333
- Brown MH, Paulsen IT, Skurray RA (1999) The multidrug efflux protein NorM is a prototype of a new family of transporters. *Mol Microbiol* **31**: 394–395
- Butler PJ, Ubarretxena-Belandia I, Warne T, Tate CG (2004) The Escherichia coli multidrug transporter EmrE is a dimer in the detergent-solubilised state. *J Mol Biol* **340**: 797–808. doi:10.1016/j.jmb.2004.05.014
- Cantor RS (1997) The Lateral Pressure Profile in Membranes: A Physical Mechanism of General Anesthesia. *Biochemistry* **36**: 2339–2344. doi:10.1021/bi9627323
- Cantor RS (1999) Lipid composition and the lateral pressure profile in bilayers. *Biophys J* **76**: 2625–2639
- Castellani F, van Rossum B, Diehl A, Schubert M, Rehbein K, Oschkinat H (2002) Structure of a protein determined by solid-state magic-angle-spinning NMR spectroscopy. *Nature* **420**: 98–102. doi:10.1038/nature01070
- Chang G, Roth CB, Reyes CL, Pornillos O, Chen YJ, Chen AP (2006) Retraction. *Science* **314**: 1875+. doi:10.1126/science.314.5807.1875b
- Chen YJ, Pornillos O, Lieu S, Ma C, Chen AP, Chang G (2007) X-ray structure of EmrE supports dual topology model. *Proc Natl Acad Sci U S A* **104**: 18999–19004. doi:10.1073/pnas.0709387104

- Cheng Y, Prusoff WH (1973) Relationship between the inhibition constant ( $K_1$ ) and the concentration of inhibitor which causes 50 per cent inhibition ( $I_{50}$ ) of an enzymatic reaction. *Biochem Pharmacol* **22**: 3099–3108
- Chevelkov V, Faelber K, Schrey A, Rehbein K, Diehl A, Reif B (2007) Differential line broadening in MAS solid-state NMR due to dynamic interference. *J Am Chem Soc* **129**: 10195–10200. doi:10.1021/ja072024c
- Chi-Rosso G, Toole BP (1987) Hyaluronate-binding protein of simian virus 40-transformed 3T3 cells: membrane distribution and reconstitution into lipid vesicles. *J Cell Biochem* **33**: 173–183. doi:10.1002/jcb.240330304
- Chung YJ, Saier MH (2001) SMR-type multidrug resistance pumps. *Curr Opin Drug Discov Devel* **4**: 237–245
- Chung YJ, Saier MH (2002) Overexpression of the Escherichia coli sugE gene confers resistance to a narrow range of quaternary ammonium compounds. *J Bacteriol* **184**: 2543–2545
- Colangeli R, Helb D, Sridharan S, Sun J, Varma-Basil M, Hazbon MH, Harbacheuski R, Megjugorac NJ, Jacobs WR, Holzenburg A, Sacchettini JC, Alland D (2005) The Mycobacterium tuberculosis iniA gene is essential for activity of an efflux pump that confers drug tolerance to both isoniazid and ethambutol. *Mol Microbiol* **55**: 1829–1840. doi:10.1111/j.1365-2958.2005.04510.x
- Costello MJ, Viitanen P, Carrasco N, Foster DL, Kaback HR (1984) Morphology of proteoliposomes reconstituted with purified lac carrier protein from Escherichia coli. *J Biol Chem* **259**: 15579–15586
- Cox H, Kebede Y, Allamuratova S, Ismailov G, Davletmuratova Z, Byrnes G, Stone C, Niemann S, Ruesch-Gerdes S, Blok L, Doshetov D (2006) Tuberculosis recurrence and mortality after successful treatment: impact of drug resistance. *PLoS Med* **3**: e384+. doi:10.1371/journal.pmed.0030384
- Crocker E, Patel AB, Eilers M, Jayaraman S, Getmanova E, Reeves PJ, Ziliox M, Khorana HG, Sheves M, Smith SO (2004) Dipolar assisted rotational resonance NMR of tryptophan and tyrosine in rhodopsin. *J Biomol NMR* **29**: 11–20. doi:10.1023/B:JNMR.0000019521.79321.3c

- Curnow P, Lorch M, Charalambous K, Booth PJ (2004) The reconstitution and activity of the small multidrug transporter EmrE is modulated by non-bilayer lipid composition. *J Mol Biol* **343**: 213–222. doi:10.1016/j.jmb.2004.08.032
- Daley DO, Rapp M, Granseth E, Melen K, Drew D, von Heijne G (2005) Global topology analysis of the Escherichia coli inner membrane proteome. *Science* **308**: 1321–1323. doi:10.1126/science.1109730
- Daporta MT, Bellido MJL, Guirao GY, Hernandez MS, Garcia-Rodriguez JA (2004) In vitro activity of older and newer fluoroquinolones against efflux-mediated high-level ciprofloxacin-resistant Streptococcus pneumoniae. *Int J Antimicrob Agents* **24**: 185–187. doi:10.1016/j.ijantimicag.2004.01.012
- Dawson RJP, Locher KP (2006) Structure of a bacterial multidrug ABC transporter. *Nature* **443**: 156–157. doi:10.1038/nature05155
- de Lima Santos H, Lopes ML, Maggio B, Ciancaglini P (2005) Na,K-ATPase reconstituted in liposomes: effects of lipid composition on hydrolytic activity and enzyme orientation. *Colloids Surf B Biointerfaces* **41**: 239–248. doi:10.1016/j.colsurfb.2004.12.013
- De Rossi E, Ainsa JA, Riccardi G (2006) Role of mycobacterial efflux transporters in drug resistance: an unresolved question. *FEMS Microbiol Rev* **30**: 36–52. doi:10.1111/j.1574-6976.2005.00002.x
- De Rossi E, Arrigo P, Bellinzoni M, Silva PA, Martin C, Ainsa JA, Guglierame P, Riccardi G (2002) The multidrug transporters belonging to major facilitator superfamily in Mycobacterium tuberculosis. *Mol Med* **8**: 714–724
- De Rossi E, Blokpoel MC, Cantoni R, Branzoni M, Riccardi G, Young DB, De Smet KA, Ciferri O (1998a) Molecular Cloning and Functional Analysis of a Novel Tetracycline Resistance Determinant, tet(V), from Mycobacterium smegmatis. *Antimicrob Agents Chemother* **42**: 1931–1937
- De Rossi E, Branzoni M, Cantoni R, Milano A, Riccardi G, Ciferri O (1998b) mmr, a Mycobacterium tuberculosis gene conferring resistance to small cationic dyes and inhibitors. *J Bacteriol* **180**: 6068–6071

- Dougherty DA (1996) Cation- $\pi$  interactions in chemistry and biology: a new view of benzene, Phe, Tyr, and Trp. *Science* **271**: 163–168. doi:10.1126/science.271.5246.163
- Dougherty DA (2007) Cation- $\pi$  interactions involving aromatic amino acids. *J Nutr* **137**: 1504S–1508S
- Elbaz Y, Steiner-Mordoch S, Danieli T, Schuldiner S (2004) In vitro synthesis of fully functional EmrE, a multidrug transporter, and study of its oligomeric state. *Proc Natl Acad Sci U S A* **101**: 1519–1524. doi:10.1073/pnas.0306533101
- Elbaz Y, Tayer N, Steinfels E, Steiner-Mordoch S, Schuldiner S (2005) Substrate-induced tryptophan fluorescence changes in EmrE, the smallest ion-coupled multidrug transporter. *Biochemistry* **44**: 7369–7377. doi:10.1021/bi050356t
- Eskandari S, Wright EM, Kreman M, Starace DM, Zampighi GA (1998) Structural analysis of cloned plasma membrane proteins by freeze-fracture electron microscopy. *Proc Natl Acad Sci U S A* **95**: 11235–11240
- Fang G, Friesen R, Lanfermeijer F, Hagting A, Poolman B, Konings WN (1999) Manipulation of activity and orientation of membrane-reconstituted di-tripeptide transport protein DtpT of *Lactococcus lactis*. *Mol Membr Biol* **16**: 297–304
- Federkeil SL, Winstone TL, Jickling G, Turner RJ (2003) Examination of EmrE conformational differences in various membrane mimetic environments. *Biochem Cell Biol* **81**: 61–70. doi:10.1139/o03-031
- Fiaux J, Bertelsen EB, Horwich AL, Wuethrich K (2004) Uniform and Residue-specific  $^{15}\text{N}$ -labeling of Proteins on a Highly Deuterated Background. *J Biomol NMR* **29**: 289–297. doi:10.1023/B:JNMR.0000032523.00554.38
- Fleishman SJ, Harrington SE, Enosh A, Halperin D, Tate CG, Ben-Tal N (2006) Quasi-symmetry in the cryo-EM structure of EmrE provides the key to modeling its trans-membrane domain. *J Mol Biol* **364**: 54–67. doi:10.1016/j.jmb.2006.08.072
- Frericks H, Zhou D, Yap L, Gennis R, Rienstra C (2006) Magic-angle spinning solid-state NMR of a 144 Å kDa membrane protein complex: *E. coli* cytochrome  $\text{bo}_3$  oxidase. *J Biomol NMR* **36**: 55–71. doi:10.1007/s10858-006-9070-5

- Fung BM, Khittrin AK, Ermolaev K (2000) An improved broadband decoupling sequence for liquid crystals and solids. *J Magn Reson* **142**: 97–101. doi:10.1006/jmre.1999.1896
- Genest D, Mirau PA, Kearns DR (1985) Investigation of DNA dynamics and drug-DNA interaction by steady state fluorescence anisotropy. *Nucleic Acids Res* **13**: 2603–2615
- Glaubitz C, Groeger A, Gottschalk K, Spooner P, Watts A, Schuldiner S, Kessler H (2000) <sup>31</sup>P-CP-MAS NMR studies on TPP<sup>+</sup> bound to the ion-coupled multidrug transport protein EmrE. *FEBS Lett* **480**: 127–131
- Goldberg EB, Arbel T, Chen J, Karpel R, Mackie GA, Schuldiner S, Padan E (1987) Characterization of a Na<sup>+</sup>/H<sup>+</sup> antiporter gene of Escherichia coli. *Proc Natl Acad Sci U S A* **84**: 2615–2619
- Goodenough UW, Staehelin LA (1971) Structural differentiation of stacked and unstacked chloroplast membranes. Freeze-etch electron microscopy of wild-type and mutant strains of Chlamydomonas. *J Cell Biol* **48**: 594–619
- Grage SL, Wang J, Cross TA, Ulrich AS (2002) Solid-state <sup>19</sup>F-NMR analysis of <sup>19</sup>F-labeled tryptophan in gramicidin A in oriented membranes. *Biophys J* **83**: 3336–3350
- Greener T, Govezensky D, Zamir A (1993) A novel multicopy suppressor of a groEL mutation includes two nested open reading frames transcribed from different promoters. *EMBO J* **12**: 889–896
- Grinius L, Dreguniene G, Goldberg EB, Liao CH, Projan SJ (1992) A staphylococcal multidrug resistance gene product is a member of a new protein family. *Plasmid* **27**: 119–129
- Grinius LL, Goldberg EB (1994) Bacterial multidrug resistance is due to a single membrane protein which functions as a drug pump. *J Biol Chem* **269**: 29998–30004
- Gros P, Ben Neriah YB, Croop JM, Housman DE (1986) Isolation and expression of a complementary DNA that confers multidrug resistance. *Nature* **323**: 728–731. doi:10.1038/323728a0
- Guan L, Kaback HR (2004) Binding affinity of lactose permease is not altered by the H<sup>+</sup> electrochemical gradient. *Proc Natl Acad Sci U S A* **101**: 12148–12152. doi:10.1073/pnas.0404936101

- Guenza M, Cuniberti C (1988) The ethidium bromide dimer. Absorption and fluorescence properties in aqueous solutions. *Spectrochim Acta [A]* **44**: 1359–1364
- Gutman N, Steiner-Mordoch S, Schuldiner S (2003) An Amino Acid Cluster around the Essential Glu-14 Is Part of the Substrate- and Proton-binding Domain of EmrE, a Multidrug Transporter from *Escherichia coli*. *J Biol Chem* **278**: 16082–16087. doi: 10.1074/jbc.M213120200
- Hartmann SR, Hahn EL (1962) Nuclear Double Resonance in the Rotating Frame. *Phys Rev* **128**: 2042+. doi:10.1103/PhysRev.128.2042
- Heir E, Sundheim G, Holck AL (1995) Resistance to quaternary ammonium compounds in *Staphylococcus* spp. isolated from the food industry and nucleotide sequence of the resistance plasmid pST827. *J Appl Bacteriol* **79**: 149–156
- Higgins CF (2007) Multiple molecular mechanisms for multidrug resistance transporters. *Nature* **446**: 749–757. doi:10.1038/nature05630
- Hillen W, Berens C (1994) Mechanisms underlying expression of Tn10 encoded tetracycline resistance. *Annu Rev Microbiol* **48**: 345–369. doi: 10.1146/annurev.mi.48.100194.002021
- Hiller M, Krabben L, Vinothkumar KR, Castellani F, van Rossum BJ, Kuehlbrandt W, Oschkinat H (2005) Solid-state magic-angle spinning NMR of outer-membrane protein G from *Escherichia coli*. *Chembiochem* **6**: 1679–1684. doi:10.1002/cbic.200500132
- Hong M, Isailovic D, McMillan RA, Conticello VP (2003) Structure of an elastin-mimetic polypeptide by solid-state NMR chemical shift analysis. *Biopolymers* **70**: 158–168. doi:10.1002/bip.10431
- Hong M, Jakes K (1999) Selective and extensive <sup>13</sup>C labeling of a membrane protein for solid-state NMR investigations. *J Biomol NMR* **14**: 71–74
- Horsefield R, Yankovskaya V, Törnroth S, Luna-Chavez C, Stambouli E, Barber J, Byrne B, Cecchini G, Iwata S (2003) Using rational screening and electron microscopy to optimize the crystallization of succinate:ubiquinone oxidoreductase from *Escherichia coli*. *Acta Crystallogr D Biol Crystallogr* **59**: 600–602

- Ilag LL, Ubarretxena-Belandia I, Tate CG, Robinson CV (2004) Drug binding revealed by tandem mass spectrometry of a protein-micelle complex. *J Am Chem Soc* **126**: 14362–14363. doi:10.1021/ja0450307
- Jack DL, Storms ML, Tchieu JH, Paulsen IT, Saier MH (2000) A Broad-Specificity Multidrug Efflux Pump Requiring a Pair of Homologous SMR-Type Proteins. *J Bacteriol* **182**: 2311–2313. doi:10.1128/JB.182.8.2311-2313.2000
- Jaroniec CP, MacPhee CE, Bajaj VS, McMahon MT, Dobson CM, Griffin RG (2004) High-resolution molecular structure of a peptide in an amyloid fibril determined by magic angle spinning NMR spectroscopy. *Proc Natl Acad Sci U S A* **101**: 711–716. doi:10.1073/pnas.0304849101
- Juliano RL, Ling V (1976) A surface glycoprotein modulating drug permeability in Chinese hamster ovary cell mutants. *Biochim Biophys Acta* **455**: 152–162
- Kaback HR, Dunten R, Frillingos S, Venkatesan P, Kwaw I, Zhang W, Ermolova N (2007) Site-directed alkylation and the alternating access model for LacY. *Proc Natl Acad Sci U S A* **104**: 491–494. doi:10.1073/pnas.0609968104
- Karas M, Hillenkamp F (1988) Laser desorption ionization of proteins with molecular masses exceeding 10,000 daltons. *Anal Chem* **60**: 2299–2301
- Keller RL (2004) *Optimizing the process of nuclear magnetic resonance spectrum analysis and computer aided resonance assignment*. Ph.D. thesis, Eidgenoessische Technische Hochschule ETH Zuerich
- Kikukawa T, Nara T, Araiso T, Miyauchi S, Kamo N (2006) Two-component bacterial multidrug transporter, EbrAB: Mutations making each component solely functional. *Biochim Biophys Acta* **1758**: 673–679. doi:10.1016/j.bbamem.2006.04.004
- Kim HW, Perez JA, Ferguson SJ, Campbell ID (1990) The specific incorporation of labelled aromatic amino acids into proteins through growth of bacteria in the presence of glyphosate. Application to fluorotryptophan labelling to the H(+)-ATPase of *Escherichia coli* and NMR studies. *FEBS Lett* **272**: 34–36
- Klammt C, Loehr F, Schaefer B, Haase W, Doetsch V, Rueterjans H, Glaubitz C, Bernhard F (2004) High level cell-free expression and specific labeling of integral membrane proteins. *Eur J Biochem* **271**: 568–580

- Klein C, Garcia-Rizo C, Bisle B, Scheffer B, Zischka H, Pfeiffer F, Siedler F, Oesterhelt D (2005) The membrane proteome of *Halobacterium salinarum*. *Proteomics* **5**: 180–197. doi:10.1002/pmic.200400943
- Knol J, Veenhoff L, Liang WJ, Henderson PJ, Leblanc G, Poolman B (1996) Unidirectional reconstitution into detergent-destabilized liposomes of the purified lactose transport system of *Streptococcus thermophilus*. *J Biol Chem* **271**: 15358–15366
- Kobayashi, Masatoshi, Matsuki, Yoh, Yumen, Ikuko, Fujiwara, Toshimichi, Akutsu, Hideo (2006) Signal assignment and secondary structure analysis of a uniformly [<sup>13</sup>C, <sup>15</sup>N]-labeled membrane protein, H<sup>+</sup>-ATP synthase subunit c, by magic-angle spinning solid-state NMR. *J Biomol NMR* **36**: 279–293. doi:10.1007/s10858-006-9094-x
- Korepanova A, Moore JD, Nguyen HB, Hua Y, Cross TA, Gao F (2007) Expression of membrane proteins from *Mycobacterium tuberculosis* in *Escherichia coli* as fusions with maltose binding protein. *Protein Expr Purif* **53**: 24–30. doi:10.1016/j.pep.2006.11.022
- Koteiche HA, Reeves MD, Mchaourab HS (2003) Structure of the substrate binding pocket of the multidrug transporter EmrE: site-directed spin labeling of transmembrane segment 1. *Biochemistry* **42**: 6099–6105. doi:10.1021/bi0342867
- Krueger-Koplin RD, Sorgen PL, Krueger-Koplin ST, Rivera-Torres IO, Cahill SM, Hicks DB, Grinius L, Krulwich TA, Girvin ME (2004) An evaluation of detergents for NMR structural studies of membrane proteins. *Journal of Biomolecular NMR* **28**: 43–57. doi:10.1023/B:JNMR.0000012875.80898.8f
- Kyte J, Doolittle RF (1982) A simple method for displaying the hydropathic character of a protein. *J Mol Biol* **157**: 105–132
- Lambert O, Levy D, Ranck JL, Leblanc G, Rigaud JL (1998) A new "gel-like" phase in dodecyl maltoside-lipid mixtures: implications in solubilization and reconstitution studies. *Biophys J* **74**: 918–930
- Lee AG (2004) How lipids affect the activities of integral membrane proteins. *Biochim Biophys Acta* **1666**: 62–87. doi:10.1016/j.bbamem.2004.05.012
- Lee KM, Androphy EJ, Baleja JD (1995) A novel method for selective isotope labeling of bacterially expressed proteins. *J Biomol NMR* **5**: 93–96

- Lehner I, Basting D, Meyer B, Haase W, Manolikas T, Kaiser C, Karas M, Glaubitz C (2007) The key residue for substrate transport (E14) in the EMRE dimer is asymmetric. *J Biol Chem* : advance online publication,doi:10.1074/jbc.M707899200
- Levy D, Bluzat A, Seigneuret M, Rigaud JL (1990) A systematic study of liposome and proteoliposome reconstitution involving Bio-Bead-mediated Triton X-100 removal. *Biochim Biophys Acta* **1025**: 179–190
- Levy D, Gulik A, Bluzat A, Rigaud JL (1992) Reconstitution of the sarcoplasmic reticulum Ca(2+)-ATPase: mechanisms of membrane protein insertion into liposomes during reconstitution procedures involving the use of detergents. *Biochim Biophys Acta* **1107**: 283–298
- Li XZ, Zhang L, Nikaido H (2004) Efflux pump-mediated intrinsic drug resistance in *Mycobacterium smegmatis*. *Antimicrob Agents Chemother* **48**: 2415–2423. doi: 10.1128/AAC.48.7.2415-2423.2004
- Lillebaek T, Dirksen A, Vynnycky E, Baess I, Thomsen V, Andersen AB (2003) Stability of DNA patterns and evidence of *Mycobacterium tuberculosis* reactivation occurring decades after the initial infection. *J Infect Dis* **188**: 1032–1039
- Littlejohn TG, DiBerardino D, Messerotti LJ, Spiers SJ, Skurray RA (1991) Structure and evolution of a family of genes encoding antiseptic and disinfectant resistance in *Staphylococcus aureus*. *Gene* **101**: 59–66
- Littlejohn TG, Paulsen IT, Gillespie MT, Tennent JM, Midgley M, Jones IG, Purewal AS, Skurray RA (1992) Substrate specificity and energetics of antiseptic and disinfectant resistance in *Staphylococcus aureus*. *FEMS Microbiol Lett* **74**: 259–265
- Llanes C, Hocquet D, Vogne C, Benali-Baitich D, Neuwirth C, Plesiat P (2004) Clinical strains of *Pseudomonas aeruginosa* overproducing MexAB-OprM and MexXY efflux pumps simultaneously. *Antimicrob Agents Chemother* **48**: 1797–1802
- Lorch M, Fahem S, Kaiser C, Weber I, Mason AJ, Bowie JU, Glaubitz C (2005a) How to prepare membrane proteins for solid-state NMR: A case study on the alpha-helical integral membrane protein diacylglycerol kinase from *E. coli*. *Chembiochem* **6**: 1693–1700. doi:10.1002/cbic.200500054

- Lorch M, Lehner I, Siarheyeva A, Basting D, Pflieger N, Manolikas T, Glaubitz C (2005b) NMR and fluorescence spectroscopy approaches to secondary and primary active multidrug efflux pumps. *Biochem Soc Trans* **33**: 873–877. doi:10.1042/BST0330873
- Luck LA, Falke JJ (1991) <sup>19</sup>F NMR studies of the D-galactose chemosensory receptor. 1. Sugar binding yields a global structural change. *Biochemistry* **30**: 4248–4256
- Luedtke NW, Liu Q, Tor Y (2005) On the electronic structure of ethidium. *Chemistry* **11**: 495–508. doi:10.1002/chem.200400559
- Ma C, Chang G (2004) Structure of the multidrug resistance efflux transporter EmrE from *Escherichia coli*. *Proc Natl Acad Sci U S A* **101**: 2852–2857
- Margolles A, Putman M, van Veen HW, Konings WN (1999) The purified and functionally reconstituted multidrug transporter LmrA of *Lactococcus lactis* mediates the transbilayer movement of specific fluorescent phospholipids. *Biochemistry* **38**: 16298–16306
- Markley JL, Bax A, Arata Y, Hilbers CW, Kaptein R, Sykes BD, Wright PE, Wüthrich K (1998) Recommendations for the presentation of NMR structures of proteins and nucleic acids—IUPAC-IUBMB-IUPAB Inter-Union Task Group on the standardization of data bases of protein and nucleic acid structures determined by NMR spectroscopy. *Eur J Biochem* **256**: 1–15
- Martin RW, Zilm KW (2003) Preparation of protein nanocrystals and their characterization by solid state NMR. *J Magn Reson* **165**: 162–174
- Masaoka Y, Ueno Y, Morita Y, Kuroda T, Mizushima T, Tsuchiya T (2000) A two-component multidrug efflux pump, EbrAB, in *Bacillus subtilis*. *J Bacteriol* **182**: 2307–2310. doi:10.1128/JB.182.8.2307-2310.2000
- Masi M, Pages JM, Pradel E (2003) Overexpression and purification of the three components of the *Enterobacter aerogenes* AcrA-AcrB-TolC multidrug efflux pump. *J Chromatogr B Analyt Technol Biomed Life Sci* **786**: 197–205
- Mason AJ, Siarheyeva A, Haase W, Lorch M, van Veen H, Glaubitz C (2004) Amino acid type selective isotope labelling of the multidrug ABC transporter LmrA for solid-state NMR studies. *FEBS Letters* **568**: 117–121. doi:10.1016/j.febslet.2004.05.016

- Mason AJ, Turner GJ, Glaubitz C (2005) Conformational heterogeneity of transmembrane residues after the Schiff base reprotonation of bacteriorhodopsin: 15N CPMAS NMR of D85N/T170C membranes. *FEBS J* **272**: 2152–2164. doi:10.1111/j.1742-4658.2005.04633.x
- Maycox PR, Deckwerth T, Jahn R (1990) Bacteriorhodopsin drives the glutamate transporter of synaptic vesicles after co-reconstitution. *EMBO J* **9**: 1465–1469
- McDermott A, Polenova T, Bockmann A, Zilm KW, Paulson EK, Martin RW, Montelione GT, Paulsen EK (2000) Partial NMR assignments for uniformly (<sup>13</sup>C, <sup>15</sup>N)-enriched BPTI in the solid state. *J Biomol NMR* **16**: 209–219
- Miroux B, Walker JE (1996) Over-production of proteins in Escherichia coli: mutant hosts that allow synthesis of some membrane proteins and globular proteins at high levels. *J Mol Biol* **260**: 289–298. doi:10.1006/jmbi.1996.0399
- Moffatt BA, Studier FW (1987) T7 lysozyme inhibits transcription by T7 RNA polymerase. *Cell* **49**: 221–227
- Molloy MP, Herbert BR, Williams KL, Gooley AA (1999) Extraction of Escherichia coli proteins with organic solvents prior to two-dimensional electrophoresis. *Electrophoresis* **20**: 701–704
- Mootha VK, French S, Balaban RS (1996) Neutral carrier-based "Ca(2+)-selective" microelectrodes for the measurement of tetraphenylphosphonium. *Anal Biochem* **236**: 327–330. doi:10.1006/abio.1996.0174
- Mordoch SS, Granot D, Lebendiker M, Schuldiner S (1999) Scanning cysteine accessibility of EmrE, an H<sup>+</sup>-coupled multidrug transporter from Escherichia coli, reveals a hydrophobic pathway for solutes. *J Biol Chem* **274**: 19480–19486. doi:10.1074/jbc.274.27.19480
- Morein S, Andersson AS, Rilfors L, Lindblom G (1996) Wild-type Escherichia coli Cells Regulate the Membrane Lipid Composition in a "Window" between Gel and Non-lamellar Structures. *J Biol Chem* **271**: 6801–6809. doi:10.1074/jbc.271.12.6801
- Morgner N, Kleinschroth T, Barth HD, Ludwig B, Brutschy B (2007) A novel approach to analyze membrane proteins by laser mass spectrometry: from protein sub-

- units to the integral complex. *J Am Soc Mass Spectrom* **18**: 1429–1438. doi: 10.1016/j.jasms.2007.04.013
- Muchmore DC, McIntosh LP, Russell CB, Anderson DE, Dahlquist FW (1989) Expression and nitrogen-15 labeling of proteins for proton and nitrogen-15 nuclear magnetic resonance. *Methods Enzymol* **177**: 44–73
- Muth TR, Schuldiner S (2000) A membrane-embedded glutamate is required for ligand binding to the multidrug transporter EmrE. *EMBO J* **19**: 234–240
- Neal S, Nip AM, Zhang H, Wishart DS (2003) Rapid and accurate calculation of protein <sup>1</sup>H, <sup>13</sup>C and <sup>15</sup>N chemical shifts. *J Biomol NMR* **26**: 215–240
- Neralla S, Glassroth J (2003) Mycobacterium tuberculosis: the treatment of active disease. *Semin Respir Infect* **18**: 292–306
- Ninio S, Rotem D, Schuldiner S (2001) Functional analysis of novel multidrug transporters from human pathogens. *J Biol Chem* **276**: 48250–48256. doi: 10.1074/jbc.M108231200
- Ninio S, Schuldiner S (2003) Characterization of an archaeal multidrug transporter with a unique amino acid composition. *J Biol Chem* **278**: 12000–12005. doi: 10.1074/jbc.M213119200
- Nishino K, Yamaguchi A (2001) Analysis of a complete library of putative drug transporter genes in Escherichia coli. *J Bacteriol* **183**: 5803–5812. doi: 10.1128/JB.183.20.5803-5812.2001
- Noguchi N, Suwa J, Narui K, Sasatsu M, Ito T, Hiramatsu K, Song JH (2005) Susceptibilities to antiseptic agents and distribution of antiseptic-resistance genes qacA/B and smr of methicillin-resistant Staphylococcus aureus isolated in Asia during 1998 and 1999. *J Med Microbiol* **54**: 557–565. doi:10.1099/jmm.0.45902-0
- Nury H, Dahout-Gonzalez C, Trezeguet V, Lauquin G, Brandolin G, Pebay-Peyroula E (2005) Structural basis for lipid-mediated interactions between mitochondrial ADP/ATP carrier monomers. *FEBS Lett* **579**: 6031–6036. doi: 10.1016/j.febslet.2005.09.061

- Oesterhelt D, Stoeckenius W (1974) Isolation of the cell membrane of *Halobacterium halobium* and its fractionation into red and purple membrane. *Methods Enzymol* **31**: 667–678
- Oh BH, Markley JL (1989) Complete  $^{13}\text{C}$  resonance assignments of tryptophan in L-lysyl-L-tryptophyl-L-lysine by single-bond and multiple-bond correlated  $^1\text{H}$  &  $^{13}\text{C}$  two-dimensional NMR. *Biopolymers* **28**: 1833–1837. doi:10.1002/bip.360281015
- Ohmizo C, Yata M, Katsu T (2004) Bacterial cytoplasmic membrane permeability assay using ion-selective electrodes. *J Microbiol Methods* **59**: 173–179. doi:10.1016/j.mimet.2004.06.008
- Olmsted J, Kearns DR (1977) Mechanism of ethidium bromide fluorescence enhancement on binding to nucleic acids. *Biochemistry* **16**: 3647–3654
- Omote H, Hiasa M, Matsumoto T, Otsuka M, Moriyama Y (2006) The MATE proteins as fundamental transporters of metabolic and xenobiotic organic cations. *Trends Pharmacol Sci* **27**: 587–593. doi:10.1016/j.tips.2006.09.001
- Pao SS, Paulsen IT, Saier MH (1998) Major facilitator superfamily. *Microbiol Mol Biol Rev* **62**: 1–34
- Park RBB, Biggins J (1964) Quantasome: Size and Composition. *Science* **144**: 1009–1011. doi:10.1126/science.144.3621.1009
- Patching SG, Brough AR, Herbert RB, Rajakarier JA, Henderson PJ, Middleton DA (2004) Substrate affinities for membrane transport proteins determined by  $^{13}\text{C}$  cross-polarization magic-angle spinning nuclear magnetic resonance spectroscopy. *J Am Chem Soc* **126**: 3072–3080. doi:10.1021/ja037163i
- Paternostre MT, Roux M, Rigaud JL (1988) Mechanisms of membrane protein insertion into liposomes during reconstitution procedures involving the use of detergents. 1. Solubilization of large unilamellar liposomes (prepared by reverse-phase evaporation) by triton X-100, octyl glucoside, and sodium cholate. *Biochemistry* **27**: 2668–2677
- Paulsen IT, Skurray RA, Tam R, Saier MH, Turner RJ, Weiner JH, Goldberg EB, Grinius LL (1996) The SMR family: a novel family of multidrug efflux proteins involved with the efflux of lipophilic drugs. *Mol Microbiol* **19**: 1167–1175

- Pearson JG, Oldfield E, Lee FS, Warshel A (1993) Chemical shifts in proteins: a shielding trajectory analysis of the fluorine nuclear magnetic resonance spectrum of the Escherichia coli galactose binding protein using a multipole shielding polarizability-local reaction field-molecular dynamics approach. *J Am Chem Soc* **115**: 6851–6862
- Peric M, Bozdogan B, Jacobs MR, Appelbaum PC (2003) Effects of an efflux mechanism and ribosomal mutations on macrolide susceptibility of Haemophilus influenzae clinical isolates. *Antimicrob Agents Chemother* **47**: 1017–1022
- Perozo E, Hubbell WL (1993) Voltage activation of reconstituted sodium channels: use of bacteriorhodopsin as a light-driven current source. *Biochemistry* **32**: 10471–10478
- Piddock LJ (2006) Clinically relevant chromosomally encoded multidrug resistance efflux pumps in bacteria. *Clin Microbiol Rev* **19**: 382–402. doi:10.1128/CMR.19.2.382-402.2006
- Pines A, Gibby MG, Waugh JS (1973) Proton-enhanced NMR of dilute spins in solids. *J Chem Phys* **59**: 569–590
- Poget SF, Cahill SM, Girvin ME (2007) Isotropic bicelles stabilize the functional form of a small multidrug-resistance pump for NMR structural studies. *J Am Chem Soc* **129**: 2432–2433. doi:10.1021/ja0679836
- Poget SF, Krueger-Koplin ST, Krueger-Koplin RD, Cahill SM, Chandra Shekar S, Girvin ME (2006) NMR assignment of the dimeric S. aureus small multidrug-resistance pump in LPPG micelles. *J Biomol NMR* **36 Suppl 1**. doi:10.1007/s10858-005-5346-4
- Poget SFF, Girvin MEE (2007) Solution NMR of membrane proteins in bilayer mimics: Small is beautiful, but sometimes bigger is better. *Biochim Biophys Acta* doi:10.1016/j.bbamem.2007.09.006
- Pornillos O, Chen YJ, Chen AP, Chang G (2005) X-ray Structure of the EmrE Multidrug Transporter in Complex with a Substrate. *Science* **310**: 1950–1953. doi:10.1126/science.1119776
- Prasad R (2007) Management of multi-drug resistant tuberculosis: practitioner's view point. *Indian J Tuberc* **54**: 3–11

- Purewal AS (1991) Nucleotide sequence of the ethidium efflux gene from *Escherichia coli*. *FEMS Microbiol Lett* **66**: 229–231
- Racker E, Stoerkenius W (1974) Reconstitution of purple membrane vesicles catalyzing light-driven proton uptake and adenosine triphosphate formation. *J Biol Chem* **249**: 662–663
- Ramon-Garcia S, Martin C, De Rossi E, Ainsa JA (2007) Contribution of the Rv2333c efflux pump (the Stp protein) from *Mycobacterium tuberculosis* to intrinsic antibiotic resistance in *Mycobacterium bovis* BCG. *J Antimicrob Chemother* **59**: 544–547
- Rankin SE, Watts A, Roder H, Pinheiro TJ (1999) Folding of apocytochrome c induced by the interaction with negatively charged lipid micelles proceeds via a collapsed intermediate state. *Protein Sci* **8**: 381–393
- Rapp M, Granseth E, Seppaelae S, von Heijne G (2006) Identification and evolution of dual-topology membrane proteins. *Nat Struct Mol Biol* **13**: 112–116. doi:10.1038/nsmb1057
- Rapp M, Seppaelae S, Granseth E, von Heijne G (2007) Emulating membrane protein evolution by rational design. *Science* **315**: 1282–1284. doi:10.1126/science.1135406
- Rath A, Deber CM (2007) Membrane protein assembly patterns reflect selection for non-proliferative structures. *FEBS Lett* **581**: 1335–1341. doi:10.1016/j.febslet.2007.02.050
- Rath A, Melnyk RA, Deber CM (2006) Evidence for assembly of small multidrug resistance proteins by a "two-faced" transmembrane helix. *J Biol Chem* **281**: 15546–15553. doi:10.1074/jbc.M600434200
- Raynaud C, Laneelle MA, Senaratne RH, Draper P, Laneelle G, Daffe M (1999) Mechanisms of pyrazinamide resistance in mycobacteria: importance of lack of uptake in addition to lack of pyrazinamidase activity. *Microbiology* **145**: 1359–1367
- Rienstra CM, Tucker-Kellogg L, Jaroniec CP, Hohwy M, Reif B, McMahon MT, Tidor B, Lozano-Perez T, Griffin RG (2002) De novo determination of peptide structure with solid-state magic-angle spinning NMR spectroscopy. *Proc Natl Acad Sci U S A* **99**: 10260–10265. doi:10.1073/pnas.152346599

- Rigaud JL, Levy D (2003) Reconstitution of membrane proteins into liposomes. *Methods Enzymol* **372**: 65–86. doi:10.1016/S0076-6879(03)72004-7
- Roninson IB, Chin JE, Choi KG, Gros P, Housman DE, Fojo A, Shen DW, Gottesman MM, Pastan I (1986) Isolation of human mdr DNA sequences amplified in multidrug-resistant KB carcinoma cells. *Proc Natl Acad Sci U S A* **83**: 4538–4542
- Rotem D, Sal-man N, Schuldiner S (2001) In vitro monomer swapping in EmrE, a multidrug transporter from Escherichia coli, reveals that the oligomer is the functional unit. *J Biol Chem* **276**: 48243–48249. doi:10.1074/jbc.M108229200
- Rotem D, Schuldiner S (2004) EmrE, a multidrug transporter from Escherichia coli, transports monovalent and divalent substrates with the same stoichiometry. *J Biol Chem* **279**: 48787–48793. doi:10.1074/jbc.M408187200
- Rotem D, Steiner-Mordoch S, Schuldiner S (2006) Identification of Tyrosine Residues Critical for the Function of an Ion-coupled Multidrug Transporter. *J Biol Chem* **281**: 18715–18722. doi:10.1074/jbc.M602088200
- Rouse DA, Li Z, Bai GH, Morris SL (1995) Characterization of the katG and inhA genes of isoniazid-resistant clinical isolates of Mycobacterium tuberculosis. *Antimicrob Agents Chemother* **39**: 2472–2477
- Ruben GC, Telford JN (1980) Dimensions of active cytochrome c oxidase in reconstituted liposomes using a gold ball shadow width standard: a freeze-etch electron microscopy study. *J Microsc* **118**: 191–216
- Saier MH, Paulsen IT (2001) Phylogeny of multidrug transporters. *Semin Cell Dev Biol* **12**: 205–213. doi:10.1006/scdb.2000.0246
- Salzmann M, Wider G, Pervushin K, Senn H, Wuthrich K (1999) TROSY-type Triple-Resonance Experiments for Sequential NMR Assignments of Large Proteins. *J Am Chem Soc* **121**: 844–848. doi:10.1021/ja9834226
- Sareen M, Khuller GK (1990) Cell wall and membrane changes associated with ethambutol resistance in Mycobacterium tuberculosis H37Ra. *Antimicrob Agents Chemother* **34**: 1773–1776. doi:10.1128/AAC.

- Schaegger H, von Jagow G (1987) Tricine-sodium dodecyl sulfate-polyacrylamide gel electrophoresis for the separation of proteins in the range from 1 to 100 kDa. *Anal Biochem* **166**: 368–379
- Schluesener D, Fischer F, Kruijff J, Roegner M, Poetsch A (2005) Mapping the membrane proteome of *Corynebacterium glutamicum*. *Proteomics* **5**: 1317–1330. doi: 10.1002/pmic.200400993
- Schuldiner S (2007) When biochemistry meets structural biology: the cautionary tale of EmrE. *Trends Biochem Sci* **32**: 252–258. doi:10.1016/j.tibs.2007.04.002
- Schuldiner S, Granot D, Mordoch SS, Ninio S, Rotem D, Soskin M, Tate CG, Yerushalmi H (2001) Small is mighty: EmrE, a multidrug transporter as an experimental paradigm. *News Physiol Sci* **16**: 130–134
- Schwaiger M, Lebendiker M, Yerushalmi H, Coles M, Groeger A, Schwarz C, Schuldiner S, Kessler H (1998) NMR investigation of the multidrug transporter EmrE, an integral membrane protein. *Eur J Biochem* **254**: 610–619
- Seeger MA, Schiefner A, Eicher T, Verrey F, Diederichs K, Pos KM (2006) Structural asymmetry of AcrB trimer suggests a peristaltic pump mechanism. *Science* **313**: 1295–1298. doi:10.1126/science.1131542
- Seidel K, Eitzkorn M, Heise H, Becker S, Baldus M (2005) High-resolution solid-state NMR studies on uniformly [<sup>13</sup>C,<sup>15</sup>N]-labeled ubiquitin. *Chembiochem* **6**: 1638–1647. doi:10.1002/cbic.200500085
- Sharoni M, Steiner-Mordoch S, Schuldiner S (2005) Exploring the Binding Domain of EmrE, the Smallest Multidrug Transporter. *J Biol Chem* **280**: 32849–32855. doi: 10.1074/jbc.M504910200
- Shastri S, Vonck J, Pflieger N, Haase W, Kuehlbrandt W, Glaubitz C (2007) Protorhodopsin: Characterisation of 2D Crystals by Electron Microscopy and Solid State NMR. *Biochim Biophys Acta Biomembr* **1768(12)**: 3012–3019. doi: 10.1016/j.bbamem.2007.10.001
- Shuker SB, Hajduk PJ, Meadows RP, Fesik SW (1996) Discovering high-affinity ligands for proteins: SAR by NMR. *Science* **274**: 1531–1534. doi: 10.1126/science.274.5292.1531

- Siarheyeva A, Lopez JJ, Glaubitz C (2006) Localization of multidrug transporter substrates within model membranes. *Biochemistry* **45**: 6203–6211. doi: 10.1021/bi0524870
- Sikora CW, Turner RJ (2005a) Investigation of ligand binding to the multidrug resistance protein EmrE by isothermal titration calorimetry. *Biophys J* **88**: 475–482. doi: 10.1529/biophysj.104.049247
- Sikora CW, Turner RJ (2005b) SMR proteins SugE and EmrE bind ligand with similar affinity and stoichiometry. *Biochem Biophys Res Commun* **335**: 105–111. doi: 10.1016/j.bbrc.2005.07.051
- Smirnova IN, Kaback HR (2003) A mutation in the lactose permease of Escherichia coli that decreases conformational flexibility and increases protein stability. *Biochemistry* **42**: 3025–3031. doi:10.1021/bi027329c
- Sonnhammer EL, von Heijne G, Krogh A (1998) A hidden Markov model for predicting transmembrane helices in protein sequences. *Proc Int Conf Intell Syst Mol Biol* **6**: 175–182
- Soskine M, Adam Y, Schuldiner S (2004) Direct evidence for substrate-induced proton release in detergent-solubilized EmrE, a multidrug transporter. *J Biol Chem* **279**: 9951–9955. doi:10.1074/jbc.M312853200
- Soskine M, Mark S, Tayer N, Mizrahi R, Schuldiner S (2006) On Parallel and Antiparallel Topology of a Homodimeric Multidrug Transporter. *J Biol Chem* **281**: 36205–36212. doi:10.1074/jbc.M607186200
- Soskine M, Steiner-Mordoch S, Schuldiner S (2002) Crosslinking of membrane-embedded cysteines reveals contact points in the EmrE oligomer. *Proc Natl Acad Sci U S A* **99**: 12043–12048. doi:10.1073/pnas.192392899
- Spooner PJ, O'Reilly WJ, Homans SW, Rutherford NG, Henderson PJ, Watts A (1998) Weak substrate binding to transport proteins studied by NMR. *Biophys J* **75**: 2794–2800
- Spooner PJ, Rutherford NG, Watts A, Henderson PJ (1994) NMR observation of substrate in the binding site of an active sugar-H<sup>+</sup> symport protein in native membranes. *Proc Natl Acad Sci U S A* **91**: 3877–3881

- Srikumar R, Paul CJ, Poole K (2000) Influence of mutations in the mexR repressor gene on expression of the MexA-MexB-oprM multidrug efflux system of *Pseudomonas aeruginosa*. *J Bacteriol* **182**: 1410–1414
- Stallkamp I, Dowhan W, Altendorf K, Jung K (1999) Negatively charged phospholipids influence the activity of the sensor kinase KdpD of *Escherichia coli*. *Arch Microbiol* **172**: 295–302
- Studier FW, Moffatt BA (1986) Use of bacteriophage T7 RNA polymerase to direct selective high-level expression of cloned genes. *J Mol Biol* **189**: 113–130
- Studier FW, Rosenberg AH, Dunn JJ, Dubendorff JW (1990) Use of T7 RNA polymerase to direct expression of cloned genes. *Methods Enzymol* **185**: 60–89
- Subczynski WK, Wisniewska A, Yin JJ, Hyde JS, Kusumi A (1994) Hydrophobic barriers of lipid bilayer membranes formed by reduction of water penetration by alkyl chain unsaturation and cholesterol. *Biochemistry* **33**: 7670–7681
- Szeverenyi NM, Sullivan MJ, Maciel GE (1982) Observation of spin exchange by two-dimensional fourier transform <sup>13</sup>C cross polarization-magic-angle spinning. *J Magn Reson (1969)* **47**: 462–475. doi:10.1016/0022-2364(82)90213-X
- Tabor S, Richardson CC (1985) A bacteriophage T7 RNA polymerase/promoter system for controlled exclusive expression of specific genes. *Proc Natl Acad Sci U S A* **82**: 1074–1078
- Takegoshi K, Nakamura S, Terao T (2001) <sup>13</sup>C-1H dipolar-assisted rotational resonance in magic-angle spinning NMR. *Chem Phys Lett* **344**: 631–637
- Takiff HE, Salazar L, Guerrero C, Philipp W, Huang WM, Kreiswirth B, Cole ST, Jacobs WR, Telenti A (1994) Cloning and nucleotide sequence of *Mycobacterium tuberculosis* gyrA and gyrB genes and detection of quinolone resistance mutations. *Antimicrob Agents Chemother* **38**: 773–780
- Tate CG, Kunji ER, Lebendiker M, Schuldiner S (2001) The projection structure of EmrE, a proton-linked multidrug transporter from *Escherichia coli*, at 7 Å resolution. *EMBO J* **20**: 77–81

- Telenti A, Imboden P, Marchesi F, Lowrie D, Cole S, Colston MJ, Matter L, Schopfer K, Bodmer T (1993) Detection of rifampicin-resistance mutations in *Mycobacterium tuberculosis*. *Lancet* **341**: 647–650
- Tennent JM, Lyon BR, Gillespie MT, May JW, Skurray RA (1985) Cloning and expression of *Staphylococcus aureus* plasmid-mediated quaternary ammonium resistance in *Escherichia coli*. *Antimicrob Agents Chemother* **27**: 79–83
- Trbovic N, Klammt C, Koglin A, Löhr F, Bernhard F, Dötsch V (2005) Efficient strategy for the rapid backbone assignment of membrane proteins. *J Am Chem Soc* **127**: 13504–13505. doi:10.1021/ja0540270
- Tsarbopoulos A, Karas M, Strupat K, Pramanik BN, Nagabhushan TL, Hillenkamp F (1994) Comparative mapping of recombinant proteins and glycoproteins by plasma desorption and matrix-assisted laser desorption/ionization mass spectrometry. *Anal Chem* **66**: 2062–2070
- Ubarretxena-Belandia I, Baldwin JM, Schuldiner S, Tate CG (2003) Three-dimensional structure of the bacterial multidrug transporter EmrE shows it is an asymmetric homodimer. *EMBO J* **22**: 6175–6181
- Vazquez-Ibar JL, Guan L, Svračić M, Kaback HR (2003) Exploiting luminescence spectroscopy to elucidate the interaction between sugar and a tryptophan residue in the lactose permease of *Escherichia coli*. *Proc Natl Acad Sci U S A* **100**: 12706–12711. doi:10.1073/pnas.1835645100
- Verdegem PJ, Bovee-Geurts PH, de Grip WJ, Lugtenburg J, de Groot HJ (1999) Retinylidene ligand structure in bovine rhodopsin, metarhodopsin-I, and 10-methylrhodopsin from internuclear distance measurements using <sup>13</sup>C-labeling and 1-D rotational resonance MAS NMR. *Biochemistry* **38**: 11316–11324. doi:10.1021/bi983014e
- Viitanen P, Newman MJ, Foster DL, Wilson TH, Kaback HR (1986) Purification, reconstitution, and characterization of the lac permease of *Escherichia coli*. *Methods Enzymol* **125**: 429–452
- Wang DN, Safferling M, Lemieux MJ, Griffith H, Chen Y, Li XD (2003) Practical aspects of overexpressing bacterial secondary membrane transporters for structural studies. *Biochim Biophys Acta* **1610**: 23–36

- Wang W, Malcolm BA (1999) Two-stage PCR protocol allowing introduction of multiple mutations, deletions and insertions using QuikChange Site-Directed Mutagenesis. *Biotechniques* **26**: 680–682
- Wang Y, Jardetzky O (2002) Probability-based protein secondary structure identification using combined NMR chemical-shift data. *Protein Sci* **11**: 852–861
- Waugh DS (1996) Genetic tools for selective labeling of proteins with alpha-15N-amino acids. *J Biomol NMR* **8**: 184–192
- Welch TJ, Fricke WF, Mcdermott PF, White DG, Rosso ML, Rasko DA, Mammel MK, Eppinger M, Rosovitz MJ, Wagner D, Rahalison L, Leclerc JE, Hinshaw JM, Lindler LE, Cebula TA, Carniel E, Ravel J (2007) Multiple antimicrobial resistance in plague: an emerging public health risk. *PLoS ONE* **2**: e309+. doi: 10.1371/journal.pone.0000309
- Werner K, Lehner I, Dhiman HK, Richter C, Glaubitz C, Schwalbe H, Klein-Seetharaman J, Khorana HG (2007) Combined solid state and solution NMR studies of alpha,epsilon-15N labeled bovine rhodopsin. *J Biomol NMR* **37**: 303–312. doi: 10.1007/s10858-007-9143-0
- WHO (2007) WHO report 2007 (WHO/HTM/TB/2007.376)
- Wilkins MR, Gasteiger E, Sanchez JC, Bairoch A, Hochstrasser DF (1998) Two-dimensional gel electrophoresis for proteome projects: the effects of protein hydrophobicity and copy number. *Electrophoresis* **19**: 1501–1505. doi: 10.1002/elps.1150190847
- Winstone TL, Duncalf KA, Turner RJ (2002) Optimization of expression and the purification by organic extraction of the integral membrane protein EmrE. *Protein Expr Purif* **26**: 111–121
- Winstone TL, Jidenko M, le Maire M, Ebel C, Duncalf KA, Turner RJ (2005) Organic solvent extracted EmrE solubilized in dodecyl maltoside is monomeric and binds drug ligand. *Biochem Biophys Res Commun* **327**: 437–445. doi:10.1016/j.bbrc.2004.11.164
- Wollman FA, Olive J, Bennoun P, Recouvreur M (1980) Organization of the photosystem II centers and their associated antennae in the thylakoid membranes: a comparative

- ultrastructural, biochemical, and biophysical study of *Chlamydomonas* wild type and mutants lacking in photosystem II reaction centers. *J Cell Biol* **87**: 728–735
- Xie H, Patching SG, Gallagher MP, Litherland GJ, Brough AR, Venter H, Yao SY, Ng AM, Young JD, Herbert RB, Henderson PJ, Baldwin SA (2004) Purification and properties of the *Escherichia coli* nucleoside transporter NupG, a paradigm for a major facilitator transporter sub-family. *Mol Membr Biol* **21**: 323–336. doi: 10.1080/09687860400003941
- Yamaguchi S, Tuzi S, Bowie JU, Saito H (2004) Secondary structure and backbone dynamics of *Escherichia coli* diacylglycerol kinase, as revealed by site-directed solid-state <sup>13</sup>C NMR. *Biochim Biophys Acta* **1698**: 97–105. doi:10.1016/j.bbapap.2003.10.013
- Yamazaki T, Otomo T, Oda N, Kyogoku Y, Uegaki K, Ito N, Ishino Y, Nakamura H (1998) Segmental Isotope Labeling for Protein NMR Using Peptide Splicing. *JACS* **120**: 5591–5592
- Yerushalmi H, Lebendiker M, Schuldiner S (1995) EmrE, an *Escherichia coli* 12-kDa multidrug transporter, exchanges toxic cations and H<sup>+</sup> and is soluble in organic solvents. *J Biol Chem* **270**: 6856–6863. doi:10.1074/jbc.270.12.6856
- Yerushalmi H, Lebendiker M, Schuldiner S (1996) Negative dominance studies demonstrate the oligomeric structure of EmrE, a multidrug antiporter from *Escherichia coli*. *J Biol Chem* **271**: 31044–31048
- Yerushalmi H, Mordoch SS, Schuldiner S (2001) A single carboxyl mutant of the multidrug transporter EmrE is fully functional. *J Biol Chem* **276**: 12744–12748. doi: 10.1074/jbc.M010979200
- Yerushalmi H, Schuldiner S (2000a) A common binding site for substrates and protons in EmrE, an ion-coupled multidrug transporter. *FEBS Lett* **476**: 93–97
- Yerushalmi H, Schuldiner S (2000b) An essential glutamyl residue in EmrE, a multidrug antiporter from *Escherichia coli*. *J Biol Chem* **275**: 5264–5269. doi: 10.1074/jbc.275.8.5264
- Yerushalmi H, Schuldiner S (2000c) A model for coupling of H<sup>(+)</sup> and substrate fluxes based on "time-sharing" of a common binding site. *Biochemistry* **39**: 14711–14719

- Yin Y, He X, Szewczyk P, Nguyen T, Chang G (2006a) Structure of the Multidrug Transporter EmrD from *Escherichia coli*. *Science* **312**: 741–744. doi:10.1126/science.1125629
- Yin Y, Jensen, Tajkhorshid E, Schulten K (2006b) Sugar binding and protein conformational changes in lactose permease. *Biophys J* **91**: 3972–3985. doi:10.1529/biophysj.106.085993
- Zacharias N, Dougherty DA (2002) Cation- $\pi$  interactions in ligand recognition and catalysis. *Trends Pharmacol Sci* **23**: 281–287
- Zech SG, Olejniczak E, Hajduk P, Mack J, McDermott AE (2004) Characterization of protein-ligand interactions by high-resolution solid-state NMR spectroscopy. *J Am Chem Soc* **126**: 13948–13953. doi:10.1021/ja040086m
- Zhang Z, Ma C, Pornillos O, Xiu X, Chang G, Saier MH (2007) Functional characterization of the heterooligomeric EbrAB multidrug efflux transporter of *Bacillus subtilis*. *Biochemistry* **46**: 5218–5225. doi:10.1021/bi7001604
- Zheleznova EE, Markham PN, Neyfakh AA, Brennan RG (1999) Structural basis of multidrug recognition by BmrR, a transcription activator of a multidrug transporter. *Cell* **96**: 353–362
- Zignol M, Hosseini MS, Wright A, Weezenbeek CL, Nunn P, Watt CJ, Williams BG, Dye C (2006) Global incidence of multidrug-resistant tuberculosis. *J Infect Dis* **194**: 479–485. doi:10.1086/505877

# Curriculum Vitae

## Persönliche Daten

|               |  |
|---------------|--|
| Name          | Daniel Basting                                       |
| Geburtsdatum  | 6. März 1977   |
| Geburtsort    | Göttingen  |
| Eltern        | Dirk Basting und Barbara Basting-Menzel, geb. Menzel |
| Familienstand | ledig  |

## Schule & Universität

|                                 |  |
|---------------------------------|--|
| Seit September 2003             | Promotion an der J. W. Goethe Universität Frankfurt a. Main, bei Prof. Dr. Clemens Glaubitz am Institut für Biophysikalische Chemie  |
| November 1997 bis November 2002 | Diplom-Studium der Chemie an der TU München, Diplomarbeit bei Prof. Dr. W. A. Herrmann am Lehrstuhl für Anorganische Chemie:<br>„Theoretische Untersuchung der Reaktionspfade von Ga(CH <sub>3</sub> ) <sub>3</sub> + NH <sub>3</sub> als klassisches System in der GaN CVD“ |
| Mai 1996                        | Abitur am Theodor-Heuss-Gymnasium, Göttingen   |
| September 1993 bis Juni 1994    | Auslandsjahr an der Middlesex School, Concord, MA, USA   |

## Veröffentlichungen

Lehner, I., Basting, D., Meyer, B., Haase, W., Manolikas, T., Kaiser, C., Karas, M., and Glaubitz, C. (2007) *The Journal of Biological Chemistry*, published online before print as doi: 10.1074/jbc.M707899200

Basting, D., Lorch, M., Lehner, I., and Glaubitz, C. (2007) Transport Cycle Intermediate in Small Multidrug Resistance Protein is revealed by Substrate Fluorescence. *The FASEB Journal*, published online before print as doi: 10.1096/fj.1007-9162com.

Basting, D., Lehner, I., Lorch, M., and Glaubitz, C. (2006) Investigating transport proteins by solid state NMR. *Naunyn-Schmiedeberg's archives of pharmacology* **372**, 451-464

Lorch, M., Lehner, I., Siarheyeva, A., Basting, D., Pflieger, N., Manolikas, T., and Glaubitz, C. (2005) NMR and fluorescence spectroscopy approaches to secondary and primary active multidrug efflux pumps. *Biochemical Society transactions* **33**, 873-877

Schmid, R., and Basting, D. (2005) Gas phase chemistry in gallium nitride CVD: Theoretical determination of the Arrhenius parameters for the first Ga-C bond homolysis of trimethylgallium. *The Journal of physical chemistry* **109**, 2623-2630